University of Miami
Scholarly Repository

Open Access Dissertations | Electronic Theses and Dissertations

2013-10-18

Development of Anti-Inflammatory Biomaterials for Islet Transplantation

Jessica D. Weaver
University of Miami, weaver.d.jessica@gmail.com

Follow this and additional works at: https://scholarlyrepository.miami.edu/oa_dissertations

Recommended Citation
Weaver, Jessica D., "Development of Anti-Inflammatory Biomaterials for Islet Transplantation" (2013). *Open Access Dissertations*. 1100.
https://scholarlyrepository.miami.edu/oa_dissertations/1100

This Embargoed is brought to you for free and open access by the Electronic Theses and Dissertations at Scholarly Repository. It has been accepted for inclusion in Open Access Dissertations by an authorized administrator of Scholarly Repository. For more information, please contact repository.library@miami.edu.

UNIVERSITY OF MIAMI

DEVELOPMENT OF ANTI-INFLAMMATORY BIOMATERIALS FOR ISLET TRANSPLANTATION

By

Jessica D. Weaver

A DISSERTATION

Submitted to the Faculty
of the University of Miami
in partial fulfillment of the requirements for
the degree of Doctor of Philosophy

Coral Gables, Florida

December 2013

©2013

Jessica D. Weaver

All Rights Reserved

UNIVERSITY OF MIAMI

A dissertation submitted in partial fulfillment of
the requirements for the degree of
Doctor of Philosophy

DEVELOPMENT OF ANTI-INFLAMMATORY BIOMATERIALS FOR ISLET TRANSPLANTATION

Jessica D. Weaver

Approved:

_____ Cherie L. Stabler, Ph.D. Professor of Biomedical Engineering	_____ Fotios Andreopoulos, Ph.D. Professor of Biomedical Engineering
_____ Edward Dauer, M.D./M.S. Professor of Biomedical Engineering	_____ Peter Buchwald, Ph.D. Professor of Molecular and Cellular Pharmacology
_____ Angel Kaifer, Ph.D. Professor of Chemistry	_____ M. Brian Blake, Ph.D. Dean of the Graduate School

_____
Antonello Pileggi, M.D./Ph.D.
Professor of Microbiology and Immunology

WEAVER, JESSICA D. (Ph.D., Biomedical Engineering)

Development of Anti-Inflammatory Biomaterials for Islet Transplantation (December 2013)

Abstract of a dissertation at the University of Miami.

Dissertation supervised by Professor Cherie L. Stabler.
No. of pages in text. (112)

Type 1 Diabetes Mellitus (T1DM) is a disease characterized by the autoimmune destruction of beta cells within the pancreatic islet. Islet replacement via transplantation of allogeneic islets demonstrates promise as a viable cure for this disease. Despite clinical success in the mitigation of T1DM symptoms, the islet transplant technique has been plagued by issues that limit graft survival and duration. Inflammation plays a significant role in the destruction of islet grafts, particularly during early engraftment. Therefore, strategies that provide alleviation of inflammation could substantially improve graft outcomes, particularly in the design of alternative islet graft transplant environments. This dissertation presents two biomaterial-based strategies for the local mitigation of inflammation in the islet transplant microenvironment: 1) the development and optimization of an implantable anti-inflammatory drug-eluting organosilicone construct; and 2) the supplementation of islets with antioxidant cerium oxide nanoparticle (CONP)-doped encapsulation polymers. The aim of this work was to develop biomaterials with the capacity to reduce local inflammation in an islet transplant site, thereby improving long-term viability and function of the transplanted cells.

Acknowledgements

I would like to acknowledge the individuals who supported me throughout and contributed significantly to the outcome of this dissertation, in particular my dissertation committee, whose time and effort is greatly appreciated. The many unique resources in the University of Miami's core facilities and the experts in their field who assisted in educating and assisting me on the use of their equipment and services have been invaluable. These include Dr. Pileggi and Dr. Molano and their talented team in the Diabetes Research Institute's (DRI) Translational Core, without whom our islet and transplant studies would not have been realized; Kevin Johnson of the DRI Histology Core, whose prompt and efficient sample processing and stimulating conversation has been greatly appreciated; Dr. Peggy Bates, Dr. Jeffrey Prince and the various experts among UM's light and electron microscope cores. I'd like also to thank Dr's Kenyon and Mendez and their teams for graciously allowing the shared use of equipment and resources when necessary, and their support through my time at the DRI. Great thanks also to all of Dr. Stabler's team for their support and camaraderie, in particular Maria Coronel and Irayme Labrada, without whom the lab would likely collapse. Lastly, my greatest appreciation for Dr. Cherie Stabler, who gave me this priceless opportunity to pursue higher education in this incredible field, and whose endless support and unfailing guidance throughout this experience, has provided me the platform to succeed in my future career.

Table of Contents

List of Figures

List of Tables

Chapter 1. Specific Aims

1.1 INTRODUCTORY REMARKS

Current clinical islet transplantation, where islets are intraportally infused into the liver, has demonstrated superior blood glucose control for Type 1 diabetics; however, detrimental inflammation during engraftment contributes to poor islet efficacy and long-term duration. As such, when seeking to engineer an artificial pancreas, the incorporation of strategies to mitigate inflammation at the local transplant microenvironment is critical.

1.2 SPECIFIC AIMS

The **long-term goal** of this project is to develop and evaluate novel bioengineering strategies for protecting donor islet cells from adverse inflammatory reactions instigated during transplantation. The **objective** of this dissertation was to develop anti-inflammatory biomaterials to alleviate and mitigate the *local* acute and chronic inflammatory reactions observed post-islet transplantation. Two independent strategies were investigated: the engineering of a steroid-based biomaterial to dampen acute inflammation in the transplant environment; and the engineering of a cerium oxide nanoparticle biomaterial capable of scavenging excessive environmental reactive oxygen (ROS) and reactive nitrogen species (RNS). **We hypothesized** that, through the fabrication of novel biomaterials capable of combating local inflammation, improvement in islet engraftment and function would be observed. We tested our central hypothesis through the pursuit of the following aims:

AIM 1. Fabricate, optimize, and assess organosilicone-based implants capable of sustained and controlled release of steroids at the implant site for reduction of acute and chronic inflammatory response in islet transplantation. We designed and assessed temporal release of a model steroid from PDMS, a hydrophobic biomaterial. Steroid-releasing biomaterial constructs of varying geometries were engineered to meet a therapeutic drug range and studied for release characteristics. Dexamethasone was used as the model steroid. Following benchtop measurements, multi-physics modeling was used to develop predictive models for drug release. These results were translated to optimize final prototypes.

Subsequently, we evaluated dexamethasone-PDMS constructs via long-term release studies and the evaluation of their capacity to reduce activation of inflammatory cells *in vitro*. Additional assessment of construct effect on islet function was performed.

Lastly, we evaluated the capacity of steroid–releasing biomaterials to alleviate local inflammation following graft implantation. Rodent studies were conducted with optimal PDMS prototypes, where local host response was evaluated. The effect of local steroid release on graft function was observed in both syngeneic and allogeneic models.

AIM 2. Engineer and evaluate biomaterials doped with cerium oxide nanoparticles (CONPs) for local and sustained scavenging of reactive oxygen and nitrogen species. We synthesized stable, catalytically active anti-oxidant CONPs of homogeneous size and coating. CONP particle size and concentration, as well as the homogeneity and topography of the coating, were subsequently characterized. Catalytic

antioxidant activity of the nanoparticles and their resulting cytotoxic and cytoprotective effects using a beta cell line and islets were explored.

CONPs were conjugated with biomaterials to generate a novel, self-renewing, free-radical scavenging materials**.** Fabricated CONPs were incorporated within hydrogels to generate anti-inflammatory biomaterials. Alginate was used as the model encapsulation hydrogel, where CONPs were incorporated within our hydrogel platform. CONP concentration was optimized within the gels, and evaluated for retention of catalytic activity, and cytotoxic and cytoprotective effects on a beta cell line and islets.

1.3 CONTENTS OF THIS DISSERTATION

The overarching objective of this dissertation was to demonstrate the development of two distinct anti-inflammatory biomaterials for enhancement of islet function *in vivo*: a corticosteroid-eluting construct for co-transplantation with an islet-laden scaffold; and a catalytic enzyme-mimetic cell encapsulation hydrogel for *in vivo* antioxidant protection. **Chapter 2** details background information pertaining to Type I Diabetes and current therapies and alternative strategies for its treatment, as well as the prominent issue of inflammation.

Chapter 3 delves into the optimization of PDMS-based drug-eluting constructs through the characteristics of surface area and drug loading using finite element modeling. *In vitro* release studies were compared to in silica results, which were utilized to elaborate on observed *in vivo* spatial delivery characteristics of the constructs. **Chapter 4** further explores the drug-eluting PDMS-based constructs for localized delivery in an islet transplant site. *In vitro* studies investigated construct impact on islets

and inflammatory cells, and syngeneic murine transplant model studies demonstrated *in vivo* efficacy of the construct through reduced inflammatory cell infiltration.

Chapter 5 investigates the development of novel antioxidant encapsulation hydrogels using catalytic nanoparticles. Nanoparticles were synthesized, developed, and characterized for catalytic activity, cytotoxicity, and cytoprotection. The development of nanoparticle-functionalized encapsulation hydrogels and their capacity for cytotoxicity and cytoprotection was explored in beta cells and islets. **Chapter 6** summarizes the work contained within this dissertation, and elaborates on recommendations for future work to further the research contained herein.

Chapter 2. Background and Significance

2.1 TYPE I DIABETES AND CURRENT TREATMENTS

Type 1 Diabetes Mellitus (T1DM) is an autoimmune disorder characterized by immune-targeted destruction of beta cells within the pancreatic islet of Langerhaans. Clinical successes have demonstrated the ability of clinical islet transplantation (CIT) to reverse diabetes and restore insulin independence (Pileggi et al., 2004). In this technique, islets, isolated from a donor pancreas, are injected into the portal vein of the liver, where they become trapped in the hepatic microvasculature (Harlan et al., 2009). Clinically, significant loss of the islet graft is observed from 18 months to five years post-transplant, likely due to inflammation and immune response.(Pileggi et al., 2004) The prominent effect of inflammation on islet survival is illustrated by studies exhibiting significant islet loss for syngeneic intrahepatic transplants, whereby allo- and auto-immune responses are not a factor(Barshes et al., 2005; Koulmanda et al., 2012; Zhu et al., 2010).

Inflammation spurs the release of reactive oxygen species (ROS) such as superoxide (O_2^-) and hydrogen peroxide (H_2O_2), and reactive nitrogen species (RNS) such as nitric oxide (NO), in addition to pro-inflammatory cytokines, which have a known cytotoxic effect on β-cells(Hume, P. S. et al., 2011a) (Lenzen et al., 1996; Oberley, 1988). Compared to hepatic tissue, pancreatic islets demonstrate low gene expression and activity for several important antioxidant enzymes, such as superoxide dismutase (SOD) and catalase, which normally alleviate damagingly high concentrations of reactive species (Ho et al., 1999).

2.2 ALTERNATIVE BIOMEDICAL ENGINEERING STRATEGIES TOWARDS A BIOARTIFICIAL PANCREAS

2.2.1 ENGINEERING NEW TRANSPLANT SITES

A persistent problem in cell therapies for diabetes treatment is the placement of donor islet cells within the host body. The current preferred site for islet transplantation is within the portal vein of the liver, where islets trapped in the vasculature are in direct contact with blood flow, and have access to ample amounts of vital nutrients, particularly oxygen. The hepatic site, however, is plagued with problems that lead to islet death and dysfunction, in part due to the islets' direct contact with the blood stream. Islets are negatively impacted by the instant blood-mediated inflammatory reaction (IBMIR) post islet infusion, which results in activation of coagulation and complement cascades, as well as infiltration of leukocytes. (Bennet et al., 2000; Broe et al., 2000; Johansson, H. et al., 2005; Johansson, U. et al., 2003; Mattson et al., 2004; Moberg et al., 2002; Yang et al., 2004) In addition, the liver is the location of drug breakdown, resulting in the release of toxins detrimental to islet graft survival. Further, islets are subjected to unnatural mechanical stresses during transplantation and engraftment, resulting in stress and potential apoptosis(van der Windt et al., 2007).

In an effort to mitigate the observed detrimental responses associated with the hepatic transplant site, alternate sites have been explored, such as the muscular, subcutaneous, ocular, and omentum sites (Berman et al., 2009; Kim, H. I. et al., 2010a; Merani et al., 2008). Alternative islet transplant sites must incorporate strategies to mimic pancreatic tissue in order to improve graft survival, as these sites typically face challenges such as sub-optimal vascularization, higher mechanical stress than the native

tissue, and islet pelleting within the transplant site.(Kim, H. I. et al., 2010a) These are important factors to consider when engineering an alternative site, and various strategies have been explored for adaptation of the islet environment. Our group has chosen to explore the omentum as the optimum location in which to engineer a bioartificial pancreas, as this site benefits from high vascularization, low mechanical stresses, space for large graft volumes, in addition to being a non-vital organ, which may lower transplant risks.

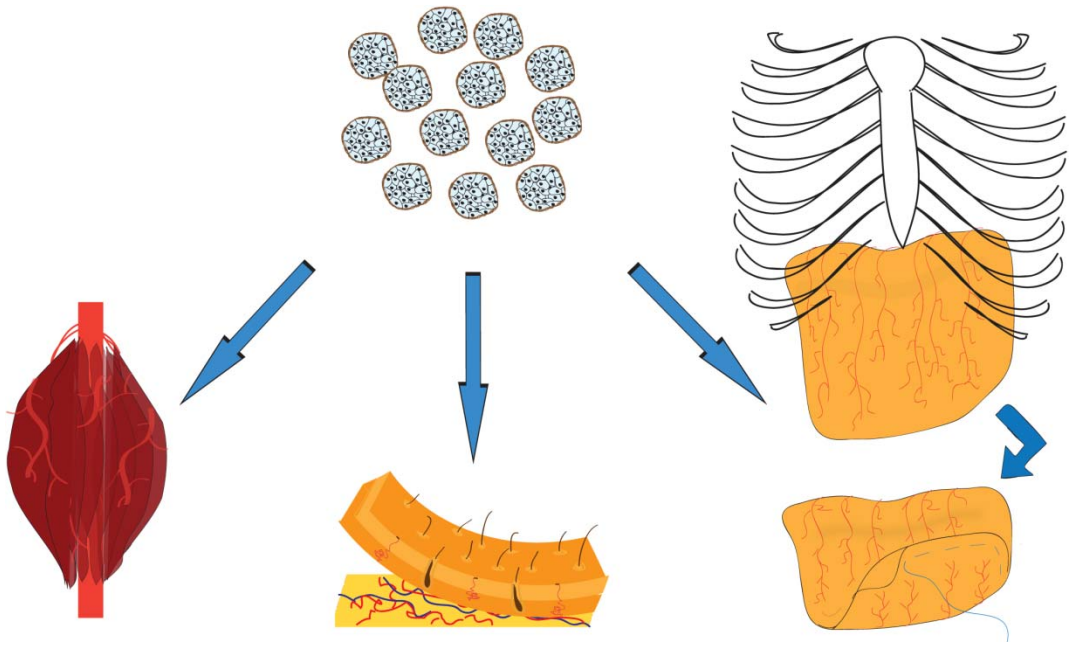

Figure 2-1 Schematic demonstrating proposed alternative sites for islet transplantation. The intramuscular (left), subcutaneous (center, bottom), and omental sites have all been investigated as alternative islet transplantation locations due to their high level of vascularization. The omental pouch is advantageous due to its lower potential for mechanical stresses compared to the other locations.

2.2.2 BIOMIMETIC SCAFFOLDS AS A MULTIFUNCTIONAL PLATFORM FOR ISLET TRANSPLANTATION

Upon removal from their native three-dimensional environment during isolation, islets suffer in function and viability. The native microvasculature and three-dimensional matrix are typically disrupted during islet isolation from pancreatic tissue, and in techniques where this is not restored islet grafts suffer.(Salvay et al., 2008; Weber, L. M. et al., 2007) In typical non-hepatic islet transplant strategies, the islets are loaded in the transplant site in large amounts in a single location. The result is a pellet of islets which quickly may become anoxic in the core of the pellet due to a large mass of cells rapidly consuming oxygen within a small volume.(Weber, L. M. et al., 2008)

An environment that is similar in structure to the islet's native pancreatic site may improve graft function and nutrient diffusion. While groups have investigated hydrogel-based matrices for use as cell scaffolding, they generally lack mechanical strength and their water-saturated structures may impede nutrient diffusion through the construct.(Van Vlierberghe et al., 2011) A promising material for the design of macroporous scaffolds with both high mechanical stability and high oxygen diffusion is polydimethylsiloxane (PDMS), which has additional benefits in that it is bioinert and has a long-standing clinical profile.(Malcolm, K. et al., 2003)

As such, Pedraza, et al. developed a highly porous silicone scaffold that allows for a wide spatial distribution of islets. The scaffolds were designed using finite element modeling to permit optimum oxygen diffusion and account for the high metabolic rate of islets.(Pedraza et al., 2013a; Pedraza et al., 2013b) This scaffold design may alleviate the

necrotic core of the implanted islets by supporting improved nutrient gradients, as well as providing mechanical support and structure for vascular infiltration.

Figure 2-2 Macroporous silicone scaffolds developed for islet transplantation by Pedraza et al.

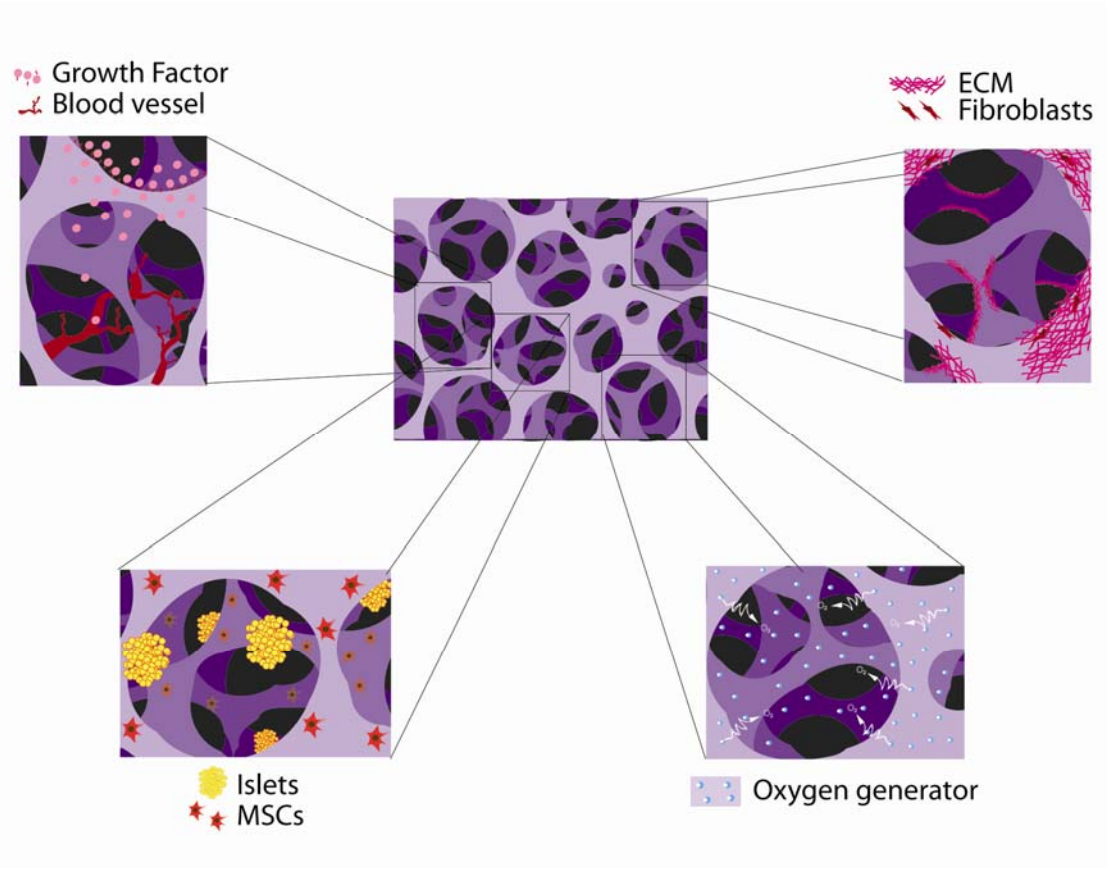

Figure 2-3 Illustration of the concept of a bioactive scaffold for islet transplantation. Potential features of a bioactive scaffold platform are illustrated: oxygen generation, islet

and supporting cells, drug/growth factor delivery to modulate the local environment, and site remodeling by fibroblasts and ECM deposition.

2.2.3 ALTERNATIVES TO SYSTEMIC IMMUNOSUPPRESSIVE THERAPIES

In addition to the IBMIR response, an aggressive immune response is generated by the host's body towards the foreign alloantigens in the implanted tissue. Foreign antigens of donor tissues present to the host in two primary ways: the direct and indirect antigen presentation pathway. In the direct antigen presentation pathway, host immune cells sense foreign antigens through direct cell-to-cell contact. Once host cells identify the presence of foreign cell-surface proteins, a cascade of signals initiate the host's immune system to full-scale attack. The indirect antigen presentation pathway is characterized by the shedding of donor antigens from the cell surface, which travel freely until they are detected and sequestered by host antigen-presenting cells, such as resident dendritic cells, which then present the foreign proteins to host immune cells(Baecher-Allan et al., 2006; Reffet et al., 2006). To alleviate this reaction, which invariably results in complete and targeted destruction of the foreign tissue, immunosuppressive, or anti-rejection, therapies are systemically administered to transplant recipients(Berney et al., 2004; Cheung, C. Y. et al., 2006; Guo et al., 2001; Ryan et al., 2001). While these drug regimens may prevent graft rejection, they come with a host of undesirable side-effects, including a higher incidence of cancer and infections due to lowered immune capabilities.(Hafiz et al., 2005)

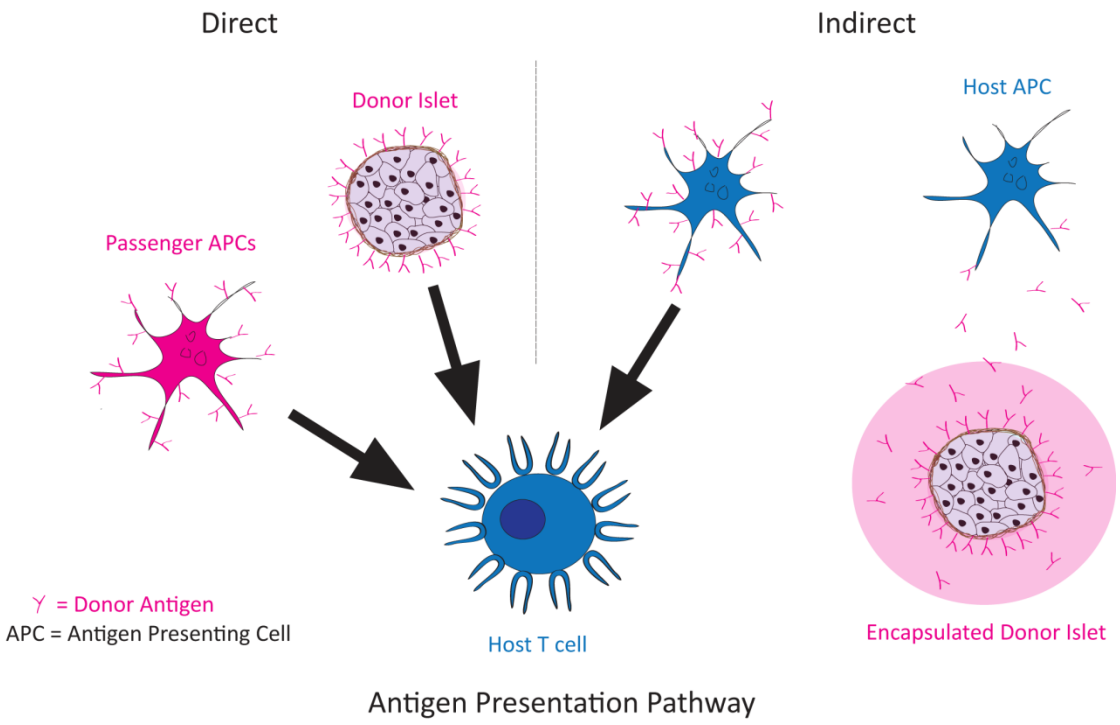

Figure 2-4 Demonstration of the antigen presentation pathway. Schematic demonstrating donor islet antigen presentation to host APCs via the indirect or direct pathway. While islet encapsulation prevents direct antigen recognition, indirect presentation may still occur.

Several strategies have been evaluated with the goal of mitigating the complex immune response to donor tissues. While common approaches to block immunorecognition through biomaterials seek to block the direct antigen presentation pathway, the alternative pathway is still a critical means to rejecting foreign tissue.(Scott et al., 1998). Thus, it is likely that not one, but multiple strategies are necessary to combat the destructive inflammatory and immune responses described above which lead to islet graft loss in vivo. Of the many possible methods, this thesis focuses on two main engineering strategies for ***local*** reduction of inflammation and its impact on islet grafts within a transplant site: localized delivery of anti-inflammatory drugs, and encapsulation of cells within an antioxidant encapsulation hydrogel.

Chapter 3. Optimization of Localized Drug Delivery: Analytical and Histological Comparisons of Corticosteroid-Releasing Organosilicone Constructs with Varying Geometries

3.1 INTRODUCTORY REMARKS

Inflammation is a prominent challenge in the optimal engraftment of tissue engineered implants. Inflammation partially arises from tissue trauma during to the transplant procedure itself (Anderson, 1988), but potent responses primarily arise due to reactions instigated by the implanted cells and/or material(Anderson, 2001). Inflammatory responses can dictate the failure or success of a graft, whereby successful implants exhibit resolution of inflammation within a few weeks, while failed grafts display sustained inflammation, hallmarked by long-term recruitment of macrophages and other immune cells associated with the innate immune pathway(Borg et al., 2011; Nilsson et al., 2007). Increasing biomaterial compatibility and decreasing the immunogenicity of the foreign cells may decrease generalized inflammation, although there are limitations in the flexibility of this approach. Systemic doses of potent anti-inflammatories such as glucocorticoids can substantially blunt activation of inflammation pathways; however, this form of delivery is suboptimal due to detrimental side effects, both generalized to the patient, as well as to the engraftment and function of the transplanted cells (Qi, D. et al., 2007).

Localized drug delivery presents many advantages over systemic exposure, particularly in the context of poorly soluble agents and/or drugs that are potentially harmful in doses required for systemic delivery (Buchwald et al., 2010; Wu et al., 2006). Localized, controlled drug delivery has demonstrated wide application in tissue engineering and would be particularly beneficial for the transplantation of allogeneic

cells, as dampening inflammation mitigates adaptive immune responses(Croxatto, 2002; Sipos et al., 2005; Sivin et al., 2002; Udipi et al., 2007). With this unique advantage, the generation of multiple drug delivery platforms has been explored, with the aim of providing sustained, controlled release alternatives to systemic injections (Di Colo, 1992; Langer, R., 1983). Matrix systems for controlled, sustained drug delivery have been evaluated in a multitude of applications(Galdi et al., 2012; Malcolm, R. K. et al., 2004; Ranade et al., 2005; Schmidt et al., 2008; Siepmann et al., 2000; Snorradottir et al., 2009; Zisch et al., 2003b), and possess the unique advantage of facile and low cost fabrication, where diffusion-driven delivery, constrained by the material matrix properties, facilitates tailoring to a targeted therapeutic dose, with a low risk of dose dumping(Zhou et al., 1997). In the development of anti-inflammatory delivery devices, organosilicones such as polydimethylsiloxane (PDMS) are advantageous in that steroids are highly soluble within the hydrophobic matrix, and provide controlled and tailorable release rates(Malcolm, R. K. et al., 2004).

The potential of localized anti-inflammatory platforms in the context of three-dimensional cellular grafts, specifically in islet transplantation, has not been previously explored. The transplantation of pancreatic islets is particularly challenging due to the potent effects of inflammation on islet survival, as well as their sensitivity to immunomodulatory steroids (Chatenoud, 2008; Kenyon, N. S. et al., 1998; Krautz et al., 2013; Marzorati et al., 2009). Islet engraftment and vascularization are strongly correlated to graft function and long-term survival, which requires the precise application of localized immunomodulatory agents, wherein the delivery platform should not significantly impede angiogenesis or healthy cellular remodeling of the implantation site.

This necessitates the design of complex three-dimensional delivery devices with the capacity for uniform spatial drug distribution, with a highly controlled dose level. As such, exhaustive experimental approaches and simplistic analytical methods are neither cost-effective nor efficient in the generation of devices that meet such specific design parameters(Zhou et al., 1997).

In an effort to design a local, anti-inflammatory platform that achieves the delicate balance between inflammation suppression and permitting beneficial tissue in-growth at the site, we sought to employ multi-physics modeling to predict not only total daily release profiles, but to also evaluate spatial release patterns within the graft. Computational analysis utilizing emergent commercially available finite element modeling (FEM) software allows for pre-fabrication prediction of drug-delivery system behavior(Frenning et al., 2005), and has multiple advantages over the previously utilized, limited methods of analytical (Galdi et al., 2012; Siepmann et al., 2011) and experimental analysis(Zhou et al., 1997). In particular, three-dimensional FEM allows for accurate *in silica* prediction of temporal and spatial drug diffusion from complex geometries of highly variable volume and surface area(Zhou et al., 1997).Such tools provide the means for device design and optimization prior to construction and implementation, allowing for more predictable outcomes, particularly in complex models(Reynolds et al., 2002; Siepmann et al., 2000).

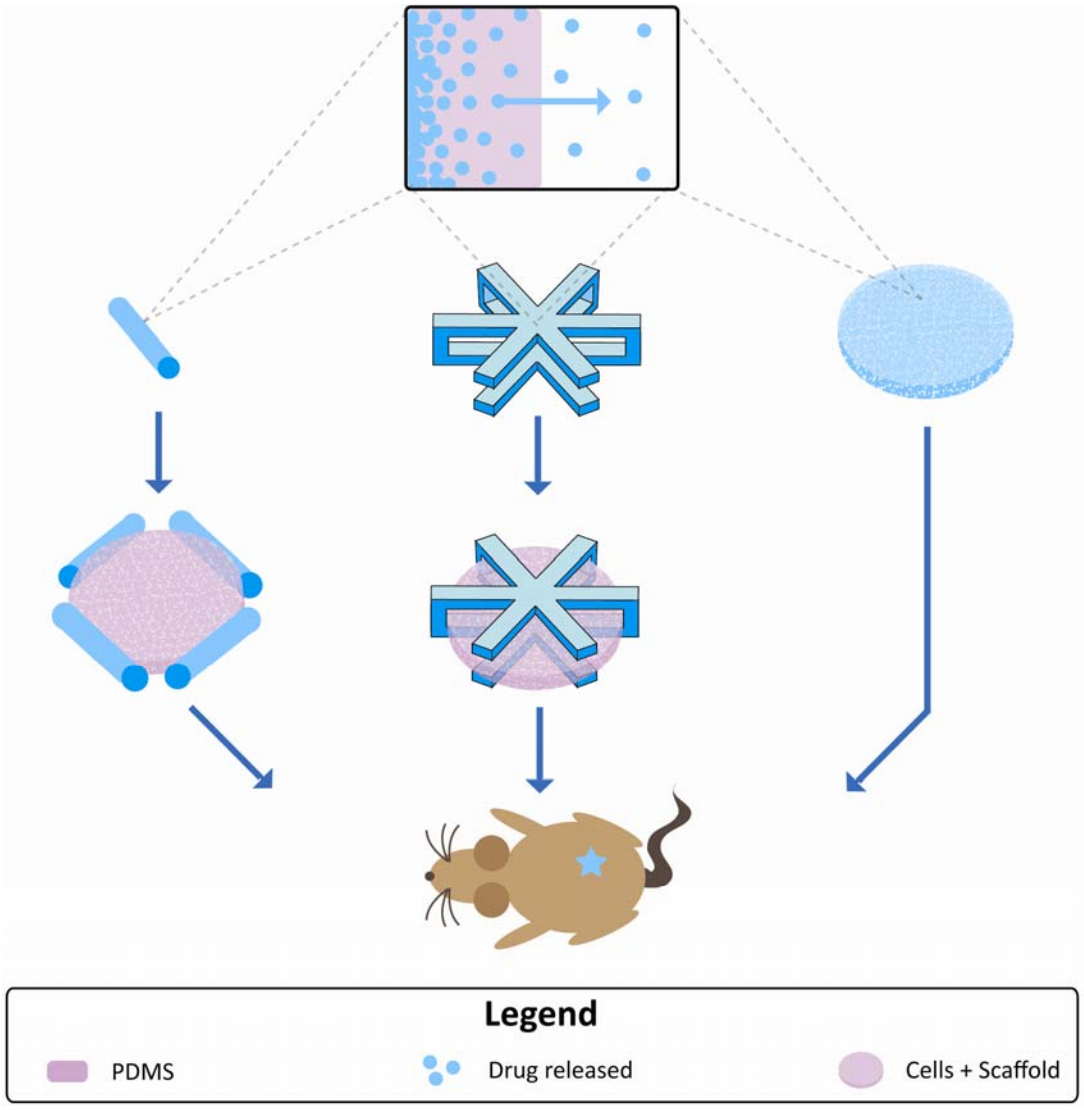

Figure 3-1 Illustration of experimental investigation of drug release from PDMS constructs of varying geometry: rod, cage, and scaffold. The rod and cage constructs are designed to provide drug delivery externally to the to the scaffold-cell combination graft, while our third strategy implements the scaffold itself as the drug delivery device. The spatial effects of these three delivery strategies are explored in vivo.

Herein, polydimethylsiloxane (PDMS), doped with the glucocorticoid dexamethasone (Dex), was chosen as the drug eluting platform. PDMS was selected not only due to its demonstrated efficacy in the sustained delivery of hydrophobic drugs(Fu,

J. C. et al., 1973; Kajihara et al., 2001; Kim, J. et al., 2008; Maeda et al., 2004; Malcolm, K. et al., 2003; Schultz et al., 2010; Snorradottir et al., 2011; Xu et al., 2011), but also due to its ease in fabrication of three-dimensional constructs of varying geometries. Dexamethasone was selected due to its potency in mitigating inflammation (Muller et al., 1994; Patil, S. D. et al., 2007b) and its ease in analytical measurement. Prototype release kinetics and spatial drug distribution was manipulated via modification of the platform geometry, and the influence of construct surface/volume ratios, geometric distribution of drug, and overall drug loading were evaluated (**Figure 3-1**). Following *in silica* analysis and *in vitro* evaluation of daily release characteristics, the impact of varying Dex-PDMS constructs on local remodeling in an islet transplant model was evaluated via assessment of graft remodeling and local inflammatory responses.

3.2 MATERIALS AND METHODS

3.2.1 DEX-PDMS CONSTRUCT FABRICATION

PDMS constructs were formed by mixing PDMS monomer with platinum catalyst per manufacturer's instructions (RTV 615 A&B, GE Silicones) at a ratio of 4:1 prior to mixing evenly with dexamethasone (Dex, Alexis Biochemicals) at 2.5, 5, or 10% w/v, and curing at 60 ºC for 24 h. The rod geometry was formed by injecting PDMS polymer into tubing (1.54mm ID, rods, Saint-Gobain); rods were cured, then cut to 8 or 4 mm in length. The cage geometry was formed by injection into a custom-made Dacron mold (BioRep) prior to curing. The scaffold geometry was formed by mixing PDMS polymer

with NaCl (250-450μm diameter) prior to curing in cylindrical molds (10mm diameter, 1mm height) and salt leaching in H_2O for 3-5 d(Pedraza et al., 2013b).

3.2.2 DEX-PDMS CONSTRUCT RELEASE STUDIES

Two rods, a single cage, or a scaffold, doped with 0-10% dexamethasone were placed in 5 mL of a 1% Benzalkonium chloride (BKC, Sigma) solution on a shaker for 30 d, with full fluid exchanges and samples taken once daily. Dexamethasone release on selected days was measured via ELISA (Neogen), which has a measurement range of 0.01-0.1 ng/mL.

3.2.3 FINITE ELEMENT DIFFUSION MODELING

Three-dimensional time-dependent finite element COMSOL models were computed using the "Transport of Diluted Species" module, which employs Fick's Law to describe diffusive transport, and model mass transport of diluted species:

$$\frac{\partial c}{\partial t} + \nabla \cdot (-D_i \nabla c_i) + \boldsymbol{u} \cdot \nabla c_i = R_i \qquad \textbf{(Equation 3-1)}$$

where c is the concentration of the species (mol/m^3), D denotes the diffusion coefficient (m^2/s), R is a reaction rate ($R = 0$ in this case), and $\boldsymbol{u}$ is the velocity vector (m/s). Full-scale geometries of cage and rod constructs were generated, and a 0.2% scale model of the silicone scaffold generated (due to limitations in geometry complexity). The initial concentration (c) of dexamethasone in the surrounding 5 mL of water was set to 0 (mol/m^3). The dexamethasone concentrations for PDMS constructs of various drug loadings are displayed in **Table 3-1**. The diffusion coefficient for Dex in water and effective diffusivity for Dex in PDMS constructs are also shown in **Table 3-1**(Buchwald et al., 2010; Pedraza et al., 2013b). The effective diffusion coefficient (D_{eff}) reflects the

impact of diffusive path tortuosity through a porous medium, and the resultant drug mobility in the polymer matrix, on the diffusion coefficient (*D*)(Langer, R. S. et al., 1981). This is due to the existence of two phases: the amorphous polymer matrix, and the pores where the drug exists within the polymer(Malcolm, K. et al., 2003); D_{eff} was computationally determined for dexamethasone in PDMS by performing parametric sweeps for this parameter within COMSOL, and total sum of squares (TSS) was used to determine best fit of modeled release profiles to *in vitro* studies:

$$TSS = \sum_{i=1}^{n}(x_i - x_m)^2 \qquad \textbf{(Equation 3-2)}$$

where x_i and x_m represent the release values at a given time point for in vitro and modeled profiles, respectively. The models were run for a time period of 30 d with intervals of 1 h, and intermediate time-stepping.

Analytical methods have previously attempted to describe steroid release from matrix silicone systems, wherein drug release deviates from matrix-controlled diffusion behavior (burst release, followed by zero-order kinetics), by application of the matrix-boundary diffusion layer model, a continuation of the Higuchi kinetics theory(Roseman, 1972; Roseman et al., 1970). Further elaborations on the Higuchi method for drug delivery from silicone polymers have acknowledged a potential resistance to drug diffusion at the surface of the device(Paul, 2011). The “Thin Diffusion Barrier” boundary condition within COMSOL was applied to all geometries to model a thin layer by which mass is transported by diffusion only. This boundary condition permits for incorporation of the potential resistance to the drug diffusion and to simulate an impedance to solvent penetration at the surface of the hydrophobic material. This modifies the standard

diffusion model sufficiently to mimic experimental observations of steroid diffusion from silicone.

Parameter		Value	Units
Thin Diffusion Barrier		1.00×10^{-7}	m
Diffusion Coefficient of Dexamethasone	in H_2O	6.00×10^{-10}	m^2/sec
	in PDMS	$2.40 \times 10^{-15\dagger}$	m^2/sec
Dexamethasone Drug Loading (% w/v)	2.5% w/v	62.5	mol/m^3
	5% w/v	125	mol/m^3
	10% w/v	250	mol/m^3

Table 3-1 Parameters used in COMSOL FE models for Dex-PDMS construct optimization †computationally determined

3.2.4 IN VIVO STUDIES

All animal studies were reviewed and approved by the University of Miami Institutional Animal Care and Use Committee. All procedures were conducted according to the guidelines of the Committee on Care and Use of Laboratory Animals, Institute of Laboratory Animal Resources (National Research Council, Washington DC). Animals were housed in microisolated cages in Virus Antibody Free rooms with free access to autoclaved food and water at the Department of Veterinary Resources of the University of Miami. The Preclinical Cell Processing and Translational Models Core at the Diabetes Research Institute assisted with rodent islet isolations, diabetes induction, and animal maintenance.

3.2.5 RODENT ISLET TRANSPLANTS

For Dex-PDMS rod and scaffold transplants, male C57BL/6 mice, weighing between 20-25 g (Jackson Labs), were used as transplant recipients. Mice were rendered diabetic by single intravenous administration of the beta-cell toxin streptozotocin (STZ, 20 mg/kg; Sigma-Aldrich) and were used as recipients only if overtly diabetic upon three consecutive readings of non-fasting blood glucose levels > 350 mg/dL, using portable glucose meters (OneTouchUltra2, Lifescan). Donor islets were isolated from male C57BL/6 mice. Recipient mice were shaved, disinfected, and a 1 cm long midline incision made through abdominal skin and peritoneum under general anesthesia (2% isofluorane USP; Baxter). The islet transplantation performed as previously described(Brady et al., 2013). Briefly, the epididymal fat pad (EFP) was gently exposed and spread, and a silicone scaffold centered on the EFP prior to islet loading (600 Islet Equivalents [IEQ]) via Hamilton syringe. Two or four 10% Dex-PDMS rods (4 mm) were placed symmetrically around the scaffold. The scaffold and rod implant was wrapped using the EFP tissue and sealed using fibrin gel (fibrinogen (8 mg/mL), thrombin (2 U/mL), aprotinin (85 μg/mL), and $CaCl_2$ (5 mM)). Grafts were explanted 30 d post-transplant.

For Dex-PDMS scaffolds, the Balb/c mice strain was used for islet donors, resulting in an allogeneic transplant. Scaffold groups included: blank or 5% Dex-PDMS scaffolds. Implants were performed as outlined above, with the exception that two transplants of 600 IEQ / scaffold were used; one scaffold per EFP site, right and left. Recipients were immunosuppressed via daily intraperitoneal injection of FTY (1mg/kg, Novartis).

For Dex-PDMS cage studies, female Lewis rats (172-180 g, Harlan Lab) were rendered diabetic by two consecutive intravenous administrations of STZ (65 mg/kg) and prepped for surgery as stated above. Male Lewis rats (220-250 g, Harlan Lab) were used as islet donors, whereby islets were isolated as previously described(Pileggi et al., 2006). Four Dex-PDMS prototypes were tested: blank cages; 5% Dex-PDMS cages; 5% Dex-PDMS ½ cages (cages longitudinally sectioned into two ½ cages); or 10% Dex-PDMS cages. Islet-loaded scaffolds (1800 IEQ) were placed inside full cages or on top of ½ cages. Constructs were then placed onto the spread omentum. The omentum was wrapped around the construct and sealed with 30μL fibrin gel (as defined above, all rats were sacrificed at 30 d post-transplant).

3.2.6 HISTOLOGICAL ASSESSMENT

All explanted grafts were formalin fixed (10%, J.T. Baker), paraffin embedded, and sectioned. Slides were stained with Masson's Trichrome (Thermo Scientific) according to manufacturer's instructions, cover-slipped and sealed using Cytoseal mounting medium (Richard Scientific), and slides imaged on a Leica DMLB with a DFC 420C camera.

3.3 RESULTS AND DISCUSSION

3.3.1 INITIAL CHARACTERIZATION OF DIFFUSION CHARACTERISTICS IN DEX-PDMS DRUG-ELUTING CONSTRUCTS USING A SIMPLE GEOMETRY: DEX-PDMS ROD

For initial investigation of release rates of dexamethasone from Dex-PDMS construct at varied drug loadings, we utilized the simple cylindrical rod geometry (8 mm

height, 1.54 mm diameter). While dexamethasone has proven highly effective for the reduction of inflammation in a variety of applications(Muller et al., 1994; Patil, S. D. et al., 2007b), islet toxicity and impairment of insulin secretion has been observed for doses in excess of 1μM (Lambillotte et al., 1997; Zawalich et al., 2006); therefore, the most pivotal characteristic constraining design of a Dex-eluting construct in an islet transplant site is the targeted plateau release range. We hypothesize that a range of 0.1-2.0μg per day of local delivery would be sufficient to strike a balance between inflammation suppression and allowing healthy remodeling and tissue in-growth at the site. Ideally, this will result in a minimal fibrotic response (characterized by dense cell infiltration and deposition of extracellular matrix), while permitting sufficient tissue remodeling to allow for graft vascularization. (Zisch et al., 2003a)

Initial release studies of Dex-PDMS rods revealed that drug loadings of 5 and 10% (w/v) dexamethasone resulted in plateau drug levels of 0.3 and 0.5 μg per day, respectively (**Figure 3-2B**, solid lines). These plateau values were within our defined therapeutic range. Release curves demonstrate a characteristic initial burst release (0-5 d)(Huang et al., 2001), followed by a lower, semi-zero order kinetic release over the duration over the remaining testing period of 30 d. These curves are characteristic to those demonstrated for hydrophobic drugs doped within hydrophobic, biostable polymers, such as paclitaxel or sirolimus within polyisobutylene or polymethacrylate copolymers(Wu et al., 2006). This burst release has been theorized to be due to the ready solubilization of the mobile agent at the construct surface, followed by the slower diffusion of solute immobilized within the matrix(Huang et al., 2001).

Subsequently, we used the finite element modeling program COMSOL to model the release of dexamethasone from PDMS rods of the same dimensions (**Figure 3-2A**) and drug loadings, and thereby determine an effective diffusion coefficient (D_{eff}) for dexamethasone in PDMS. This coefficient of diffusion for dexamethasone within our PDMS substrate is 'effective,' as the diffusion is not occurring through a pure polymer (Malcolm, K. et al., 2003). The effective diffusion coefficient is an aggregate value, influenced by multiple parameters associated with the matrix and the drug, such as the interconnectivity and tortuosity of the pores within the polymer, the density of polymer within the matrix, diffusional characteristics of the drug itself, and the ability of the solvent to navigate between the hydrophobic polymer chains. Assessment of drug migration out of polymer matrices has been typically describe in terms of a 'jumping' diffusion mechanism, wherein the penetrating solvent moves between pockets via temporary channels, and the rate of diffusion varies due to the rate and distance of this jumping mechanism (Brandt, 1959; Frisch et al., 1983). Thus, the diffusion mechanism is largely governed by the molecular weight and dispersion of the drug, or distance between pockets, through the polymer (Malcolm, K. et al., 2003).

Best fit of the modeled release profiles to *in vitro* results was determined by total sum of squares (TSS) method on the plateau release region (after day 5), where TSS for modeled rods was optimal for 5% (0.08) and 10% (0.16) drug loadings at $D_{eff} = 2.4 \times 10^{-15}$ m^2/sec (**Figure 3-2B**, dashed lines). The effective diffusion coefficient determined via our approximation method was three orders of magnitude smaller than that previously reported via analytical determination methods(Malcolm, K. et al., 2003; Malcolm, R. K. et al., 2004) using similar silicone-steroid systems, and one order of magnitude smaller

than those reported for other dexamethasone-releasing silicone systems(Kim, J. et al., 2008; Kim, J. et al., 2010b). This slight discrepancy may be due to the complexity of our FEM system and conditions compared with 1-D analytical methods. Further, effective diffusivity is greatly weighted by the properties of the silicone elastomer used, as variations in fillers and degree of crosslinking results in high variations in the tortuosity of the diffusion pathway(Fu, Y. et al., 2010; Johansson, E. D. et al., 2004; Roseman, 1972; Snorradottir et al., 2011).

Color maps of rod construct sagittal section concentrations demonstrate spatial drug distribution within the rods over the course of release (**Figure 3-2C**, slice). For both 5 and 10% drug loadings, drug was released from the surface of the construct inward, and surface mapping of Dex-PDMS rod constructs over time reveal surface depletion of drug within the first day (**Figure 3-2C**, surface).

3.3.2 DRUG-RELEASE MODELING AND PREDICTION IN A COMPLEX DEX-PDMS GEOMETRY: DEX-PDMS CAGE

Using the effective diffusion coefficient determined in our Dex-PDMS rod construct study, we sought to evaluate the robustness of our model by applying a more complicated geometry. Given that the desired spatial distribution of the localized drug delivery is uniform, three-dimensional distribution, concentrated on the periphery of the implant, we designed and developed a cage-like construct within which our islet-loaded silicone scaffolds may be inserted prior to transplantation (**Figure 3-1 & Figure 3-3A**).

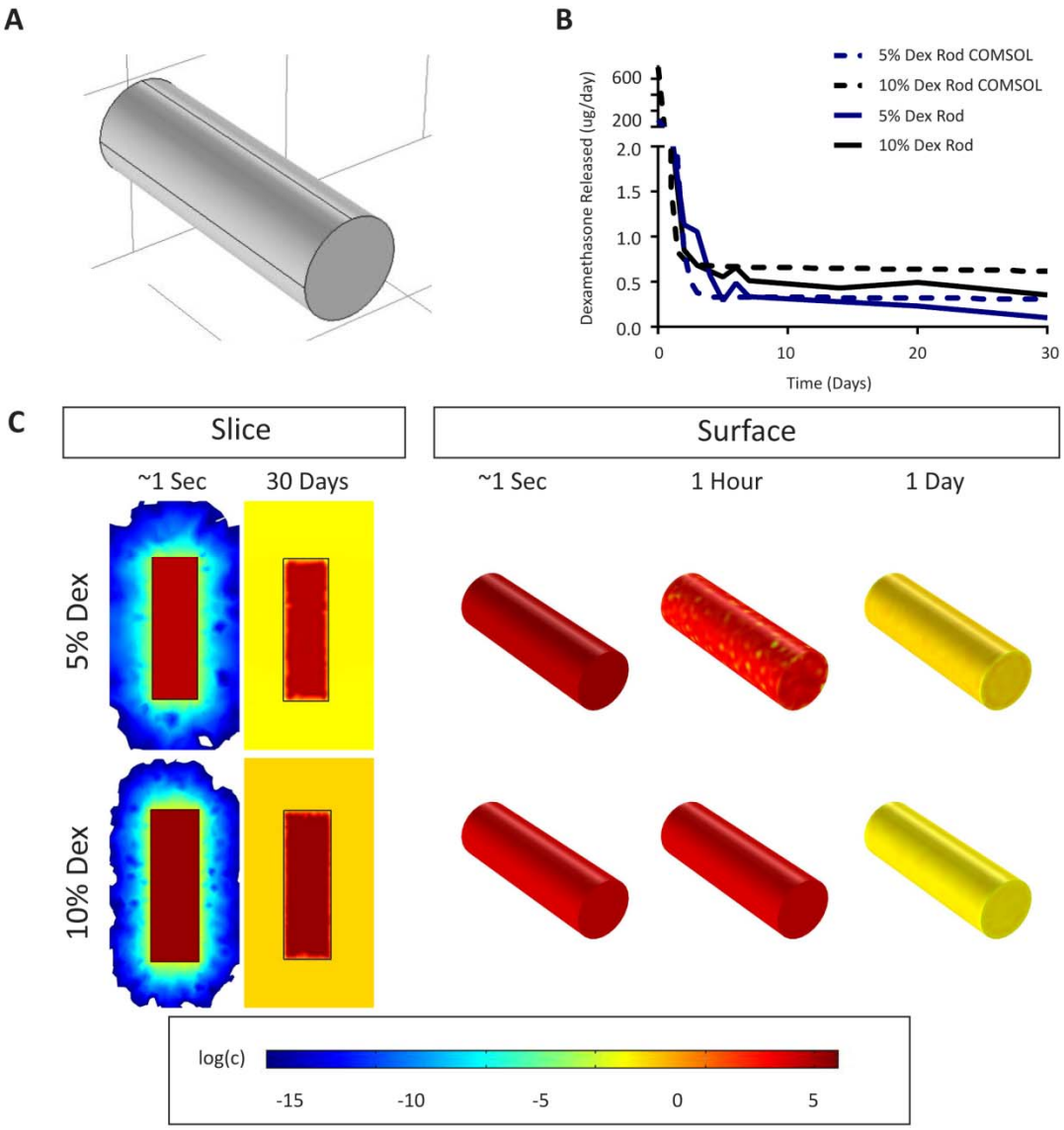

Figure 3-2 Dex-PDMS rod (A) release profiles measured (solid lines) and predicted via COMSOL model (dashed lines) (B) from 5 or 10% w/v rod constructs. Longitudinal slices (C, left) and surface maps (C, right) at specified time points illustrate predicted spatial distribution of Dexamethasone in constructs over time.

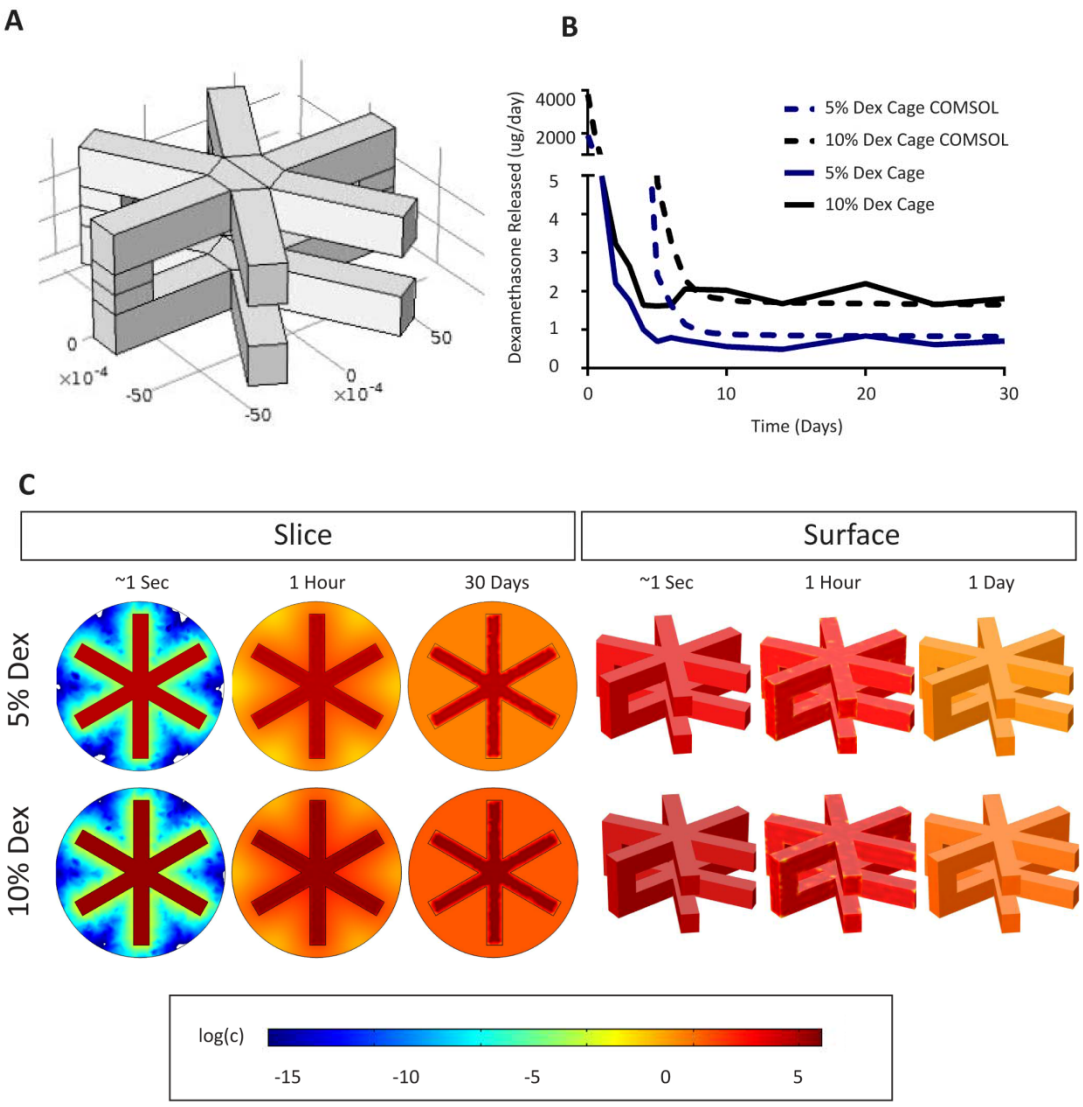

Figure 3-3 Dex-PDMS cages (A) release profiles measured (solid lines) and predicted via COMSOL model (dashed lines) (B) from 5 or 10% w/v cage constructs. Longitudinal slices (C, left) and surface maps (C, right) at specified time points illustrate predicted spatial distribution of Dexamethasone in constructs over time**.**

Application of our previously determined effective diffusivity to this more complicated geometry revealed COMSOL-generated release profiles consistent with in vitro release studies (**Figure 3-3B**) for both 5 (TSS = 1.19) and 10% (3.11) drug loadings. Transverse slices through the cage construct illustrate prediction of gradual

depletion of drug from the construct surface, with slow inward erosion of drug concentration over time (**Figure 3-3C**, Slice). Additionally, surface maps demonstrate temporal reduction in drug concentration similar to the rod geometry, with near total surface depletion after 1 day regardless of drug loading (**Figure 3-3C**, Surface).

3.3.3 DRUG-RELEASE MODELING AND PREDICTION IN A HIGH-SURFACE AREA, COMPLEX GEOMETRY: DEX-PDMS SCAFFOLD

With the establishment of an approximate value for dexamethasone effective diffusivity, and accurate prediction of release profiles for both rod and cage constructs, we sought to investigate whether the model could be accurately applied to a highly complex geometry with high surface area. The macroporous scaffold was originally designed to contain 90% open space, with pore size optimized (250-425 μm) for islet dispersion within the three dimensional matrix. (Pedraza et al., 2013a; Pedraza et al., 2013b) This void space allows for graft vascularization and tissue in-growth. Due to limitations in memory allotted to geometry construction, a 0.2% scale piece of scaffold was modeled in COMSOL (**Figure 3-4A**). As shown **Figure 3-4B**, the predicted release kinetics were remarkably consistent with in vitro release data for both 2.5 (TSS = 1.63) and 5% (13.46) drug loadings. The TSS value for the 5% scaffold is largest of all the predicted release curves at 13.46. This may be due to multiple factors, including the estimation of the complex and unpredictable scaffold geometry surface area, and the necessary scaling up to a full-size model (scale factor of 500), which inevitably inflates inherent error.

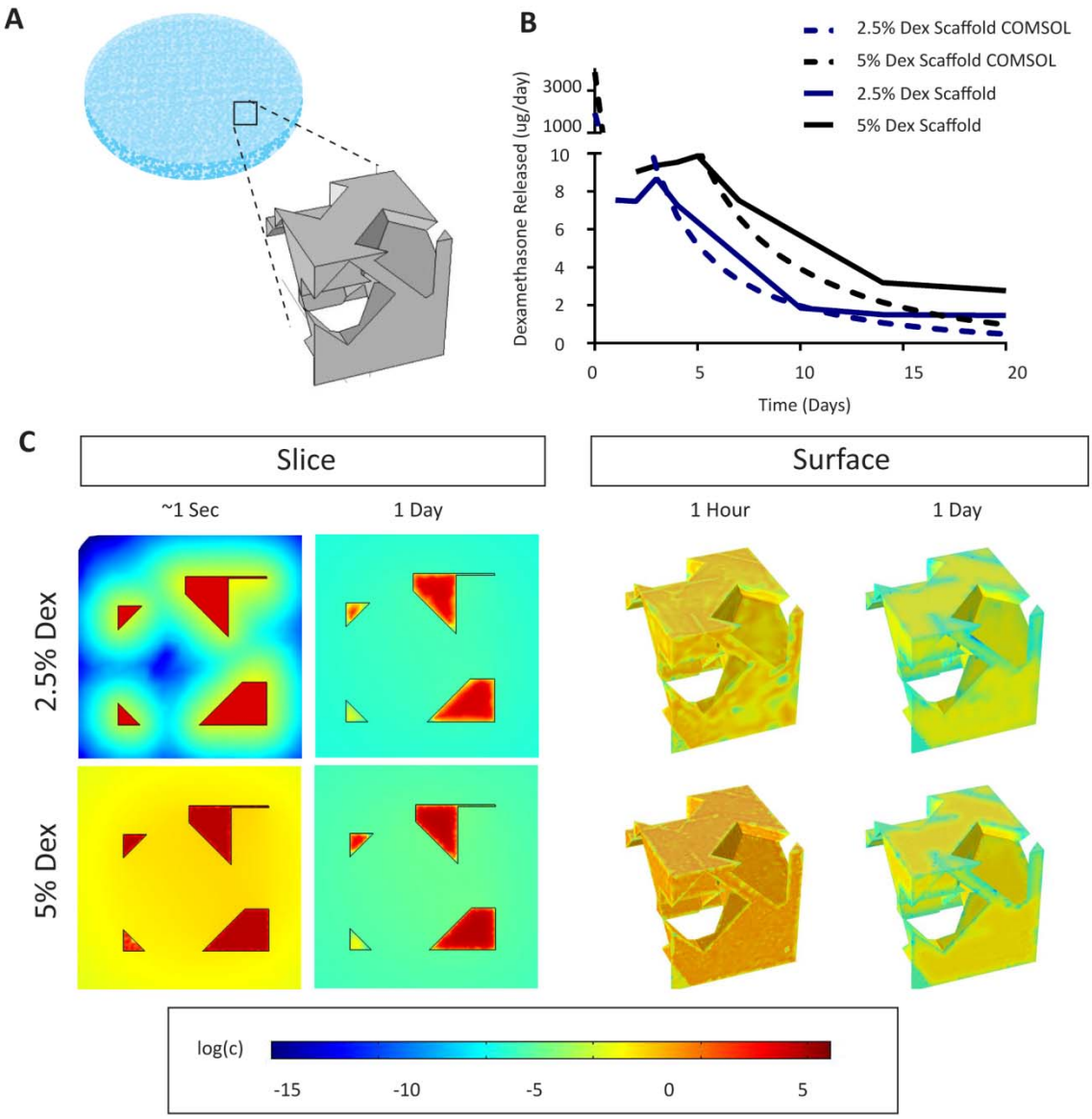

Figure 3-4 Dex-PDMS scaffold (A) release profiles measured (solid lines) and predicted via COMSOL model (dashed lines) (B) from 5 or 2.5% w/v scaffold constructs. Longitudinal slices (C, left) and surface maps (C, right) at specified time points illustrate predicted spatial distribution of Dexamethasone in constructs over time.

Slices of Dex-PDMS scaffolds at both 2.5 and 5% drug loadings demonstrate a rapid depletion of internal drug reserves, particularly in comparison to the rod and cage (**Figure 3-4C, Slice**). This was further evidenced by rapid exhaustion of surface

dexamethasone within one hour (**Figure 3-4C, Surface)**, compared to one day for the other two geometries. This behavior is likely due to the 10-fold higher surface area–to–volume ratio(Reynolds et al., 2002) of the scaffold geometry ($4.02x10^4$ m^{-1}) compared to the rod ($1.83x10^3$ m^{-1}) and cage ($2.13x10^3$ m^{-1}), resulting in a larger proportion of Dex-PDMS being directly exposed to the surrounding solvent.

3.3.4 EVALUATION OF DEX-PDMS CONSTRUCT GEOMETRY IMPACT ON ISLET TRANSPLANT ENGRAFTMENT AND REMODELING

With the previous studies, we established consistent and predictable release profiles from Dex-PDMS constructs *in vitro*. We next sought to determine the impact of construct loading and geometry on localized remodeling in an islet transplant graft. We hypothesized that increasing the surface area of construct, and therefore the overall drug release, will result in a greater impedance of tissue in-growth and local remodeling. Additionally, we hypothesized that locus of delivery, either internal (scaffold) or external (rod and cage), would result in variations in spatial remodeling within the graft.

Rod Dex-PDMS constructs were evaluated in a murine syngeneic transplant model, whereby islets, loaded within macroporous scaffolds, were transplanted within the epididymal fat pad (EFP) site(Brady et al., 2013). Dex-PDMS rods transplants (4 mm) were placed peripherally to the scaffold (**Figure 3-1**). Three groups were investigated: two PDMS-only rods (control); two 10% (w/v) Dex-PDMS rods; and four 10% (w/v) Dex-PDMS rods. Daily dexamethasone release from a 10% Dex-PDMS rod plateaus at approximately 0.75 µg per day (8 mm rods), indicating that the four 4-mm Dex-PDMS rod group would receive a maximal exposure of 1.5 µg per day, although the true

physiological concentration of the local drug is dependent on multiple, unpredictable parameters, such as physiological clearance and local vascularization. Islet graft function for diabetic recipients was assessed via nonfasting blood glucose values, whereby two consecutive measurements < 200 mg/dL indicated diabetes reversal. As outlined in greater detail in **Chapter 4**, blood glucose values and transplant efficacy were not statistically disparate between implants containing Dex-PDMS rods and control animals. Histological evaluation of explanted grafts was performed 96 d post-transplant. Masson's trichrome staining was used to observe cell infiltration and extracellular matrix deposition within the grafts (**Figure 3-5**). Islets were visualized in all grafts as dense clusters of spheroidal cells. While cellular infiltration and extracellular matrix (ECM) deposition were observed in all groups, migration patterns and ECM deposition appears less uniform for the four Dex-PDMS rod group, whereby cellular infiltration and ECM deposition proximal to the rod location was mitigated (**Figure 3-5, left column**). This suggests an impact of local dexamethasone concentrations on graft remodeling, which appears nonuniform with sections closest to the dexamethasone-eluting material exhibiting the greatest effect. The uniformity of drug diffusion throughout the implant was likely limited by varying factors such as fluid flow due to site vascularization, the hydrophobicity of the drug, and its resulting limited solubility. Additionally, overall dense collagen deposition was less observable in Dex-PDMS rod groups compared to controls (**Figure 3-5, right column**), indicating correlation between local dexamethasone delivery and dense ECM deposition.

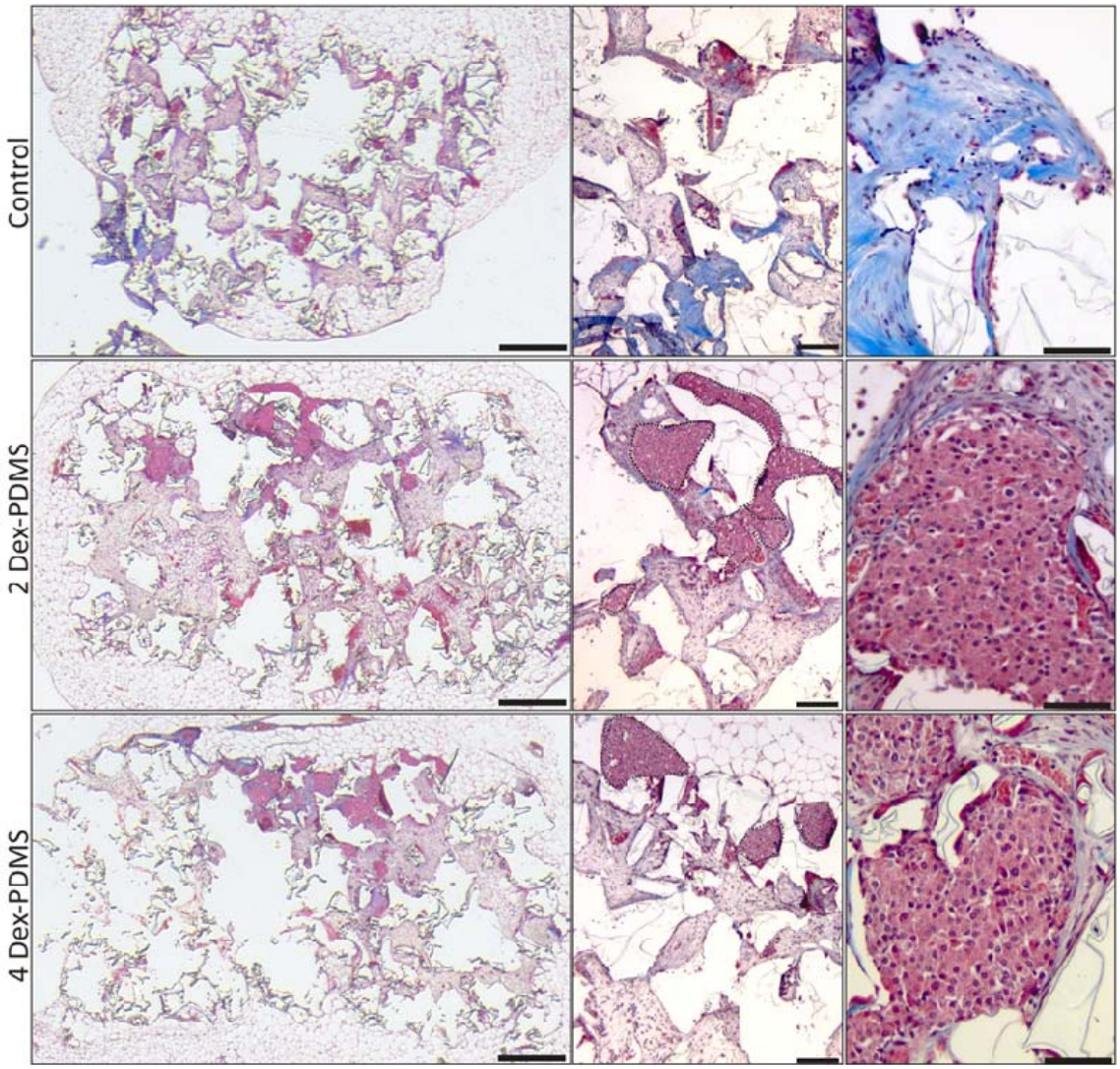

Figure 3-5 Masson's Trichrome Staining of implants containing syngeneic islet-loaded silicone scaffolds transplanted with 2 or 4 10% Dex-PDMS rods (4 mm) or 2 blank PDMS rods (4mm) (Control). Low (left column), moderate (middle column), and high (right column) magnification images illustrate infiltrating cells (cytoplasm = red, nuclei = purple) and collagen (blue). Scale bars: left column=0.5 mm; middle column = 100 μm; and right column = 50 μm

Following establishment of the effects of local dexamethasone release from simple rod geometry, we sought to evaluate the Dex-PDMS cage geometry, which was designed specifically for peripheral drug delivery in a rat model. We hypothesized that diffusion limitations within the graft, which were observed in the mouse rod model,

would limit the bulk of drug exposure to the periphery of the scaffold. The use of a rat model was due to the scale of the cage, which could not be easily minimized, using our available resources, for implantation in the mouse model. In this model, transplantation into the rat omentum was a more appropriate transplant site. For these transplants, a macroporous silicone scaffold, seeded with 1800 IEQ, was inserted into the PDMS cages, and wrapped in the omentum (**Figure 3-1**). Three groups were investigated: scaffold only (control); a single 10% (w/v) Dex-PDMS cage; a single 5% (w/v) Dex-PDMS cage; and a half 5% (w/v) Dex-PDMS cage. For half cages, the cage was sectioned longitudinally and the scaffold was placed onto the cage. These groups permit evaluation of drug dosage on remodeling and engraftment, as well as the effects of spatial release (half cage). Release studies indicate that the 5% Dex-PDMS cage releases well within our targeted therapeutic range (maximum 1 μg / day), and the 10% Dex-PDMS cage releases at the upper limit (maximum 2 μg / day).

Islet graft function for rat diabetic recipients was assessed via nonfasting blood glucose values, whereby two consecutive measurements < 200 mg/dL indicated diabetes reversal. Blood glucose values and transplant efficacy were statistically disparate between implants containing Dex-PDMS rods and control animals. All grafts containing Dex-PDMS cages (n=2 per group) remained diabetic, while controls stabilized to normoglycemia after 2 d post-transplant.

Histological evaluation of explanted grafts was performed 30 d post-transplant via Masson's Trichrome staining (**Figure 3-6**). Although these grafts were implanted for a fraction of the time of the rod model, cellular infiltration and ECM deposition appears more robust, with significantly more pronounced remodeling within the control scaffold.

Visualization of transverse sections revealed dense concentrations of collagenous matrix visible throughout the control scaffold, in addition to a uniform distribution of infiltrating cells. The half 5% cage group demonstrates limited remodeling on the side proximal to the Dex-PDMS; conversely, scaffold sections distal to the cage exhibited remodeling similar to that of drug-free controls, with an apparent gradient of tissue in-growth between. The 5% Dex-PDMS cage group exhibits a significant reduction in tissue in-growth in the central portion of the scaffold, with a gradual increase in visible tissue in-growth radially out towards the scaffold periphery. The 10% Dex-PDMS cage group demonstrates a marked decrease in visible remodeling throughout the graft, with minimal collagenous deposition at the periphery of the scaffold.

The evident spatially-limited remodeling in the half 5% Dex-PDMS cage group demonstrates the diffusion limitations of dexamethasone within the graft, and the importance of graft proximity to the Dex-PDMS. At 5% dexamethasone loading for a half cage, total daily flux was approximately 0.5 μg per day, well within our targeted therapeutic range; however, diffusion within the graft appears limited to half-way (or 0.5 mm) through the graft. In the 5% Dex-PDMS cage group, the pattern of tissue in-growth reduction in the inward radial direction could be attributed to the higher amount of surface area at the center of the cage's star-like structure. This larger surface area can result in a higher local drug delivery, leading to the central region receiving the highest drug exposure. In the 10% Dex-PDMS cage group, remodeling at the graft site appears to be nearly completely inhibited by the localized drug release. This outcome suggests that release from this construct, which reaches the upper limit of our targeted therapeutic

range at 2 µg per day, exceeds the dosage by which positive host remodeling was unimpaired.

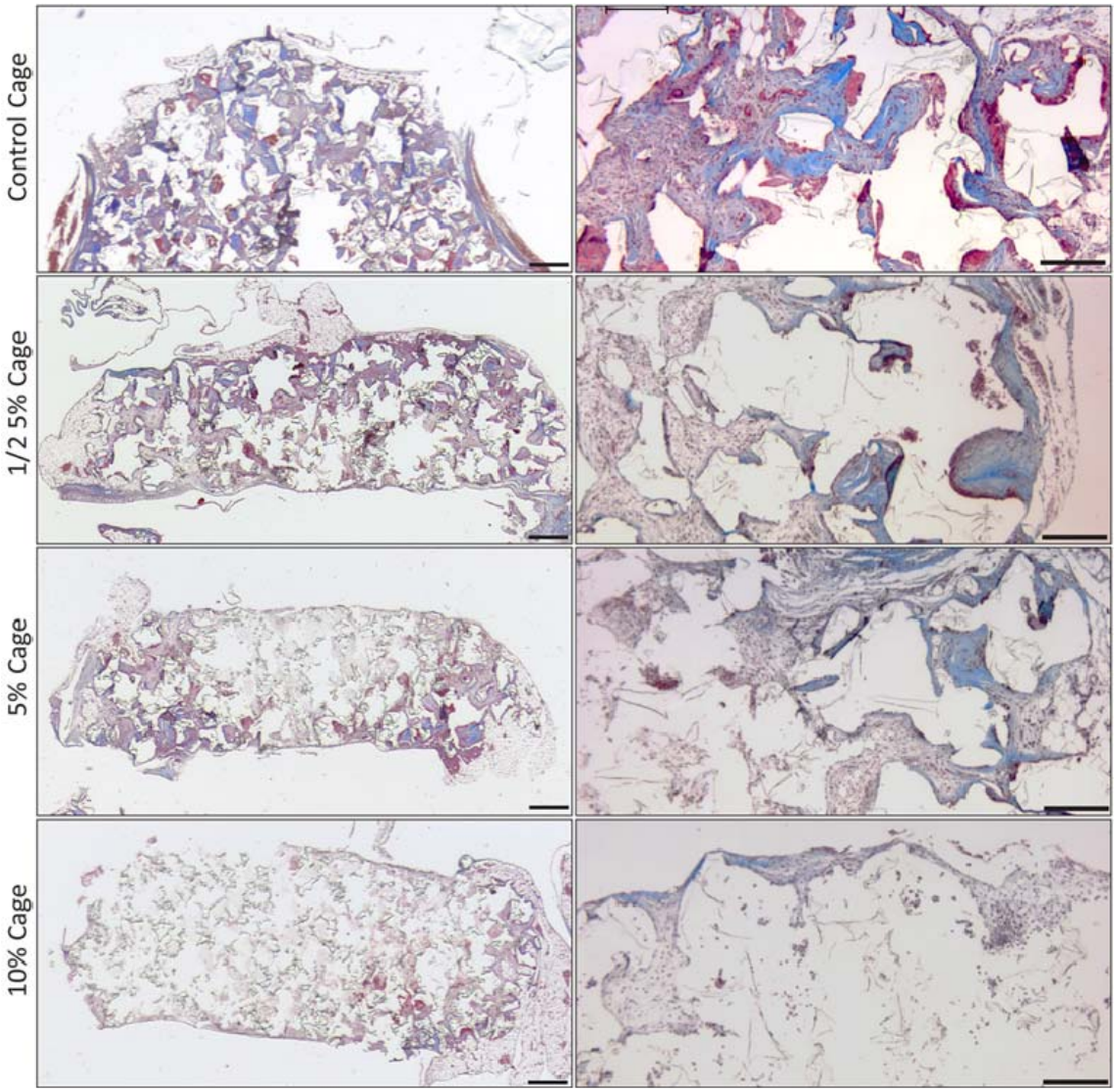

Figure 3-6 Masson's Trichrome staining of implants containing syngeneic islet-loaded silicone scaffolds transplanted without or with a full 10%, full 5 %, or half 5 % w/v Dex-PDMS cage. Low (left column) and high (right column) magnification images illustrate infiltrating cells (cytoplasm = red, nuclei = purple) and collagen (blue). Scale bars: left column =0.5 mm; right column = 200 µm

To investigate the impact of internal anti-inflammatory delivery on an allogeneic transplant model, we evaluated the effect of Dex-PDMS scaffolds on function and graft remodeling in a murine model. Allogeneic transplants in immunocompetent animals results in a robust immune response, typically necessitating a larger number of IEQ to reproducibly achieve function (1200 vs. 600 IEQ)(Pedraza et al., 2013a). We hypothesized that an allogeneic transplant would likely result in a more vigorous early host response to the graft, and that the higher initial release observed in the Dex-PDMS scaffold could serve to counteract this response. Two groups were screened: PDMS-only (control) or 5% w/v Dex-loaded PDMS scaffolds. Scaffolds were loaded with islets and placed within the EFP of STZ-induced diabetic male C57BL/6 mice, similar in method to the Dex-PDMS rod transplants. Graft rejection was mitigated via delivery of FTY720 (1 mg/kg/day) (Chiba et al., 2005; Habicht et al., 2006; Ueda et al., 2005). The initial 5-day burst release was removed from 5% Dex-PDMS scaffolds prior to implantation via washes. Release studies indicate a drop in local delivery from 6 to 3 μg per day from day 5 to 15 of release, corresponding to days 1 through 10 post-transplantation; delivery from day 20 post-transplant onward drops to within our targeted release range. Monitoring of nonfasting blood glucose revealed a significant impact of the local dexamethasone release on islet function. All of the Dex-PDMS scaffold implants (n=2) exhibited primary nonfunction, with minimal decrease in blood glucose levels, while controls exhibited normoglycemia 24 h post-transplant.

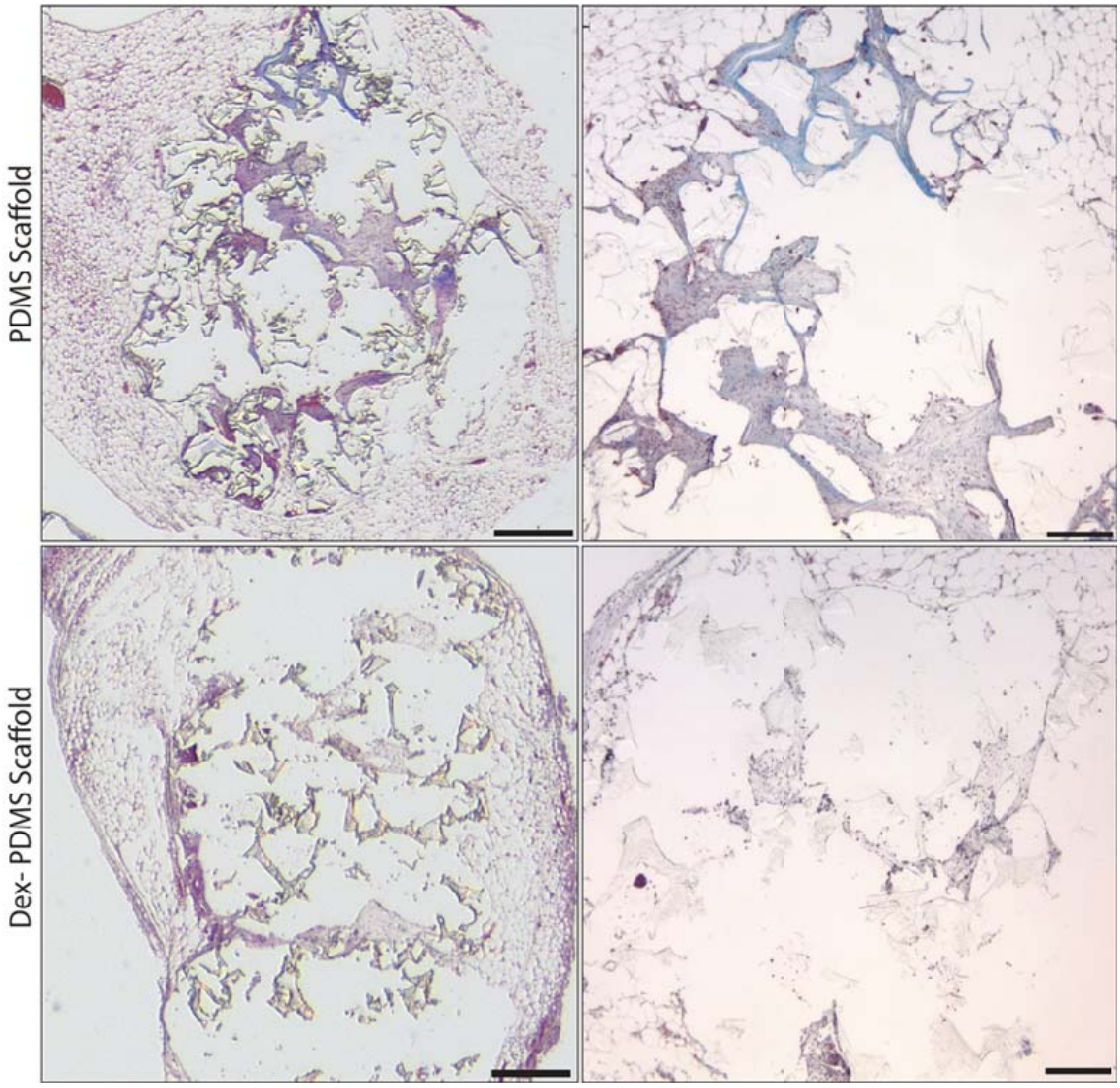

Figure 3-7 Masson's Trichrome staining of implants containing allogeneic islet-loaded PDMS or 5% w/v Dex-PDMS scaffolds. Low (left column) and high (right column) magnification images illustrate infiltrating cells (cytoplasm = red, nuclei = purple) and collagen (blue). Scale bars: left column=0.5 mm; right column = 200 μm

Histological evaluation of explanted grafts was performed 42 d post-transplant via Masson's Trichrome staining (**Figure 3-7**). The control scaffold performed similarly to the syngeneic murine islet transplant control above, with moderate noticeable collagen deposition and cell infiltration. Dex-PDMS grafts indicate that the release of

dexamethasone from the PDMS scaffold results in a dramatic impact on local remodeling (**Figure 3-7**). Cellular infiltration and ECM deposition was extremely limited to sparse sections at the periphery of the scaffold implant. This pronounced effect on remodeling in the Dex-PDMS scaffold group was likely due to a combination of potent local delivery, resulting from the high surface area for release, and the spatial proximity of Dex-PDMS to the infiltrating tissue.

The histological evaluation of implants from all three construct geometries indicates an evident relationship between reduction in remodeling and graft proximity to the Dex-eluting construct. Additionally, a consistent reduction of overall collagen deposition and cell infiltration in all three Dex-PDMS geometries was observed, indicating the capacity for limited diffusion of the hydrophobic drug throughout the graft, as clearly evidenced by tissue gradients in the Dex-PDMS cage experiment. Thus, the external dexamethasone delivery methods (rod and cage) have the advantage of limited islet proximity to Dex-PDMS construct (**Figure 3-8A**), with highest dexamethasone exposure at the periphery of the scaffold. The diffusion of dexamethasone through the graft was spatially limited, with internal dose dependent on construct loading, as demonstrated in the rod and cage spatial diffusion gradients illustrated in **Figure 3-8**, which correlate with observed *in vivo* engraftment results. By contrast, the Dex-PDMS scaffold provides internal delivery, wherein every surface within the transplanted graft elutes drug, resulting extensive coverage of dexamethasone throughout the scaffold. This was evidenced by internal diffusion gradients depicted in **Figure 3-8**, where drug distribution in scaffold pores appears nearly uniform. This leads to negligible remodeling and tissue in-growth, and prevents positive graft integration, a noted response observed in

local delivery of dexamethasone (Pires et al., 2005). For the application of islet transplantation, whereby islet engraftment and vascularization is critical to a successful implant, the uniform delivery of this dosage of dexamethasone is detrimental.

The application of the apparent diffusion coefficient to all three geometries resulted in an accurate shift in release curves when compared with in vitro release studies. As total drug flux from the construct was clearly dependent on available surface area, change in construct surface area should result in a predictable shift in release curves. The rod geometry (7.38×10^{-5} m^2) has 11.5% of the surface area of the cage (6.44×10^{-4} m^2); however, the rod geometry release profile plateaus at approximately one third that of the cage (scaffold geometry was incomparable due to non-zero-order release kinetics), indicating that plateau range does not linearly correlate with construct surface area.

This observed behavior was likely due to varied construct geometry, wherein the cage and scaffold possess internal void space, which accumulates drug faster than external construct surfaces that were exposed to a larger void space. The drug accumulation in void spaces results in a faster reduction in driving forces for diffusion (i.e. the concentration gradient) at internally-oriented surfaces. This would limit diffusion from internal surfaces, as reflected in the COMSOL-generated release profiles: the rod geometry possesses external surfaces only, and exhibits a characteristic burst followed by sustained release; the cage possesses a large internal void space with a high potential for exchange with external void space, resulting in a release profile comparable to that of the rod, with a slightly longer burst release and more gradual plateau; and the scaffold possesses a high surface area geometry containing many small void spaces with minimal

potential for passive exchange with the external void, resulting in high release rate with a rapid decline over 20 days.

.

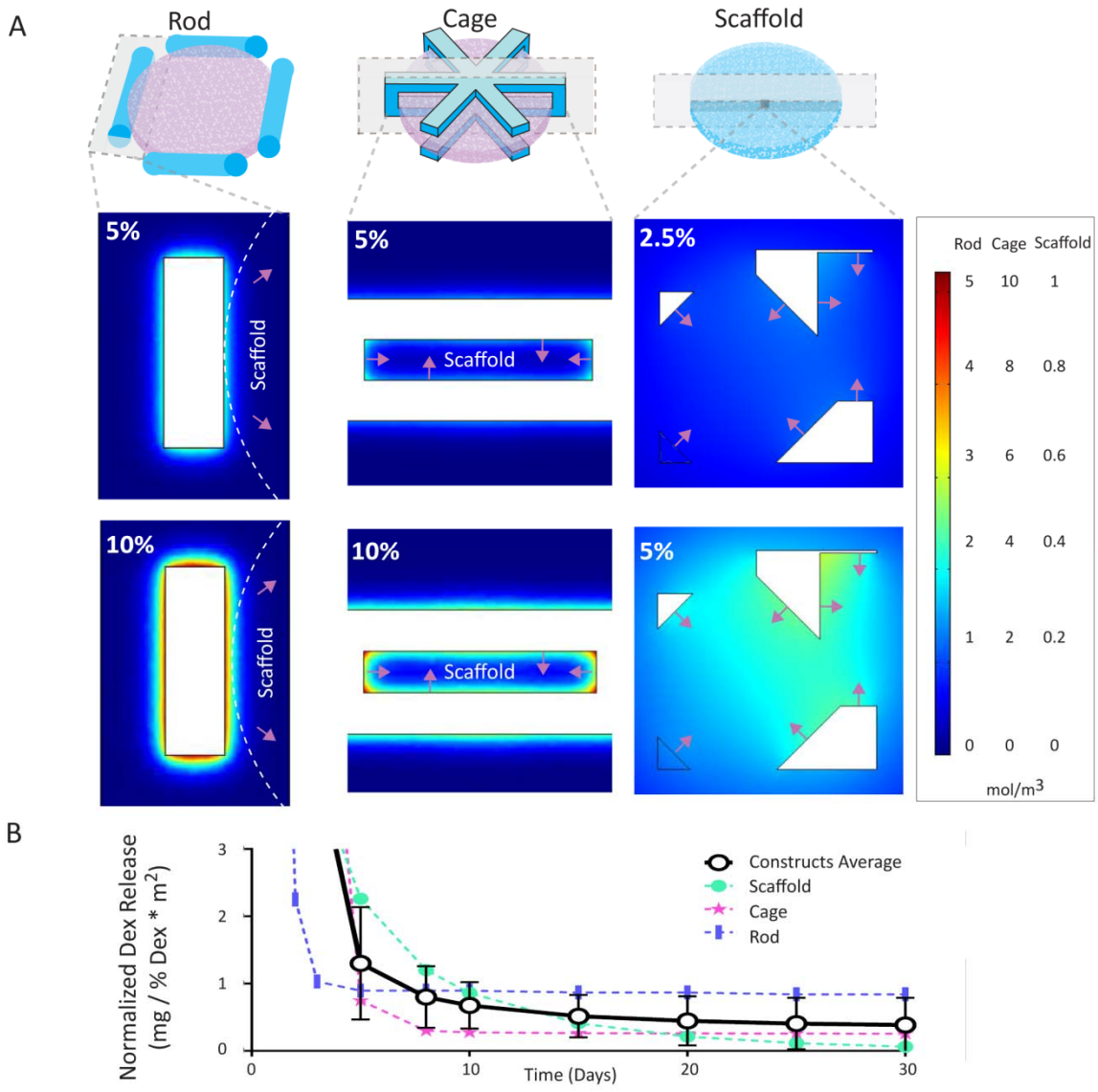

Figure 3-8 Spatial release characteristics of varying geometries demonstrate spatial gradients of dexamethasone throughout construct (A). Planar sections within defined locations of the Dex-PDMS/cell-scaffold implants were modeled via COMSOL. Dexamethasone release, normalized to percent drug loading and surface area (B), for scaffold, cage, and rod geometries, as well as average value for all 3 constructs. Error bars represent standard deviation.

Despite the potential impedance of internal void space, the three geometries resulted in similar temporal release profiles. To assess whether dexamethasone delivery via a PDMS platform exhibits consistent behavior when surface area and drug loading were accounted, COMSOL-generated release profiles were normalized by their total construct surface area and drug loading. Normalized dexamethasone release profiles for the scaffold (green), cage (red) and rod (blue) geometries, as well as the average of the three constructs, were plotted (**Figure 3-8B)**. The average normalized profile (black) indicates controlled, sustained release, with an initial burst release complete within the first 5 days. This relationship demonstrates the capacity for facile optimization of a localized Dex-PDMS construct of any geometry, wherein simple variation of surface area and drug loading enable design to meet any targeted dose

3.4 CONCLUSIONS

Within this study, we investigated three Dex-PDMS prototypes of variable geometry for local suppression of inflammation in an islet transplant site. Three-dimensional finite element modeling enabled the approximation of dexamethasone effective diffusivity in silicone, with subsequent prediction of temporal and spatial drug release profiles *in vitro*. The use of dexamethasone proved to be highly effective as a model drug for combating local inflammation *in vivo*, where prototypes could be easily adapted and release profiles tailored for a variety of applications. The potential for dexamethasone to negatively impact islet engraftment, however, prevents the ease of use of this anti-inflammatory agent without careful and extensive predictive analysis to ensure low local levels of the agent. Exploration into alternative drugs, which exhibit

minimal effects on islet engraftment, for use within this platform is the focus of future studies in the local modulation of inflammation in an islet transplant site.

Chapter 4. Local, Controlled Release of Glucocorticoids from Organosilicone Constructs for Modulation of Inflammation in Islet Transplantation

4.1 INTRODUCTORY REMARKS

Inflammation during cellular transplantation can lead to significant cell loss and dysfunction. Inflammation is a particular challenge for islet transplantation, whereby islets transplanted in the absence of immunological rejection (e.g. syngeneic transplants) have demonstrated substantial cell loss associated with elevation of generalized inflammatory processes (Barshes et al., 2005; Korsgren et al., 2009; Wilson et al., 2008a). The intra-portal hepatic transplantation site is strongly associated with elevated inflammation, whereby islets in direct contact with blood instigate the instant blood-mediated inflammatory reaction (IBMIR) (Berman et al., 2007). IBMIR results in activation of coagulation and complement cascades, as well as the infiltration of leukocytes(Bennet et al., 2000), resulting in a highly unfavorable transplant microenvironment.(McDaniel et al., 1996) In an effort to mitigate islet loss associated with the hepatic transplant site, we and others have explored the omentum as an alternative location (Berman et al., 2009; Kenyon, N. et al., 2010; Kenyon, NS et al., 2011; Kim, H. I. et al., 2010a; Pedraza et al., 2013a; Salvay et al., 2008). In one approach, a macroporous organosilicone (polydimethylsiloxane, PDMS) scaffold was implemented within this alternative site to generate a three-dimensional islet microenvironment.(Pedraza et al., 2013a; Pedraza et al., 2013b). While this technique presents many advantages over the intra-hepatic method of islet delivery, inflammation still remains a prominent challenge to islet graft survival.

The implantation of cells in conjunction with a biomaterial invariably elicits an inflammatory response due to tissue injury and a generalized foreign body response (FBR). The initial acute phase is characterized by infiltration of neutrophils and monocytes, which release factors meant to degrade and facilitate phagocytosis foreign material (Nilsson et al., 2007; Onuki et al., 2008; Ward et al., 2002). Chemoattractants released by these cells recruit macrophages, signaling the chronic inflammatory phase. When aggravated macrophages are unsuccessful in removal of the foreign material, they cluster into foreign body giant cells (FBGC) and recruit fibroblasts, resulting in fibrotic encapsulation of the implant in thick layers of FBGCs and fibroblasts(Ratner et al., 2004). Generalized inflammation and FBR are highly detrimental to the transplanted cells, as exposure to cytokines and free radicals secreted by activated immune cells results in apoptosis, while hypoxia induced by fibrotic encapsulation promptly leads to necrosis (Walker et al., 1988). Supplementation of islet grafts with anti-inflammatory agents for the duration of this inflammatory period may improve cell survival via mitigation of these inflammatory processes.

Systemic delivery of potent anti-inflammatory drugs has the potential for adverse side effects in the host, while also requiring high dosing levels and cost (Qi, D. et al., 2007). Alternatively, local delivery of immunomodulatory agents at the transplant site has several advantages, including reduced overall dosage and systemic side effects, as well as the potential to utilize drugs that are not amenable to systemic delivery. There are a number of studies supporting the feasibility of local supplementation with therapeutic agents such as glucocorticoids (Freise et al., 1991; Ozcay et al., 1997; Ruers et al., 1986; Ruers et al., 1988; Weber, T. et al., 1997) for delaying cell or tissue allograft rejection.

Preliminary studies exploring the injection of anti-inflammatory agents (e.g. dexamethasone phosphate and loteprednol etabonate) within the islet transplant site have observed prolonged islet graft survival using doses a hundred-fold smaller than those typically used in systemic treatments (Bocca et al., 2010; Bocca et al., 2008; Buchwald, 2008). Local injections, however, typically face complications of aqueous solubility arising from drug stability and hydrophobicity, requiring potentially toxic co-solvents (e.g. ethylene glycol, dimethylsulfoxide, and ethanol) (Allen et al., 2004). Further, the labor intensive nature of daily injections likely decreases their translation. These challenges motivated the exploration of options for delivering agents in a controlled, temporal manner via biomaterials.

Implantable sustained or controlled release systems of various polymer matrices have existed for decades and have shown strong promise in both the local and systemic delivery of agents therapeutically, with a wide variety of agents (Langer, R., 1983). Of particular interest to us is the application of these sustained-release systems to hydrophobic or poorly soluble drugs, the feasibility of which is well-supported by the existence of several FDA approved drug-eluting biomaterial implants (e.g. steroid-releasing rings, such as Estring® and Nuvaring®; subdermal contraceptive implants, such as Norplant®, Jadelle®, Implanon)(Croxatto, 2002; Sivin et al., 2002). Of note is that many implants are based on cross-linked silicone devices, leading to ease in translation to our PDMS-based scaffold platform (Malcolm, K. et al., 2003). Numerous hydrophobic agents (steroids, NSAIDs, antibiotics, and proteins) have been incorporated into silicones to achieve modulated release rates (Fu, J. C. et al., 1973; Kajihara et al., 2001; Kim, J. et al., 2008; Maeda et al., 2004; Malcolm, R. K. et al., 2004; Schultz et al.,

2010; Snorradottir et al., 2011; Xu et al., 2011), and the biostability and non-adhesive nature of PDMS-based materials enable facile, minimally invasive replacement when materials expire. PDMS is also ideal in that it is easily fabricated into a variety of geometries, enabling the design of drug delivering constructs optimized to fit the transplant site.

Dexamethasone (Dex) is a potent hydrophobic corticosteroid that is well suited for incorporation into hydrophobic polymers (Buchwald, 2008; Buchwald et al., 2010; Muller et al., 1994; Song et al., 2011); their relatively low molecular weight to volume ratio results in high solubility in silicone (Malcolm, K. et al., 2003). Part of dexamethasone's potent anti-inflammatory action is derived from reduction of leukocyte recruitment to the site of inflammation through modulation of surface adhesion molecules, such as ICAM-1 (CD54), and co-stimulatory molecule expression, such as CD86. (Cronstein et al., 1992; Goulding, 2004; Greenwald et al., 2005; Tuckermann et al., 2005; Vital et al., 2003) While local delivery of glucocorticoids alleviates many issues with systemic drug effects, the potential for islet exposure to high corticosteroid concentrations at the transplant site must be considered. Previous studies have demonstrated that dexamethasone concentrations in excess of 1 μM have the capacity to inhibit insulin secretion in rat islets (Lambillotte et al., 1997; Zawalich et al., 2006). Therefore, Dex-PDMS construct design would ideally consider an appropriate therapeutic delivery range, as well as aim to deliver the drug at the periphery of the scaffold, in an effort to prevent inflammatory cell activation prior to migration into the site, and limit islet exposure to the drug within the scaffold.

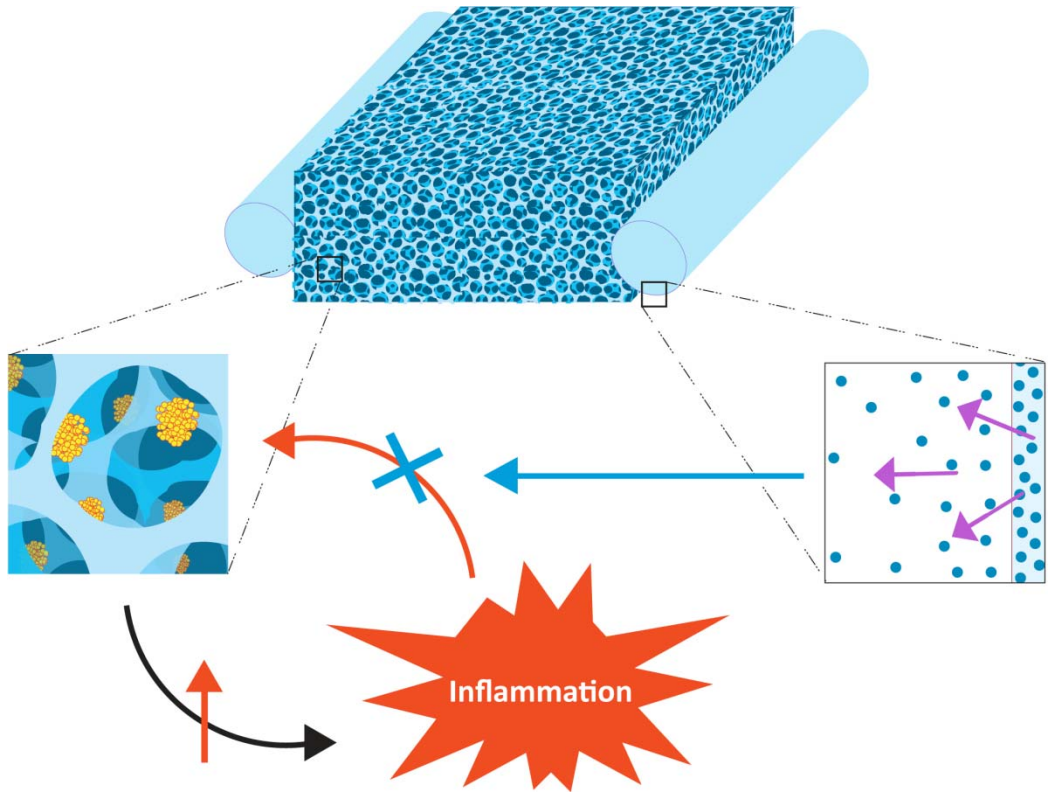

Figure 4-1 Illustration demonstrating Dex-PDMS construct method of action. Dex-PDMS rods positioned around a silicone scaffold housing islets; drug release from PDMS constructs aims to combat the localized inflammation at the transplant site caused by implantation of scaffold and cells.

We describe herein the development and evaluation of a Dex-eluting PDMS construct designed to reduce inflammation in an islet transplant site (**Figure 4-1**). Via correlation of dexamethasone release rate from PDMS polymer to construct surface area and drug loading, we explored the tailoring of drug release profiles to target the therapeutic dose. Following optimization in vitro, the effects of Dex-PDMS constructs on the functional efficacy of islet transplant grafts, as well as modulation of the local inflammatory response, was evaluated.

4.2 MATERIALS AND METHODS

4.2.1 DEX-PDMS CONSTRUCT FABRICATION

PDMS constructs were formed by mixing PDMS monomer with platinum catalyst per manufacturer's instructions (RTV 615 A&B, GE Silicones) at a ratio of 4:1 prior to mixing evenly with Dexamethasone (Dex, Alexis Biochemicals) at 5 or 10% w/v. PDMS and Dex-PDMS mixtures were cured at 60 ºC for 24 h in either a petri dish (1mm height, disks) or Tygon tubing (1.54mm ID, rods, Saint-Gobain). Disks were fabricated by stamping from the Dex-PDMS slab (5.6mm diameter) and Dex-PDMS rods were cut to size after extraction from the Tygon tubing (8mm length).

4.2.2 DEX-PDMS CONSTRUCT RELEASE STUDIES

Two disks or rods were placed in 5 mL of a 1% Benzalkonium chloride (BKC, Sigma) solution on a shaker for 30 d, with full fluid exchanges and samples taken once daily. Dexamethasone release on selected days was measured by ELISA (Neogen), which has a measurement range of 0.01-0.1 ng/mL.

4.2.3 THP-1 MONOCYTE CULTURE AND ACTIVATION

THP-1 monocytes (ATCC) were cultured in complete RPMI (c-RPMI, Gibco) supplemented with 1% penicillin/streptomycin (P/S, CellGro) and 10% fetal bovine serum (FBS, Thermo Scientific). Dex-PDMS disks were pre-eluted for one to five weeks prior to incubation with monocytes for 24h. Monocytes were activated via incubation with 1 μg/mL lipopolysaccharide (LPS) from Escherichia coli 055:B5 (Sigma) in c-RPMI for 48 h. After activation, monocytes were stained with monoclonal mouse anti-human

FITC-CD54 antibody and mouse anti-human PE-CD86 antibody (BD Biosciences) according to manufacturer's instructions. Cells were analyzed using a BD LSR II Flow Cytometer (BD Biosciences) and FlowJo software (Tree Star, Inc).

4.2.4 THP-1 MACROPHAGE DIFFERENTIATION AND ACTIVATION

THP-1 monocytes were cultured as described in c-RPMI. For macrophage differentiation, cells were plated at 3x105 cells per well in a 24-well TCT plate and cultured for 48 h in the presence of 100 nM phorbol-12-myristate-acetate (PMA, Sigma). Adhered cells were washed and cultured an additional 7 days to full differentiation, with media changes every two days. PDMS disks containing 0, 5, 10, or 20% Dexamethasone (w/v) were pre-eluted for 5 d to remove the burst release and added to appropriate wells 48 h prior to macrophage stimulation. Pre-treated macrophages were exposed to 100 ng/mL LPS in low serum (1% FBS) RPMI for 6 h; cell supernates were collected and assessed for IL-6 concentration by ELISA (R&D Systems) according to manufacturer's instructions.

4.2.5 ISLET CYTOTOXICITY STUDIES

Mouse islets were isolated from 20 C57BL/6 mice, plated at 2500 IEQ per dish (Buchwald et al., 2009) (nTCT petri) in complete CMRL (Gibco, 10% FBS, 1% P/S) and incubated with PDMS disks loaded with 0, 5, 10% Dexamethasone for 48 h. Islets were assessed for viability via MTT (Promega), with a minimum of 500 IEQ per well, as previously described (Pedraza et al., 2012). Islet function was determined through static incubation of sequential exposure to basal and elevated glucose levels using the column glucose stimulated insulin response assay, as previously described (Pedraza et al., 2012).

Briefly, islets are aliquotted into columns (150IEQ) in a bed of Sephadex beads (GE Healthcare), and exposed to glucose (60 or 300mg/dL) in KRBB buffer (99mM $NaCl_2$, 5mM KCl, 1.2mM KH_2PO_4, 1.2mM $MgSO_4$, 2.6mM $CaCl_2$, 26mM $NaHCO_3$, 25mM HEPES, 0.2% BSA).Samples elute from columns and collected after a 1hr incubation at low, high, and low glucose concentrations. Insulin content in samples was determined by ELISA (Mercodia).

4.2.6 ANIMAL GENERAL CARE

All animal studies were reviewed and approved by the University of Miami Institutional Animal Care and Use Committee. All procedures were conducted according to the guidelines of the Committee on Care and Use of Laboratory Animals, Institute of Laboratory Animal Resources (National Research Council, Washington DC). Animals were housed in microisolated cages in Virus Antibody Free rooms with free access to autoclaved food and water at the Department of Veterinary Resources of the University of Miami. The Preclinical Cell Processing and Translational Models Core at the Diabetes Research Institute performed the rodent islet isolations, diabetes induction, and animal maintenance.

4.2.7 INTRAPERITONEAL TRANSPLANTATION OF DEX-PDMS DISKS

Male C57BL/6 mice, weighing between 20-25 g (Jackson Labs) were used as recipients. Under general anesthesia (2% isofluorane USP; Baxter), a 1 cm long midline incision made through abdominal skin and peritoneum and two Dex-PDMS disks (pre-eluted for 3-5 d to remove burst release) were inserted within the abdominal cavity; the

animal's peritoneum was sutured and epithelium stapled. Urine and blood samples were periodically collected over a 96 d period.

4.2.8 SYNGENEIC CO-TRANSPLANTATION OF DEX-PDMS RODS WITH PDMS SCAFFOLD-SUPPORTED ISLETS

Male C57BL/6 mice, weighing between 20-25 g (Jackson Labs), were used as transplant recipients. Mice were rendered diabetic by intravenous administration of the beta-cell toxin streptozotocin (60 mg/kg; Sigma-Aldrich) and were used as recipients of syngeneic islets only if overtly diabetic upon three consecutive readings of non-fasting blood glucose levels > 350 mg/dL, using portable glucose meters (OneTouchUltra2, Lifescan). Donor islets were isolated from male C57BL/6 mice, counted, and 600 IEQ aliquots prepared for transplantation. Mice were prepped for surgery as stated above, and islet transplantation performed as previously described (Brady et al., 2013). Briefly, the epididymal fat pad (EFP) was gently exposed and spread and a silicone scaffold centered on the EFP prior to islet loading via Hamilton syringe. One or two 10% Dex-PDMS rods (8 mm) were cut in half and placed symmetrically around the scaffold. The scaffold and rod implant was wrapped using the EFP tissue and sealed using fibrin gel (fibrinogen (8 mg/mL), thrombin (2 U/mL), aprotinin (85 μg/mL), and $CaCl_2$ (5 mM)).

4.2.9 HISTOLOGICAL ASSESSMENT OF THE TRANSPLANT MICROENVIRONMENT

Mice were sacrificed on 30 and 90 days post-transplantation, and implants excised into 10% formalin buffer (J.T. Baker), followed by paraffin-embedding and sectioning for histological evaluation. For both immunofluorescent and Masson's Trichrome

staining (MTC, Thermo Scientific), sections were de-paraffinized prior to staining; after completion of staining protocol, all sections were coverslipped and sealed with Cytoseal mounting medium (Richard Allen Scientific). MTC staining was performed according to manufacturer's protocol and sections imaged on a Leica DMLB with a DFC 420C camera. Prior to immunofluorescent staining, sections were treated for antigen decloaking in citrate buffer (Biocare Medical) at 100 ºC for 20 min. Sections were subjected to sequential staining for rat anti-mouse CD45 (Millipore, 1:100), guinea pig anti-insulin (DAKO, 1:100), and DAPI (1 μM, Sigma). The CD45 primary was incubated overnight at 4 ºC, the insulin primary for two hours at room temperature, and DAPI for 5 min. Blocking was performed with goat serum (30 min), followed by goat secondary antibodies for 1 hr at room temperature (AlexaFluor 647 anti-rat, AlexaFluor 488 anti-guinea pig; all diluted 1:100, Invitrogen). Anti-Fade ProGold (Invitrogen) was applied prior to coverslipping. Immunofluorescent staining was imaged on a Leica SP5 Inverted Confocal microscope, and all results were compared to isotype controls to ensure specificity of signal.

4.2.10 EARLY INFLAMMATORY RESPONSE AT TRANSPLANT MICROENVIRONMENT

To evaluate the effect of Dex-PDMS implant on mitigation of early inflammatory events, selected mice were euthanized 3 and 6 days post-transplantation. EFP explants, containing the scaffold and Dex-PDMS rods were minced into collagenase type II (1 mg/mL, Sigma), incubated for 20 min at 37 ºC, and the tissue filtered through a cell strainer (70 μm, BD Falcon). Rods were easily removed during digestion while PDMS scaffolds were strained out. Cells were washed with excess FACS buffer (1% FBS in

HBSS, Corning CellGro) twice by centrifugation at 1500 rpm for 5 min to separate the cells of interest from adipocytes and eliminate excess collagenase. The isolated cell fraction was incubated in AKC red blood cell lysing buffer (Gibco) for 5 min, and washed again in FACS buffer prior to antibody staining. Cells were first blocked against FcBlock (BD Biosciences, 1:100) for 15 min to reduce nonspecific binding. Anti-mouse antibodies used for staining were Pacific Blue-CD45 (30-F11, Biolegend, 1:400), AF-488-CD11b (M1/70, BD Biosciences, 1:200), PE-Cy7-F4/80 (BM8, eBioscience, 1:400), and PerCP-Cy5.5-CD86 (GL-1, Biolegend, 1:100). Compensation was performed prior to sample analysis using compensation beads (Molecular Probes). FACS analysis was performed on a FACSAria II and data analysis performed on FlowJo Software (Tree Star, Inc).

4.2.11 STATISTICAL ANALYSIS

Statistical analysis was performed on GraphPad Software. Except the reversal curve, data is represented as the mean ± SD, with number of replicates and p values indicated in the figure caption. A minimum of three independent experiments were performed for the in vitro macrophage assay and syngeneic Dex-PDMS rod transplant. A minimum of two independent experiments were performed for the release, vitro monocyte FACS, and SVF FACS studies. Analysis of THP-1 monocyte and macrophage data was performed using a student's unpaired t-test. For FACS data analyses, a two-way ANOVA was used.

4.3 RESULTS AND DISCUSSION

4.3.1 DESIGN AND DEVELOPMENT OF DEX-PDMS CONSTRUCTS

To design dexamethasone eluting PDMS implants, the first objective was in the optimization of the release profile. Given the potential of dexamethasone to dampen islet function, design of prototypes, characterization of release profiles, and targeting for controlled, sustained release within the therapeutic range was critical. To evaluate the correlation between release kinetics and surface area, two PDMS geometries with variant surface areas, a disk (66.85mm^2) and a rod (35.2mm^2), were assessed. We predicted that construct surface area would dictate rate of release; construct volume would impact duration of release; and drug loading (%) would dictate drug availability. Dexamethasone release kinetics was evaluated over the course of 30 days. Both rod and disk geometries exhibit a characteristic initial burst release prior to plateau at day 5. Plateau release ranges for both construct geometries and both drug loadings fell below 1000 ng/dy (**Figure 4-2A**), with 10% drug loadings plateauing at approximately twice the release rate of 5% loaded constructs. Drug release plateau ranges for Dex-PDMS constructs exhibits a trend dependent on construct surface area and drug availability/loading. Dex-PDMS rods (14.9 mm^2) have approximately half the available surface area of Dex-PDMS disks (24.6 mm^2), which results in a plateau range at approximately half that of the disks for both 5% (203 ng/day rod vs. 459 ng/day disk) and 10% (410 ng/day rod vs. 666 ng/day disk) drug loadings (**Figure 4-2B**). Further, a 2-fold increase in drug loading resulted in a proportional increase in plateau release range for both construct prototypes. As such, tailoring of localized drug delivery is easily achieved via modification of surface area and drug loading. Furthermore, with construct geometry only constrained by surface area,

greater flexibility in construct design, and therefore, the ability to tailor drug-releasing constructs to the needs of the transplant site, is feasible.

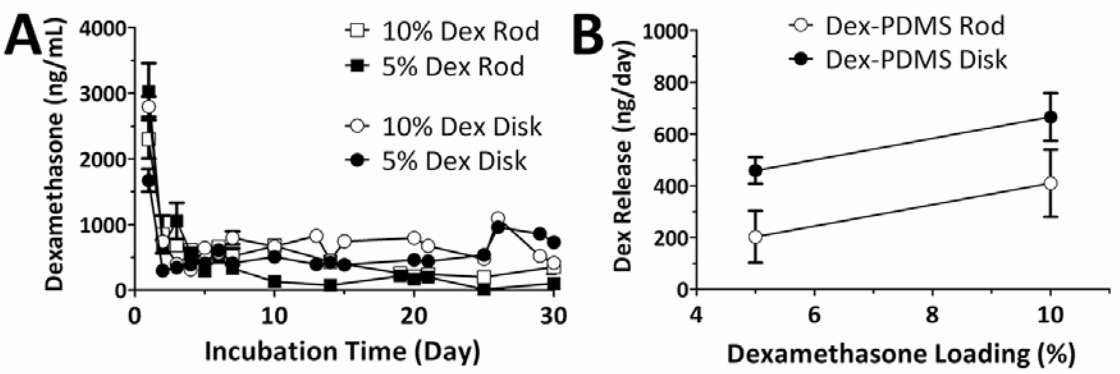

Figure 4-2 Dex-PDMS construct design and development. Release profile of dexamethasone (A) from PDMS constructs configured into disks or rods, with varied drug loadings. Average plateau release ranges (B) for Dex-PDMS rods (14.9 mm2) and disks (24.6 mm2) indicate a relationship between dexamethasone release, drug loading, and construct surface area. Error bars represent standard deviation (n=3).

4.3.2 IN VITRO EVALUATION OF DEX-PDMS CONSTRUCT IMPACT ON ISLET VIABILITY AND FUNCTION

Following optimization of dex-eluting constructs to our targeted therapeutic range, the effect of Dex-PDMS constructs on islets was evaluated. Dex-PDMS disks, loaded with 0, 5, or 10% dexamethasone, were incubated with mouse islets for 48 h, followed by evaluation of islet viability and function. Dex-PDMS constructs demonstrated no impact on islet viability as evaluated by MTT (**Figure 4-3A**), indicating negligible toxicity for Dex release within the targeted range. The glucose-stimulated insulin response (GSIR) technique was used to assess islet function, wherein islets exposed to basal (60mg/dL) and elevated (300mg/dL) glucose levels were evaluated for

their insulin secretion response. Well-functioning islets should exhibit a clear tri-phasic response to sequential exposure to basal (Low 1), elevated (High), then basal (Low 2) glucose levels. In this study, islets exposed to Dex-PDMS constructs were statistically identical to controls (**Figure 4-3B**). As such, local release of dexamethasone from Dex-PDMS constructs imparted undetectable effects on murine islets.

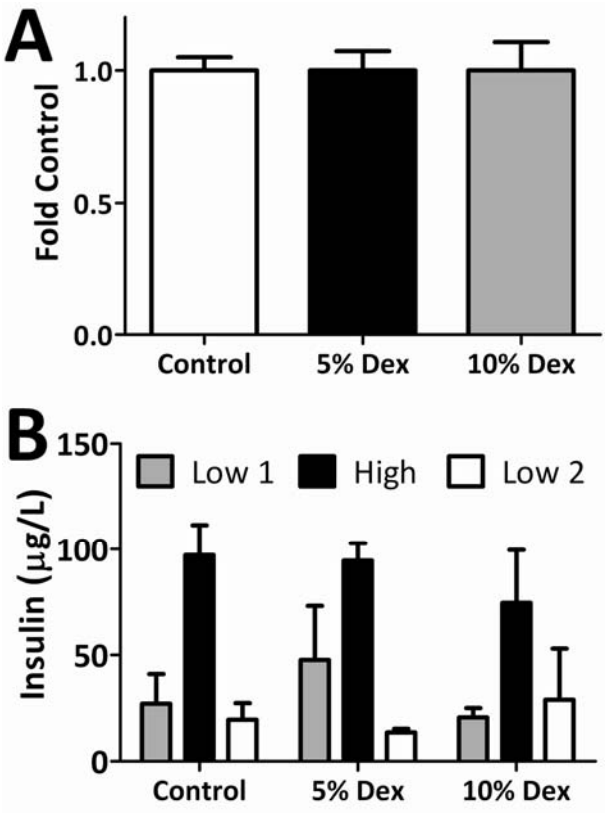

Figure 4-3 Co-incubation of dexamethasone eluting materials with islets does not impair viability or insulin secretion. In vitro assessment of mouse islets (2500 IEQ) following 72 h co-incubation with PDMS disks loaded with 0% (control), 5% or 10% dexamethasone. MTT viability (A) expressed as fold over control and insulin responsiveness. Glucose stimulated insulin secretion (B). Error bars represent standard deviation (n=3). No statistically significant effect of Dex-PDMS on insulin viability or glucose stimulated insulin secretion was observed.

4.3.3 IN VITRO EVALUATION OF INFLAMMATION SUPPRESION IN MONOCYTE AND MACROPHAGE CULTURES BY DEX-PDMS CONSTRUCTS

To evaluate the potency of Dex-PDMS constructs in impartment of inflammation cell activation, human monocytes and macrophages (THP-1 cell line) were pre-incubated with Dex-PDMS disks prior to activation via lipopolysaccharide (LPS). For monocyte studies, Dex-PDMS disks (0, 5, or 10%) were aged one to five weeks prior to co-incubation with THP-1 monocytes. Following LPS stimulation, cell activation via CD54 (intercellular adhesion molecule-1, ICAM-1) and CD86 (co-stimulatory molecule) surface markers was substantially reduced (**Figure 4-4A and 4-4B**) for both markers compared to stimulated controls for both drug loadings. CD86 activation was comparable to non-stimulated controls for all time points except for week 3. Aging of Dex-PDMS constructs for up to 5 weeks did not diminish the effect, supporting release profiles of sustained dexamethasone elution.

To evaluate Dex-PDMS construct impact on cell populations present in later stages of the FBR, THP-1 macrophages were evaluated. IL-6 secretion, following LPS stimulation, was assessed as a marker of macrophage inflammatory activation. Control macrophage cultures incubated with or without a blank PDMS construct exhibit elevated IL-6 secretion over unstimulated controls (**Figure 4-4C**), whereas cultures pre-incubated with Dex-PDMS disks (5, 10, or 20% drug loading) exhibited significant suppression of IL-6 secretion. Suppression of activation in both monocyte and macrophage cell cultures by Dex-PDMS constructs indicates the potential for this system to reduce inflammatory responses that arise in both the acute and chronic inflammatory stages of the FBR.

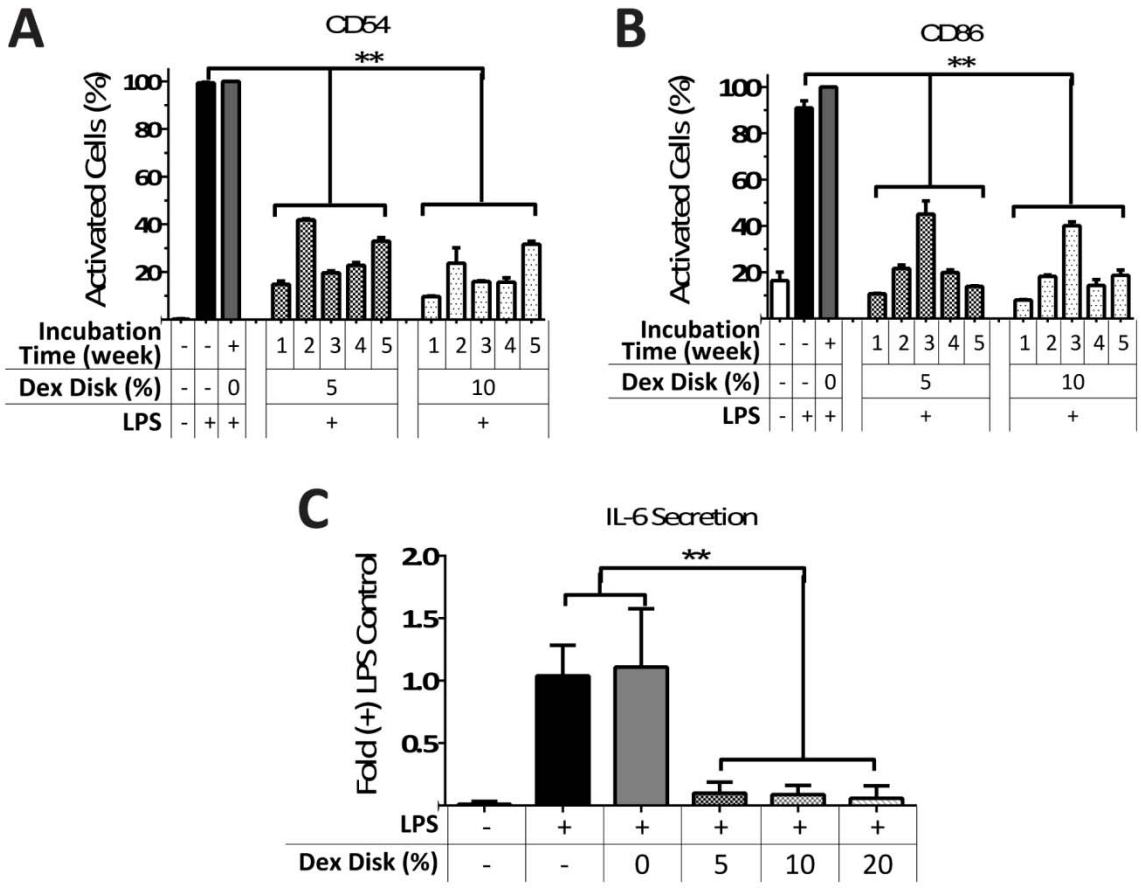

Figure 4-4 Dex-PDMS disks inhibit THP monocyte and macrophage activation following LPS stimulation. Activation of THP monocytes was assessed via CD54 (A) and CD86 (B) expression. Effects of 5% or 10% Dex-PDMS disks on inhibiting LPS activation was quantified for disks incubated for up to 5 weeks within buffer solutions. Results were compared to non-activated and LPS stimulated cells. THP macrophage activation, assessed via IL-6 secretion (C), was quantified for LPS stimulated macrophages co-incubated with 0%, 5%, 10%, or 20% Dex-PDMS disks. Error bars represent standard deviation (n=3). **P < 0.01

4.3.4 IN VIVO INVESTIGATION OF DEX-PDMS CONSTRUCT TOXICITY AND EFFICACY

Following in vitro evaluation of Dex-PDMS constructs, we sought to evaluate the effect of these implants in vivo. Initial studies sought to detect systemic dexamethasone levels following transplantation of Dex-PDMS constructs. As shown in **Figure 4-5**, urine

levels for recipients of Dex-PDMS disks were significantly elevated over blank PDMS only controls. No statistical difference was discerned for urine Dex levels between the variable drug loadings. Previous studies investigating the relationship between systemic corticosteroid injections in rodents and their detectable levels in urine have found an approximate 60% correlation between the amount injected and the amount excreted.(Kalliokoski et al., 2010)While the implanted Dex-PDMS constructs are predicted to release in the range of 250-1000 ng/mL per day, urine dexamethasone levels were 0.1-0.4% of this value, indicating that local Dex release results in minimal systemic effect.

Subsequent studies sought to evaluate the effect of local Dex-PDMS constructs on islet engraftment. A syngeneic mouse model was used in order to examine the effects of local drug delivery on engraftment efficacy, in the absence of the compounding effects of allograft rejection. Islets were loaded within macroporous silicone scaffolds in the epididymal fat pad (EFP) site (**Figure 4-6A**), as evaluated in previous studies (Brady et al., 2013). The rod geometry was selected, wherein two (**Figure 4-6B**) or four (**Figure 4-6C**) 4 mm Dex-PDMS rods were placed symmetrically around the islet-loaded scaffold to favor peripheral drug release. The EFP was then wrapped around the scaffold and rods, and sealed with fibrin glue (**Figure 4-6D**) prior to replacement within the peritoneum. **Figures 4-6E and 4-6F** demonstrate construct remodeling after 30 d in vivo for two and four Dex-PDMS rod groups, respectively. Due to low protein and cellular adhesion to PDMS, and Dex-PDMS constructs in particular, the rods tend to shift within the EFP after transplantation, as is evident in **Figure 4-6F**; however, no correlation between movement of rods and graft efficacy was observed.

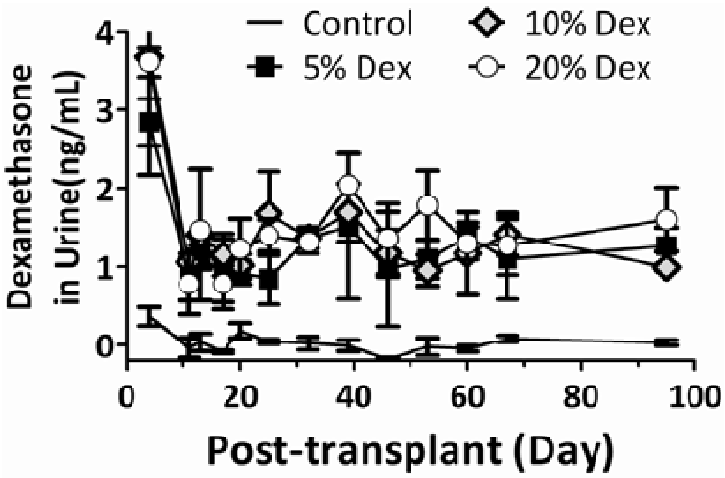

Figure 4-5 Detection of dexamethasone in urine of C57BL/6J mice following implantation of 2 Dex-PDMS disks. Levels of dexamethasone in urine for PDMS disks loaded with 0% (control), 5%, 10%, or 20% dexamethasone. Error bars represent standard error (n=2-3)

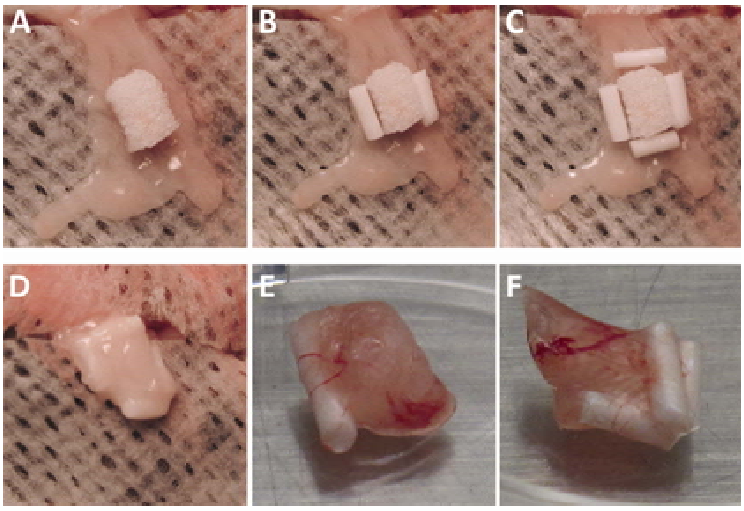

Figure 4-6 Islet-loaded silicone scaffolds transplanted in the EFP of diabetic B6 mice with 0(A), 2 (B), or 4 (C) Dex-PDMS rods, placed symmetrically around the scaffold. Explanted constructs, 30 days post-transplantation, with 0 (D), 2 (E), or 4 (F) Dex-PDMS rods.

Islet graft function was assessed via nonfasting blood glucose values, whereby two consecutive measurements < 200 mg/dL indicated diabetes reversal. Within this study, blood glucose values were not statistically disparate between implants containing

Dex-PDMS rods and control animals (**Figure 4-7A**). Mouse body weight (**Figure 4-7B**) rose steadily over the post-transplantation time-period and with no detectable difference between groups, indicating adequate graft function in all groups. Evaluation of transplant efficacy (**Figure 4-7C**) revealed no statistical difference between groups. Following reversal to normoglycemia, stability of function was observed for all groups. Transplantation of islet-scaffold constructs alone (Control) resulted in normoglycemia in 100% of the transplants (n=7), with an average time to reversal of 9.3 ± 13.9 days post-transplantation. By comparison, transplants containing 2 Dex-PDMS rods exhibited 100% reversal (n=7), with an average time to reversal of 17.6 ± 11.7 days post-transplantation. For transplants containing 4 Dex-PDMS rods, 6 of the 8 transplants (75%) reverted within 30 days post-transplant, with an average time to reversal for functioning grafts of 15.8 ± 13.8 days post-transplantation. While statistically insignificant, this data suggests that Dex-PDMS rods may impart a delay in efficiency in engraftment, when higher levels of dexamethasone are present within the graft microenvironment. Although no effect on islet functional characteristics was observed in vitro, indicating minimal effects on the islets themselves, engraftment efficacy in vivo is highly correlated to vascularization of the graft (Brady et al., 2013; Pileggi et al., 2006). Given that dexamethasone has been shown to delay angiogenesis, the observed trend of decreased engraftment efficacy observed may be due to Dex-induced impairment of islet revascularization (Hori et al., 1996; Logie et al., 2010).

Urine samples demonstrate measurable dexamethasone for Dex-PDMS groups. (**Figure 4-7D**), confirming controlled, sustained release of drug over the full time course. Interestingly, systemic dexamethasone levels were similar to Dex-PDMS disks

transplanted intraperitoneally; this limited systemic exposure is a unique advantage to localized drug delivery. No significant difference of dexamethasone detected in urine was observed between the two and four rod groups, and systemic levels are not likely to correlate to localized delivery in the graft.

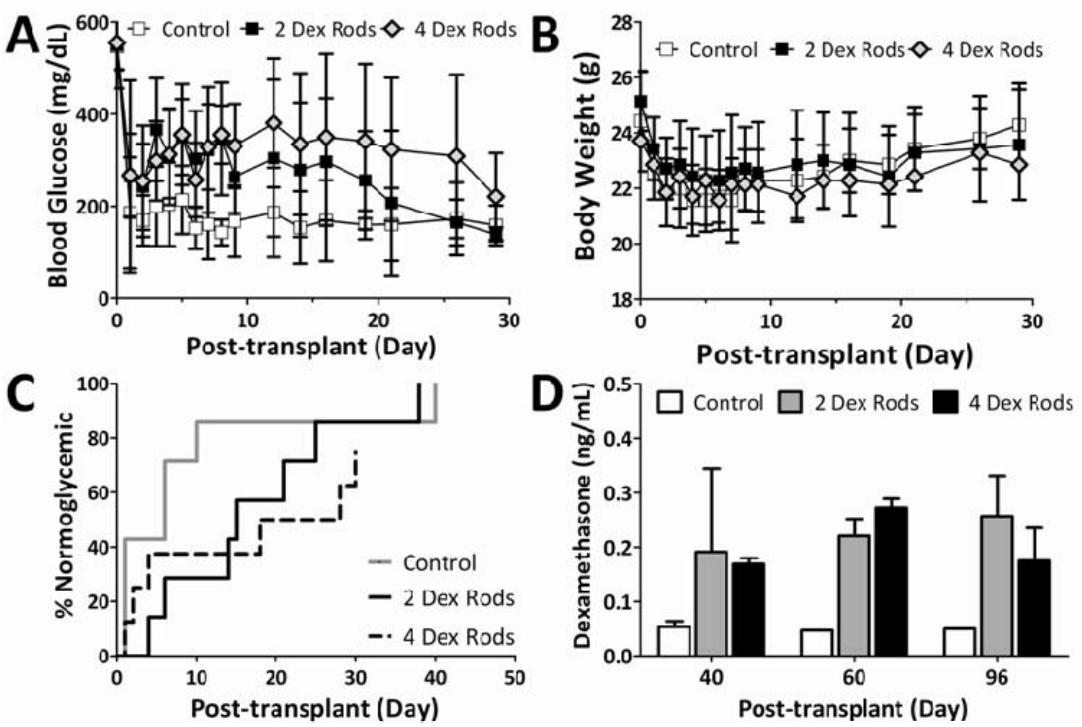

Figure 4-7 Dex-PDMS rods within islet transplant microenvironment resulted in no impairment of transplant efficacy in diabetic syngeneic mouse model. Nonfasting blood glucose levels (A) and body weight (B) of recipients following transplantation of 600 IEQ without (control; n=7) or with two 10% Dex-PDMS rod (2 Dex Rods; n=7) or four 10% Dex-PDMS rods (4 Dex Rods; n=8). No statistical difference in blood glucose or body weight following transplant was observed between groups. Error bars = standard deviation. Time to reversal to normoglycemia (C) for implanted grafts. Reversal is defined as two readings < 200 mg/dL. Quantification of dexamethasone levels within urine (D) for selected transplants. Error bars = standard error

Histological assessment was performed on explanted grafts 90 days post-transplantation to evaluate Dex-PDMS rod impact on graft remodeling. Masson's trichrome staining permits visualization of cell infiltrates and extracellular matrix

deposition within the silicone scaffold. Islets are clearly visualized (**Figure 4-8,** top row) with maintenance of islet morphology in all groups. Immunofluorescent labeling of insulin demonstrates strong insulin expression for islets within all groups (**Figure 4-8**, bottom row). Immunofluorescent staining of membrane-associated leukocyte marker CD45 revealed marked differences in expression, with significant reduction in $CD45^{+}$ cells when Dex-PDMS rods are present. This marked decrease in leukocyte infiltrating cells in Dex-PDMS rod groups indicates that the localized delivery of dexamethasone is sufficient to reduce inflammatory cell migration to the site, even 90 d post-transplant.

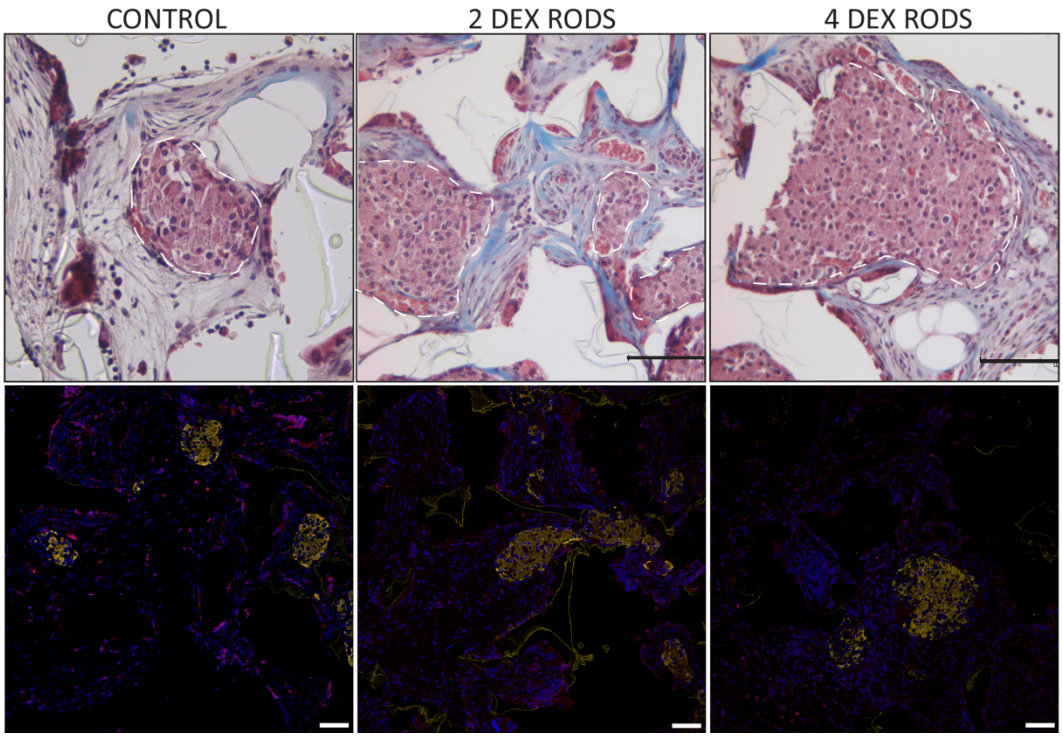

Figure 4-8 Representative histopathological images of islet-loaded implants without (control) or with two or four 10% Dex-PDMS rods, explanted from the epididymal fat pad site 90 d post-transplantation. Masson's Trichrome (top row) and immunofluorescent staining (bottom row) for insulin (yellow) and CD45+ (red) with DAPI nuclear counter stain (blue); dashed lines encircle islets; scale bar = 100 μm.

To further evaluate the effects of local dexamethasone delivery on graft integration and early inflammatory events, grafts were explanted at early time points for histological evaluation and phenotypic analysis of cells infiltrating the graft microenvironment. Histological evaluation was performed 30 days post-transplant, with immunofluorescent stating for insulin and $CD45^+$ cells (**Figure 4-9**). In all groups, islets demonstrate robust staining for insulin (yellow). A marked increase in the proportion of cells staining positive for CD45 was observed for control animals, when compared with Dex-PDMS rod groups. This trend is consistent with that seen on day 90, although comparison of controls at days 30 and 90 post-transplant indicate more robust early inflammatory events. This further support the capacity of Dex-PDMS constructs to consistently reduce general leukocyte infiltration in the early stages of transplant site remodeling.

Phenotypic analysis of cells within the graft microenvironment was perform at early time points, 3 and 6 days post-transplantation, to evaluate the impact of Dex-PDMS constructs during the acute inflammatory phase (e.g. 0-7 d). General markers of leukocytes ($CD45^+$), antigen presenting cells ($CD86^+$), monocytes ($CD11b^+$), and macrophages ($F4/80^+$) were evaluated via FACS. Results were expressed relative to the control group (**Figure 4-10**). Leukocyte populations ($CD45^+$) were significantly lower in both two and four Dex-PDMS groups on day 3 ($p < 0.01$), and in the four rod group on day 6 ($p < 0.05$), indicating sufficient dexamethasone release to impede early infiltration of general FBR cells. This correlates with our histological assessments.

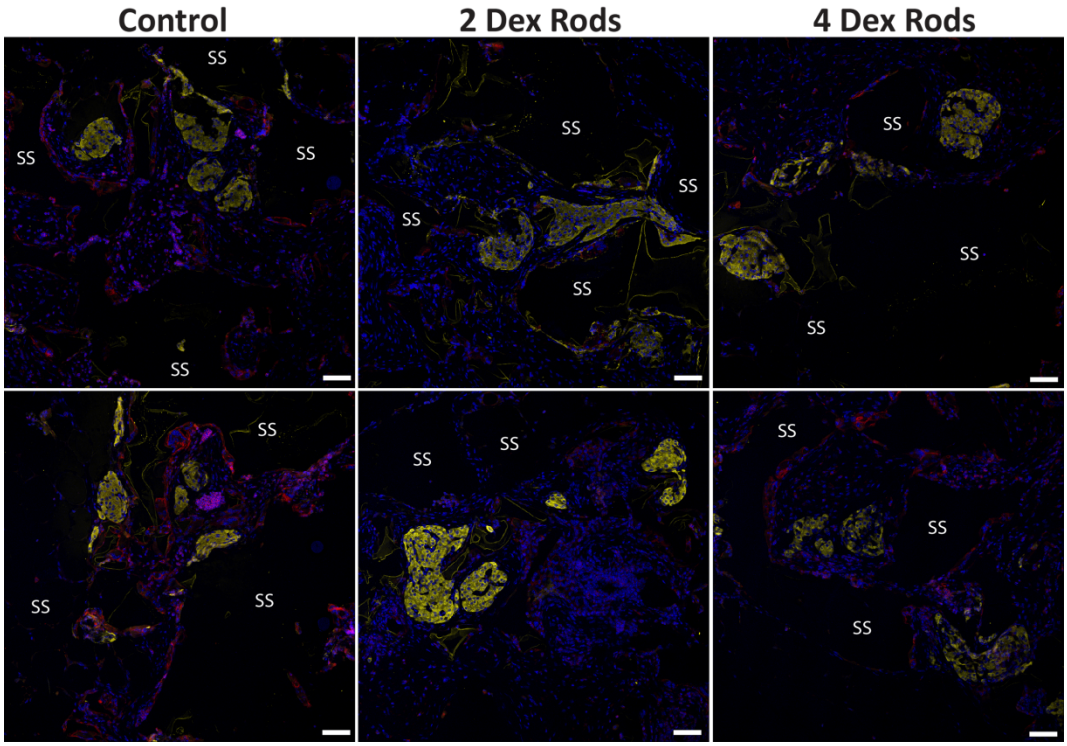

Figure 4-9 The presence of dexamethasone-eluting PDMS rods decreased infiltration of CD45+ cells, per histopathological evaluation. Immunohistochemical staining of islet-loaded implants without (control) or with two or four 10% Dex-PDMS rods, explanted from the epididymal fat pad site on day 30. Representative images of immunofluorescent staining of explants for insulin (yellow) and CD45+ (red) with DAPI nuclear counterstain (blue); scale bar = 100 μm. SS=PDMS scaffold

Monocyte ($CD11b^+$) presence was significantly lower ($p < 0.05$) in Dex-PDMS rod groups on both day 3 (2 rod: 21%, 4 rod: 25%) and 6 (2 rod: 18%, 4 rod: 30%)) relative to controls, indicating Dex-PDMS constructs successfully reduced infiltration and migration of cells common to the acute inflammatory phase. Reduced monocyte presence may also correlate with decreased recruitment of, and differentiation to, macrophages, as observed on day 3, with significant reduction of $F4/80^+$ cells in two (22%, $p < 0.05$) and two (43%, $p < 0.01$) rod groups. Interestingly, this trend was not observed on day 6, with all groups demonstrating comparable numbers of $F4/80^+$ cells. Antigen presenting cell ($CD86^+$) infiltration exhibited a trend in reduced presence for

Dex-PDMS groups, with significant reduction observed or the four Dex-PDMS rod group on day 6 ($p < 0.05$). This *in vivo* result supports earlier *in vitro* monocyte studies.

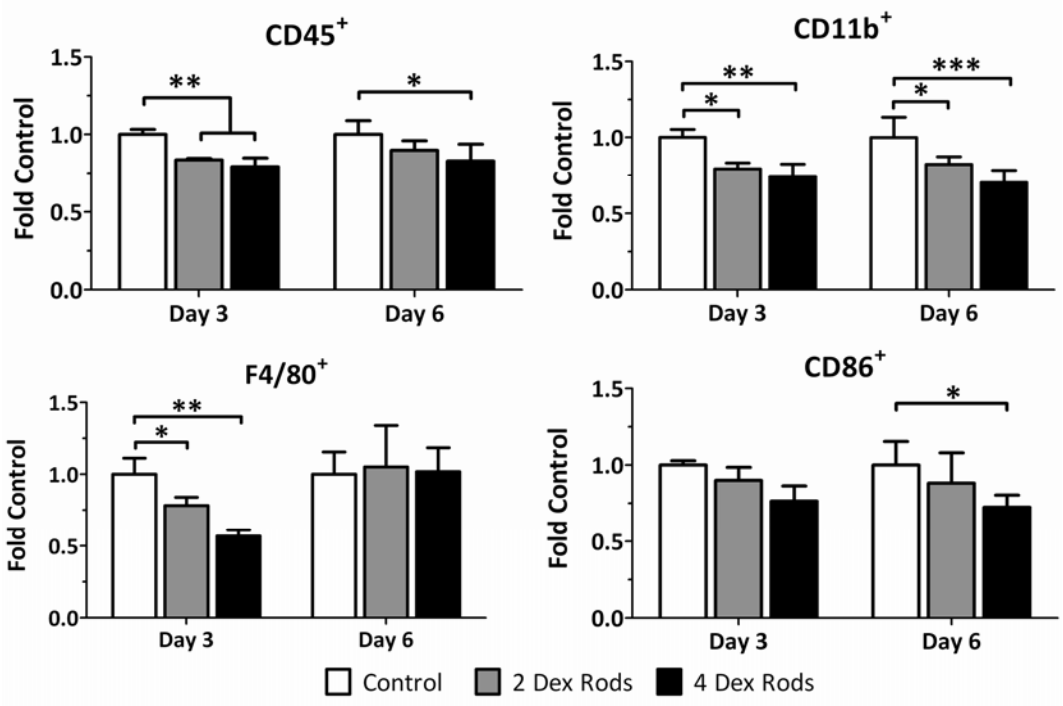

Figure 4-10 The presence of Dex-PDMS rods in the transplant microenvironment reduces inflammatory cell migration to the graft site. Assessment of CD45+, CD11b+, F4/80+, and CD86+ cell presence in the graft microenvironment via FACs following transplantation of islets without (control) or with two or four 10% Dex-PDMS rods. Grafts were assessed 3 and 6 days post-transplantation. Total % positive cells for each group was normalized by control values, e.g. fold control. Error bars represent standard deviation; n=4 per group; * $P < 0.05$; ** $P < 0.01$; *** $P < 0.001$ vs control

4.4 CONCLUSIONS

Localized delivery of anti-inflammatory agents within a cell transplant site can provide a targeted and safe means to decrease generalized inflammatory events during the early engraftment period. In this study, Dex-PDMS constructs were optimized for

targeted dexamethasone release within a therapeutic range. Resulting constructs demonstrated the capacity to significantly reduce inflammatory responses both in vitro and in vivo. This strategy has broad applications in cell and organ transplantation, and its unique advantage lies in the potential to tailor both drug delivery range and construct geometry.

Chapter 5. Antioxidant Cerium Oxide Nanoparticle Hydrogels for Cellular Encapsulation

5.1 INTRODUCTORY REMARKS

Oxidative stress is defined as the imbalance between the production of oxidants or reactive oxygen species (ROS), such as superoxide (O_2^-) and hydrogen peroxide (H_2O_2), and their elimination via antioxidants, such as superoxide dismutase (SOD) and catalase. Sustained oxidative stress results in significant destruction of cellular structures and functions and has been implicated in numerous pathological conditions, such as atherosclerosis, cancer, renal disease, and diabetes.(Griendling et al., 2003; Muhammad et al., 2009; Reuter et al., 2010) Given that oxidative stress can be induced via exposure of cells to hypoxia, cytokines, and inflammation, cellular transplants are particularly susceptible to oxidative damage, resulting in increased cell death and decreased efficacy of implants.(Tiedge et al., 1997; Tiedge et al., 1998) Protecting cellular grafts from this toxic oxidative milieu is particularly challenging in the context of pancreatic islet transplantation for treatment of Type 1 diabetes mellitus (T1DM), due to the inherently low gene expression and activity of important antioxidant enzymes in pancreatic islets.(Ho et al., 1999; Lenzen et al., 1996; Oberley, 1988) Oxidative damage of islets following transplantation is one of the contributing factors resulting in graft destabilization and decreased long-term efficacy.(Drews et al., 2010)

The encapsulation of transplanted donor islets within semi-permeable polymers is an appealing method for protecting allogeneic grafts from detrimental host responses.(Kizilel et al., 2010; Sefton et al., 2000; Wilson et al., 2008b) The encapsulating polymer permselectivity permits passage of nutrients and release of

secreting proteins or waste products, but blocks direct host cell interactions with the graft cells. The most commonly used encapsulation material is alginate, due to its high biocompatibility, ease in encapsulation method, and demonstrated efficacy in small animal models.(Cui et al., 2009; Sun, 1988; Zimmermann et al., 2007) While cellular encapsulation aids in reduction of generalized host cell responses via blocking direct cell-cell interactions, this strategy fails to protect donor cells from soluble by-products of the inflammatory response, in particular ROS.(Chen et al., 1998; Kavdia et al., 2002; Wiegand et al., 1993)

Numerous anti-oxidant agents, such as edaravone and gliclazide, have been incorporated into islet transplants, either via systemic infusion, pre-culture treatment, or transgenic overexpression, with varying degrees of protective effects;(Fukudome et al., 2008; Kimoto et al., 2003; Li, X. et al., 2004; Mancarella et al., 2008; Padmasekar et al., 2013) however, most of these approaches are limited by the need for systemic delivery, the decreased duration of effect, and the complexities of transfection. Notable biomaterial strategies have sought to scavenge free radicals via supplementation of encapsulation polymers with antioxidant enzymes such as SOD and catalase.(Cheung, Charles Y. et al., 2008; Hume, Patrick S. et al., 2011b; Kojima et al., 1996; Li, Z. et al., 2009; Nakaoka et al., 1997) Inevitably, however, the catalytic reactivity of the free radical scavenging agents is exhausted, resulting in transient protection. A more potent approach to combat the continual inflammatory assault to the transplant would be in the development of a sustainable anti-oxidant mimetic.

The unique redox properties of selected metal oxides, e.g. yttrium and cerium, have recently been explored as scavenging agents for cellular oxidative stress.(Schubert

et al., 2006) The oxide form of the rare earth element cerium, found in the lanthanide series of elements, has the ability to cycle between its cerium(III) and cerium(IV) oxidation states, due to a lattice structure with a high tolerance for reversible oxidation/reduction.(Bumajdad et al., 2009) Cerium oxide nanoparticles (CONPs) exhibit enhanced catalytic activity over bulk forms due to increased surface area, resulting in an amplified number of available oxygen vacancies.(Bumajdad et al., 2009; Pirmohamed et al., 2010) The oxidative state of CONP appears related to its catalytic activity, whereby cerium (IV) correlates with catalase-like behavior and cerium (III) exhibits SOD mimetic responses.(Heckert et al., 2008; Pirmohamed et al., 2010) The unique ability of CONPs to switch their oxidative states between III and IV lends itself to its desirable self-renewing property.(Perez et al., 2008) Further, CONPs have the potential to provide broad free radical protection, with demonstrated quenching of hydroxyl radicals, superoxide, peroxide, and nitric oxide.(Asati et al., 2009; Das et al., 2007; Heckert et al., 2008; Korsvik et al., 2007)

CONP's potent scavenging capacity, with low loading volume and unlimited auto-catalytic potential, inspired exploration of their pharmaceutical potential, with the aim of reducing oxidative damage in a variety of injury models. Co-culture of free CONPs with cells have resulted in radioprotective,(Colon et al., 2009; Das et al., 2007; Tarnuzzer et al., 2005) cardioprotective,(Niu et al., 2007) and neuroprotective effects(Schubert et al., 2006) (for full review see(Celardo et al., 2011)). Selected studies have also explored the potential of CONPs to protect beta cells and islets.(Hosseini et al., 2013; Pourkhalili et al., 2012; Tsai et al., 2007) While highly promising, cytotoxic effects have been observed, particularly for particle sizes exceeding 100 nm or at

concentrations higher than 300 μM (particle sizes 3-50nm), although broad assessment of CONP toxicity is complicated by the variable size, surface geometry, and zeta potential of the particles.(Das et al., 2007; Hussain et al., 2012; Pirmohamed et al., 2010) Cytotoxicity likely results from cellular internalization and accumulation of the nanoparticles, where autophagy-induced apoptosis has been observed, a common outcome of nanoparticle phagocytosis.(Celardo et al., 2011; Hussain et al., 2012; Patil, S. et al., 2007a; Stern et al., 2008)

A means to mitigate the cytotoxicity of CONPs may be entrapment within an encapsulation hydrogel; minimizing particle phagocytosis, while retaining their catalytic potential. Herein, we sought to engineer a nanocomposite, anti-oxidant biomaterial via incorporation of cerium oxide nanoparticles within an encapsulating hydrogel (see **Figure 5-1**). The potential of CONPs, embedded within a hydrogel, to retain their catalytic and self-renewal activity was examined. The capacity of CONPs and CONP-composite hydrogels to prevent ROS-induced beta cell death, as well as enhance cytocompatibility, was also evaluated. The benefits of this approach to provide the local presentation of potent CONPs at the transplant site, thereby reducing potential downstream or systemic effects, are discussed.

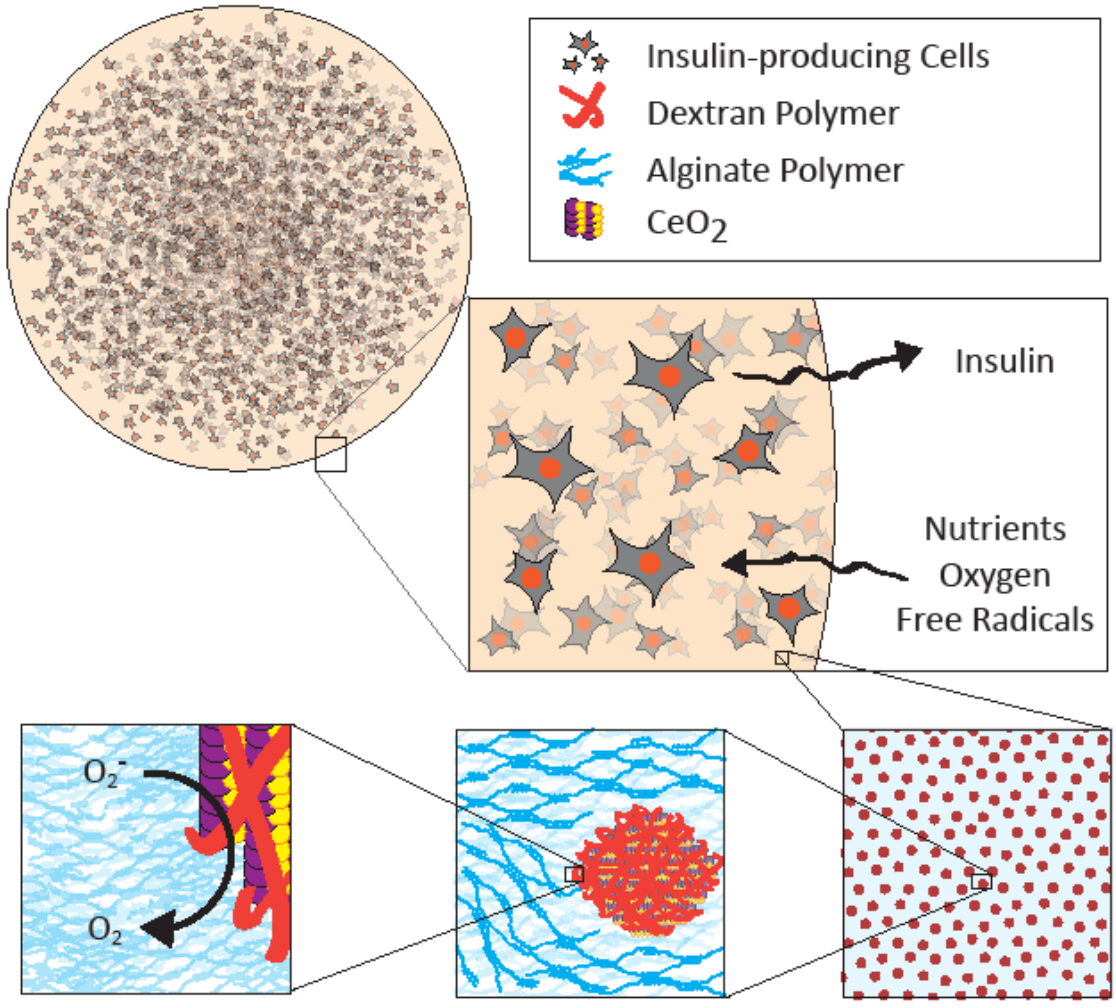

Figure 5-1 Illustration of cerium oxide nanoparticle (CONP)-alginate composite hydrogel. Alginate microbead provides matrix for cellular encapsulation and perm-selectivity to permit nutrient diffusion in and insulin secretion out of the hydrogel. CONP, embedded within the alginate matrix, provides ubiquitous, renewable, antioxidant protection from external free radical damage.

5.2 MATERIALS AND METHODS

5.2.1 CONP SYNTHESIS

A 1 mL solution of 1 M Cerium (III) Nitrate was mixed evenly with a 2 mL solution of 100 mM Dextran T-10, added drop-wise to 6mL of ammonium hydroxide

(30%), and stirred overnight. To remove excess Dextran and reaction byproducts, CONP solutions were dialyzed against PBS using 30 kDa MWCO centrifuge filters (Millipore) at 4000 rpm in 10 min intervals, until effluent pH was ~7.0. CONP solutions were further processed for analysis and cell culture by sonication, and sterile filtration (0.2 μm).

5.2.2 CONP SOLUTION CHARACTERIZATION

CONP size was characterized by dynamic light scattering (DLS) using a DynaPro Titan and Dynamics v6.0 software (Wyatt Technology), all samples diluted in PBS (Gibco). CONP solution composition was characterized by Fourier transform infrared (FTIR) analysis on a Perkin-Elmer Spectrum 100 FTIR Spectrometer (average of four scans with a resolution of 4 cm^{-1}) using a lyophilized, processed sample. HR-TEM imaging was performed at 300 kV on a FEI Tecnai F30 TEM by the Advanced Materials Processing and Analysis Center (AMPAC) at the University of Central Florida (UCF). XPS analysis was performed on a Physical Electronics 5400 ESCA, also at AMPAC UCF, and peaks identified using PeakFit v4.12 (Systat Software, 8% Savitsky-Golay smoothing, linear two-point baseline subtraction). CONP catalytic activity and renewability was assessed by addition of CONP (1 mM) to H_2O_2 (0.1 mM) and spectral analysis performed on a Molecular Devices SpectraMax M5 Microplate reader. CONP solutions were incubated with 1.25 mM 3,3',5,5'-Tetramethylbenzidine (TMB, Mercodia) and oxidation read on the aforementioned spectrophotometer at 652 nm at the indicated time points. Superoxide radicals were generated through the reaction of Xanthine (XA,100 μM) and Xanthine Oxidase (XO, 25 nM), whereby XA's conversion to urea results in the release of superoxide.(Fridovich, 1970) Superoxide generation was

measured via the rate of oxidation of cytochrome C.(Cohen et al., 1978) This reaction rate may be calculated using equation (1) below,(Hume, Patrick S. et al., 2011b)

$$\left[O_2^-\right] = \frac{\Delta A \times v}{K \times l \times t} \qquad \textbf{(Equation 5-1)}$$

where ΔA is the change in absorbance, l is the pathlength, t is time, v is volume, and K is the extinction coefficient for the difference in absorption between reduced and oxidized cytochrome C ($K = 21 \times 10^3$ cm^{-1}/M).

At the above concentrations of XA and XO, superoxide production peaked at 10 nmol/ min, with the majority of reaction completion within 10-15 min. The aforementioned XA/XO system was incubated without or with 1 mM CONP, with assessment of superoxide generation over the course of the experiment (15 min).

5.2.3 CONP MIN6 CYTOTOXICITY AND SUPEROXIDE PROTECTION

MIN6 cells (subclone C3, courtesy of Dr. Valerie Lilla and Alejandra Tomas) were cultured as monolayers in T-flasks and fed every 2-3 days with fresh medium comprised of Dulbecco's modified Eagle's medium (DMEM, Mediatech) supplemented with 10% fetal bovine serum (FBS), 1% (v/v) penicillin-streptomycin (P/S, Gibco), 1% (v/v) L-glutamine (Gibco) and 0.001% (v/v) β-mercaptoethanol . MIN6 cytotoxicity experiments were performed by exposure of 3x105 cells/well seeded within a 24-well plate to 0, 0.1, and 1.0 mM CONP-supplemented DMEM for 48 h. Cell viability was assessed by Alamar Blue (Invitrogen). Superoxide protection was assessed after a 48 h pre-incubation with CONP-supplemented DMEM. Superoxide radicals were generated using the XA/XO system defined above for 2 h in CONP-supplemented PBS, and

viability assessed by Alamar Blue and Live/Dead staining (Calcein AM/Ethidium Homodimer, Invitrogen) on a Zeiss LSM510 confocal microscope.

5.2.4 CONP-BIOMATERIAL FABRICATION

CONP-matrigel capsules were formed by thorough mixing of matrigel polymer (BD Biosciences) and CONP solution on ice, followed by droplet formation (10 μL) on glass slides, incubated at 37 ºC for 1 h to allow gelation. CONP-agarose solutions were fabricated by making a 2% solution of Agarose VII in PBS at 37 ^{o}C in a double boiler, and thoroughly mixing with CONP solution. Capsules were formed by addition of 30 mL mineral oil to 10 mL CONP-agarose in a 50 mL conical vial; the tube was capped and inverted gently several times, immersed in an ice bath between inversions to allow the agarose spheres to crosslink. CONP-agarose capsules were then washed by gentle inversion in 40mL of PBS to remove excess mineral oil. 1 mm diameter beads were selected from resulting microbeads for CONP retention experiments. CONP-alginate capsules were formed by premixing a 1.6% (w/v) alginate (UP-MVG, Novamatrix) PBS solution with CONPs prior to extrusion through a capsule generator with parallel airflow (42 psi) into a crosslinking bath of 1.5% (w/v) barium chloride , supplemented with 10mM 3-(N-morpholino)propanesulfonic acid (MOPS), 140 mM D-Mannitol, and 0.025% Tween-20. After 10 min of crosslinking, CONP-alginate capsules were washed with PBS to remove excess crosslinker. Resulting alginate microbeads were 0.922 ± 0.149 mm in diameter.

5.2.5 CONP-BIOMATERIAL CHARACTERIZATION

All three CONP-hydrogels were visually assessed for CONP retention by complete immersion of hydrogels in soluble TMB solution, and imaged on an Olympus SZX7 stereomicroscope. To further confirm visual observations, CONP-alginate beads were washed several times in excess PBS, and samples assessed in the DLS for free CONP detection. CONP-alginate hydrogel catalytic activity was further assessed quantitatively by immersing 20 CONP-alginate or pure alginate capsules in a 60 μM H_2O_2 solution for 1, 2, or 4 h. H_2O_2 levels were assessed via colorimetric hydrogen peroxide detection kit (Enzo Life Sciences) at the above time points.

5.2.6 CONP-ALGINATE MIN6 ENCAPSULATION AND SUPEROXIDE PROTECTION

MIN6 were thoroughly mixed with CONP-alginate or alginate solutions at $10x10^6$ cells/mL (short-term study) or $25x10^6$ cells/mL (long-term study), prior to capsule formation using the method described above. For both the short- and long-term study, encapsulated MIN6 were plated at 40 capsules/well (~$0.25x10^5$ or $1x10^5$ cells/well, respectively) in a 48-well plate. For the short-term CONP-alginate titration study, encapsulated MIN6 were cultured for 48 h prior to superoxide exposure (200μM XA and 50nM XO in PBS) for 2 h, and viability assessment via Alamar Blue and Live/Dead staining. For the long-term CONP-alginate encapsulation study, encapsulated MIN6 were cultured for 10 d, with superoxide exposure (200 μM XA/50 nM XO) for 2 h on day 2 and 6 post-encapsulation, with viability assessments (Alamar Blue, Live/Dead stain) performed 2, 4, 6, 8, and 10 d post-encapsulation.

5.2.7 EVALUATION OF CONP-ALGINATE AND CONP SOLUTIONS ON PRIMARY RAT ISLET VIABILITY AND FUNCTION

Rat islets were isolated from Lewis rats, plated at 2000 IEQ per dish (Buchwald et al., 2009) (nTCT petri) in complete CMRL (Gibco, 10% FBS, 1% P/S) supplemented with 0, 0.1, 1.0, or 10 mM CONP solution for 48 h. Islets were encapsulated in CONP-alginate at concentrations of 0, 0.1, 1.0, and 10 mM CONP using the encapsulation method described above, at 2000 IEQ / mL alginate. Islets in both groups were assessed for viability via MTT (Promega) or Alamar Blue (Invitrogen), with a minimum of 500 IEQ per well, as previously described (Pedraza et al., 2012). Islet function was determined through static incubation of sequential exposure to basal and elevated glucose levels using the column glucose stimulated insulin response assay, as previously described (Pedraza et al., 2012). Briefly, islets are aliquotted into columns (150IEQ) in a bed of Sephadex beads (GE Healthcare), and exposed to glucose (60 or 300mg/dL) in KRBB buffer (99mM $NaCl_2$, 5mM KCl, 1.2mM KH_2PO_4, 1.2mM $MgSO_4$, 2.6mM $CaCl_2$, 26mM $NaHCO_3$, 25mM HEPES, 0.2% BSA).Samples elute from columns and are collected after a 1hr incubation at low, high, and low glucose concentrations. Insulin content in samples was determined by ELISA (Mercodia).

5.2.8 STATISTICAL ANALYSIS

Data are presented as mean ± standard deviation (s.d.). Univariate differences between groups were evaluated using Student's *t*-test. Statistical analyses were performed using Graphpad Prism 6 for Windows (Graphpad Software).

5.3 RESULTS AND DISCUSSION

5.3.1 CONP SYNTHESIS AND CHARACTERIZATION

CONP solutions were synthesized as described, sonicated to reduce particle aggregation, and dialyzed against PBS to reduce pH and remove excess Dextran and synthesis by-products. CONP solution composition was characterized via Fourier transform infrared (FT-IR) spectroscopy, whereby characteristic bands in the 800-1300 nm range confirmed Dextran coating of the CONP (**Figure 5-2A**). CONP particle size was characterized via dynamic light scattering (DLS) and high resolution transmission electron microscopy (HR-TEM). DLS measurements indicate CONP solutions contain a relatively monodisperse (23.8% polydispersity) distribution of nanoparticles with an average radius of 2.7-9 nm (**Figure 5-2B**). HR-TEM imaging further confirms particulate size, while additionally permitting visualization of the characteristic crystalline CeO2 nanoparticle core (Figure 2C). X-ray photon spectroscopy (XPS) analysis of CONP solutions exhibits spectra for both cerium oxidative states, demonstrating characteristic cerium III (Ce2O3) and IV (CeO2) peaks (**Figure 5-2D**).

To verify the capacity of CONPs to perform enzyme-mimetic electron transfer reactions with reactive oxygen intermediates, CONP solutions were exposed to hydrogen peroxide, peroxidase substrate 3,3',5,5'-Tetramethylbenzidine (TMB), or superoxide. CONPs demonstrate catalase-mimetic behavior through their ability to reduce hydrogen peroxide (H2O2) to water and oxygen. Upon reaction with H2O2, CONP solutions (1 mM) display a red spectral shift (**Figure 5-3A**), which is hypothesized to evolve from the shifting of Cerium atoms from the +4 to +3 oxidative states.(Pirmohamed et al., 2010) The reversible nature of the particles was demonstrated via regression to pre-treatment

spectrum over time. Incubation of TMB with CONPs resulted in rapid TMB oxidation (**Figure 5-3B**), demonstrated via characteristic color shift from clear to blue, with a catalyst concentration-dependent degree of oxidation. We further sought to investigate the capacity of CONP solutions to counteract the free radical superoxide (O2-), whereby superoxide was generated via XA/XO system (see Methods section). As shown in **Figure 5-3C**, the presence of only 1 mM CONP completely abrogated superoxide levels. Overall, these results illustrate the catalytic and reversible activity of the Dextran coated CONP (summarized in **Figure 5-3D**), correlating with previous reports(Asati et al., 2009).

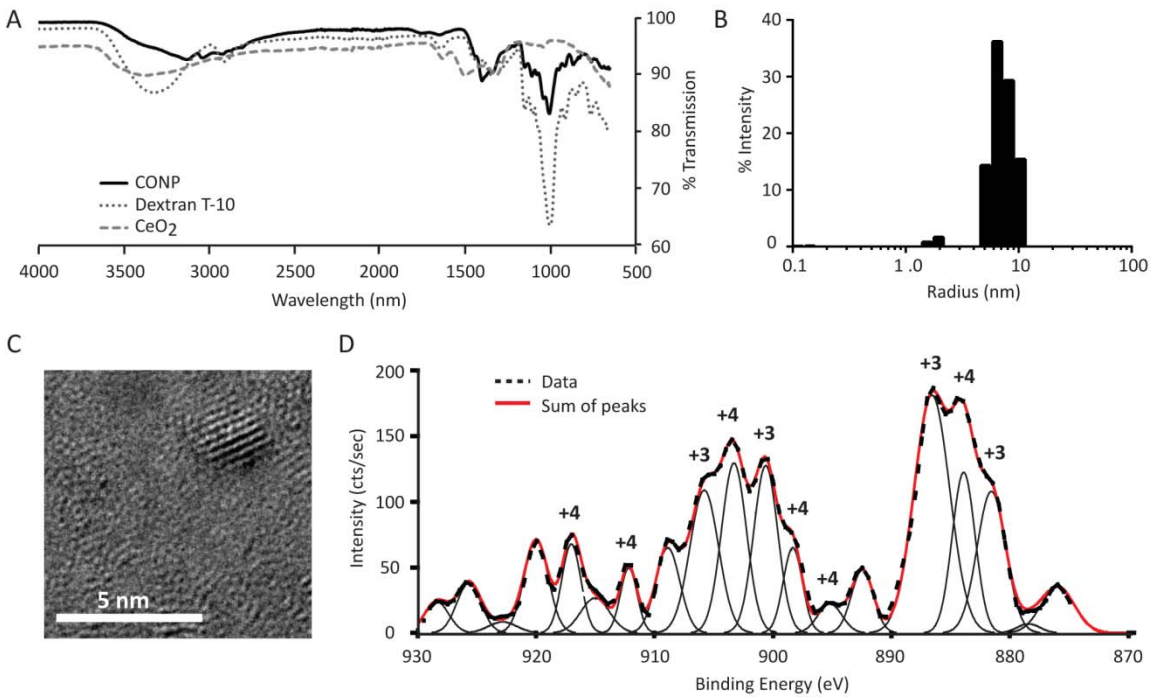

Figure 5-2 Dextran coated cerium oxide nanoparticles (CONP) exhibit characteristics of cerium oxide nanoparticles. A) FTIR of cerium dioxide prior without (CeO_2; dashed grey line) and with (CONP; black line) Dextran coating; Dextran spectra (Dextran T-10; dotted grey line) shown for comparison. B) DLS analysis of CONP particles exhibiting moderate polydispersity. C) HR-TEM image of CONP, illustrating the characteristic crystalline core. D) X-ray photon spectroscopy (XPS) analysis of CONP solutions demonstrating both characteristic cerium +3 (Ce_2O_3) and +4 (CeO_2) peaks.

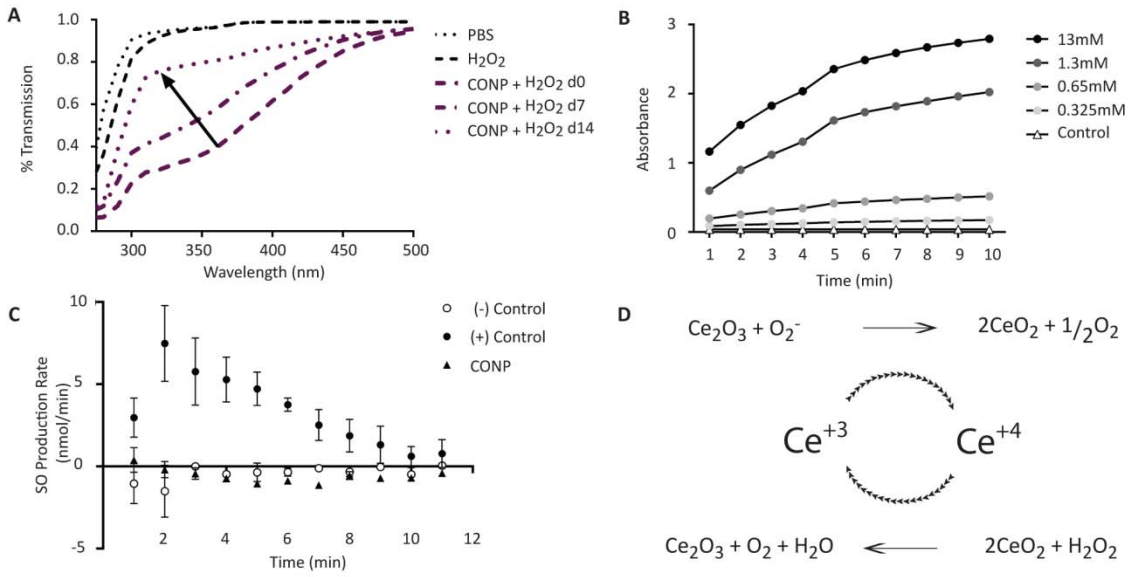

Figure 5-3 CONP in solution exhibit strong catalytic reactivity. A) Reactivity of CONP (1 mM) solutions with H_2O_2 (0.1 mM) via spectroscopic assessment of color shift. Return to initial state is tracked over 14 d. B) Effect of CONP concentration (0 – 13 mM) on TMB oxidation, measured via absorbance shift. C) Neutralization of superoxide, generated via the XA/XO system, as measured through the oxidation of cytochrome C without ($^{(+)}$ control, filled circles) and with CONP (filled diamonds). Additional control with no XA/Xo added ($^{(-)}$ control, open circles) is also shown. D) Hypothesized reactions of CONPs with ROS superoxide and hydrogen peroxide. Error = standard deviation

5.3.2 CYTOTOXIC AND PROTECTIVE EFFECTS OF CONPSOLUTIONS ON BETA CELLS

The cytocompatibility and protective effects of CONP was evaluated via co-incubation of free CONP with MIN6 cells, a murine beta cell line. For these studies, beta cells were incubated for 48 h with 0.1 or 1.0 mM CONP. While a variety of cell types have been evaluated with various CONP formulations, evaluation of CONP cytotoxicity for beta cell lines or primary pancreatic islets in the literature is minimal, with no evaluation of their protective capacity(Pourkhalili et al., 2012; Tsai et al., 2007). In this study, no toxicity was observed at 0.1 mM CONP, while a significant (20%) drop in

viability was detected at 1 mM CONP (**Figure 5-4A**). This correlates with concentration-dependent viability trends observed in experiments performed on other cell types, where investigators utilized similar CONP formulations.(Das et al., 2007; Tarnuzzer et al., 2005) Transmission electron microscopy images (TEM) of cells exposed to 1 mM CONP exhibit internalization of CONP within cellular lysosomes (**Figure 5-5**), indicating the mechanism of the observed CONP cytotoxicity was likely due to interactions with internal cellular structures after nanoparticle internalization. This mechanism of cytotoxicity is common when high concentrations of nanoparticles are present in the bathing media (Celardo et al., 2011; Hussain et al., 2012; Patil, S. et al., 2007a; Stern et al., 2008)

Following establishment of a cytotoxic CONP concentration range, we sought to evaluate the capacity of free CONPs to scavenge superoxide radicals sufficiently in a cell culture system to prevent oxidative damage. The XA/XO system was used to generate superoxide in bathing milieu. **Figure 5-4** demonstrates the detrimental impact of superoxide in control MIN6 cultures, with an 80% decrease in metabolic activity. The addition of CONPs to the media provides a protective effect, whereby MIN6 viability is preserved due to free radical neutralization by the nanoparticles. The protective effect is dose-dependent, with 0.1 mM CONP improving viability 1.5 fold over superoxide treated control cells, and 1.0 mM CONP providing total protection from superoxide, with cell viability levels statistically identical to pre-superoxide treatment levels. Representative live/dead images (**Figure 5-4B)** support metabolic results, wherein a clear decrease in viable cells was observed for superoxide-treated controls, while CONP-treated groups

demonstrate a concentration-dependent increase in viable cells. These results illustrate the potent protective capacity of CONPs against free radical damage for beta cells.

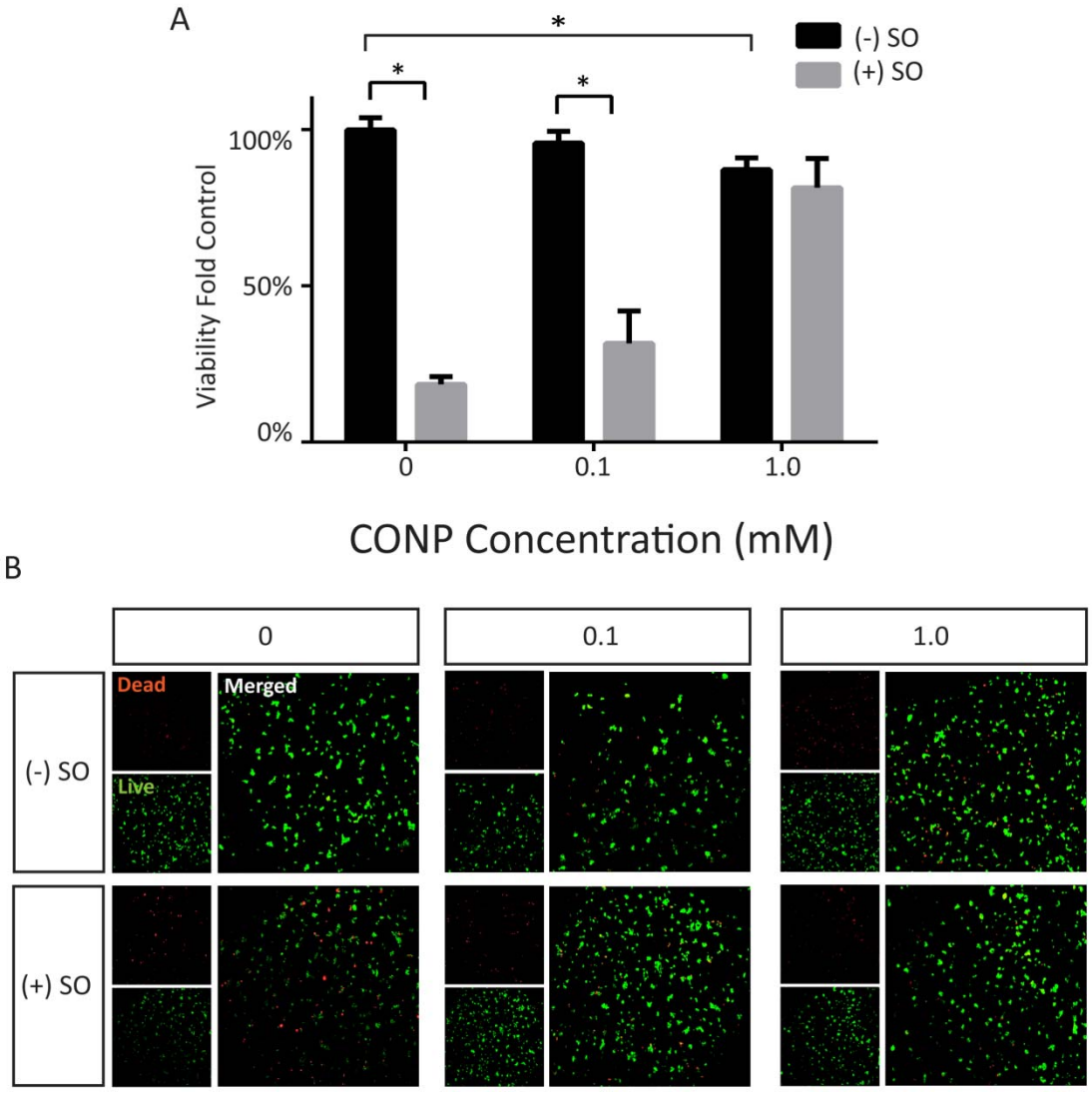

Figure 5-4 CONPs in solution provide cytoprotective effects for beta cells following exposure to superoxide. MIN6 beta cells were co-incubated with CONP (0, 0.1, or 1.0 mM), free in solution, for 48 hr. (A) Beta cell viability was evaluated after exposure to superoxide ($^{(+)}$SO; grey bars) via Alamar Blue. Controls were not exposed to superoxide ($^{(-)}$SO; black bars). Results were normalized to day 0 controls (no CONP, no superoxide). (B) Single plane Live/Dead (live, green; dead, red; merged) confocal imaging for 0, 0.1, and 1.0 mM free CONP. Error = standard deviation *$P < 0.0001$

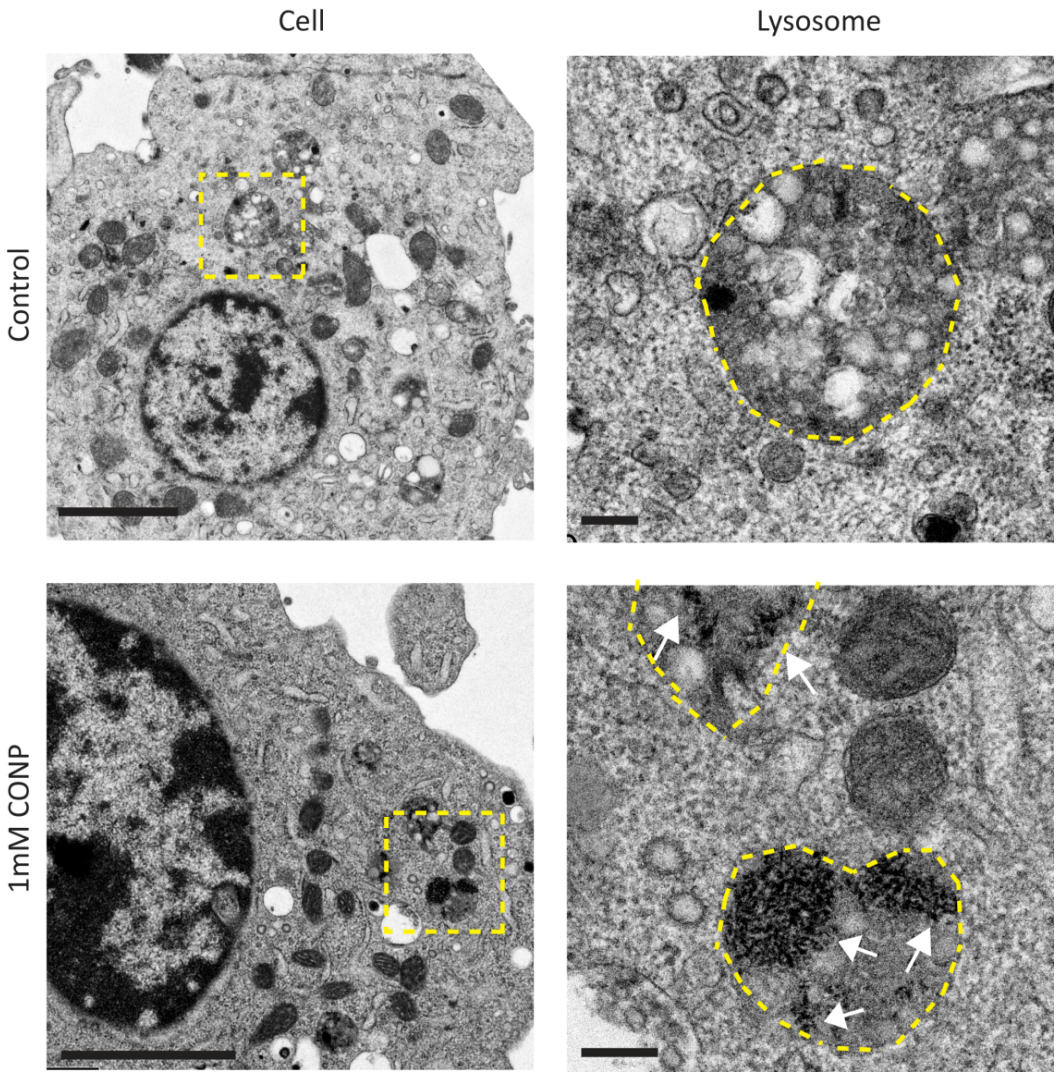

Figure 5-5 TEM imaging of MIN6 cells (left column, scale bars = 2 µm) reveals normal morphology for both control and 1 mM CONP-treated groups. Higher magnification images of cell lysosomes (right column, scale bars = 100 nm) demonstrate phagocytosis of CONPs within the cells, with a localized concentration of nanoparticles in CONP-treated cell lysosomes.

5.3.3 CONP-COMPOSITE ENCAPSULATION HYDROGEL DEVELOPMENT AND CHARACTERIZATION

With the catalytic potency of the CONPs formulations established, we sought to engineer a nanocomposite hydrogel, which would provide localization of CONPs within an encapsulation polymer and minimize cytotoxicity associated with cellular internalization. We explored three common cellular encapsulation hydrogels as platforms for CONP composites: matrigel, agarose, and alginate. These materials vary greatly in composition, pore size, and electrostatic charge. Matrigel is composed of extracellular matrix components (e.g. laminin and collagen), with an average pore size of 2000 nm.(Zaman et al., 2006) Both agarose and alginate are composed of polysaccharide chains, with average pore sizes of 300-400 nm (Pernodet et al., 1997) and 5-200 nm,(Gombotz et al., 1998) respectively. CONP-functionalized gels were fabricated via thorough mixing with the aforementioned materials prior to gelation. For initial evaluation of CONP retention, gel droplets or capsules of approximately 1 mm in diameter were fabricated with CONP concentrations of 0, 1, or 10 mM. The catalytic reactivity of the CONPs within the three materials was visually assessed through the colorimetric reaction of CONP-hydrogel composites with TMB. Generation of oxidized TMB (blue color) was visualized for all CONP-hydrogel composites, indicating reactivity of CONPs within the material (**Figure 5-6A**). Incubation of TMB with hydrogel-only controls resulted in no color change. Of note, for alginate hydrogels only, TMB, following oxidation via embedded CONPs, was retained within the hydrogel. Subsequent studies identified binding interactions between oxidized TMB and alginate hydrogels

(**Figure 5-7A-E**). This interaction was only observed for oxidized TMB. Further, this interaction was found to be independent of CONP presence.

While catalytic activity of the CONPs was observed for all hydrogels, retention of the CONPs within matrigel and agarose hydrogels was poor, as CONPs were detected in the incubating solution within minutes after fabrication (**Figure 5-7H**). CONP release from alginate hydrogels was not detected and reactivity of CONPs within the alginate hydrogel was observed over 1 year post-fabrication (**Figure 5-7F**), demonstrating the high stability of the system. Due to the stability of CONP-alginate composites, future studies were focused on the use of this system.

To quantitatively confirm catalytic activity of the CONP-alginate composite hydrogels, microcapsules doped with varying CONP concentrations (i.e. 0, 0.1, 1.0, and 10 mM) were assessed for their capacity to scavenge ambient hydrogen peroxide. As shown in **Figure 5-6B**, ambient H_2O_2 was cleared from the incubating solution by the CONP-alginate composite hydrogels in a concentration-dependent manner, with 10 mM CONP-alginate microcapsules neutralizing nearly 100% H_2O_2 within 4 h. CONP reactivity may be further confirmed via visualization of the characteristic red spectral shift within the capsules (**Figure 5-6B**, insets).

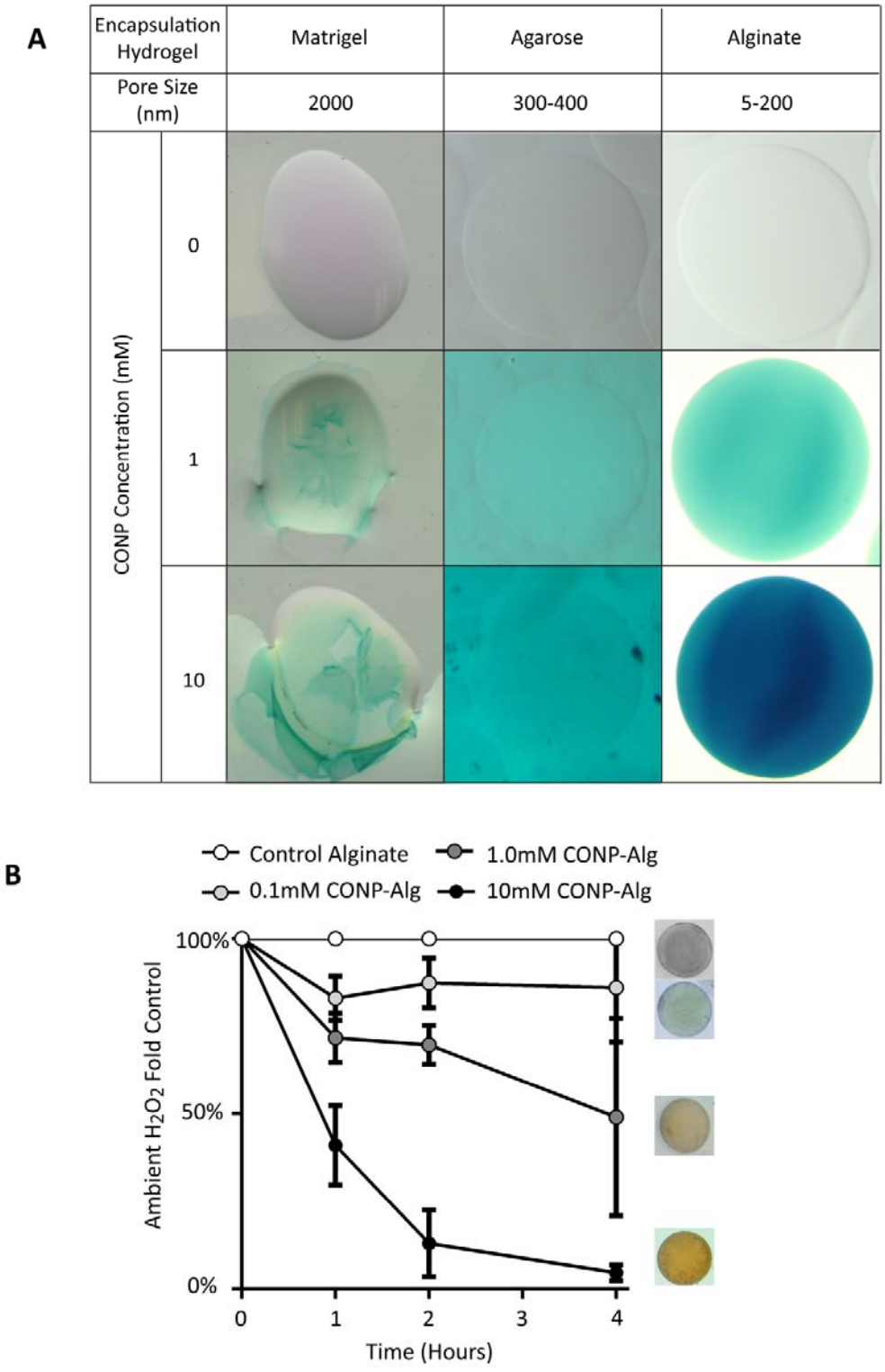

Figure 5-6 CONP within CONP-hydrogel composites retain catalytic activity. CONP (1 or 10 mM) was embedded within matrigel, agarose, or alginate hydrogels and catalytic activity verified via TMB oxidation (color shift to blue) and H_2O_2 scavenging. A) Visualization of TMB oxidation via embedded CONP after 15 min incubation. B)

Detection of ambient H_2O_2 via absorbance assay for CONP-alginate composites loaded with 0, 0.1, 1, 10 mM CONP. Results were normalized to initial ambient H_2O_2 concentration (60 μM) and assessed at 1, 2, and 4 h; CONP-alginate groups are significant ($P < 0.05$) at all time points save for 0.1mM CONP-Alg at 4 hours. Error = standard deviation.

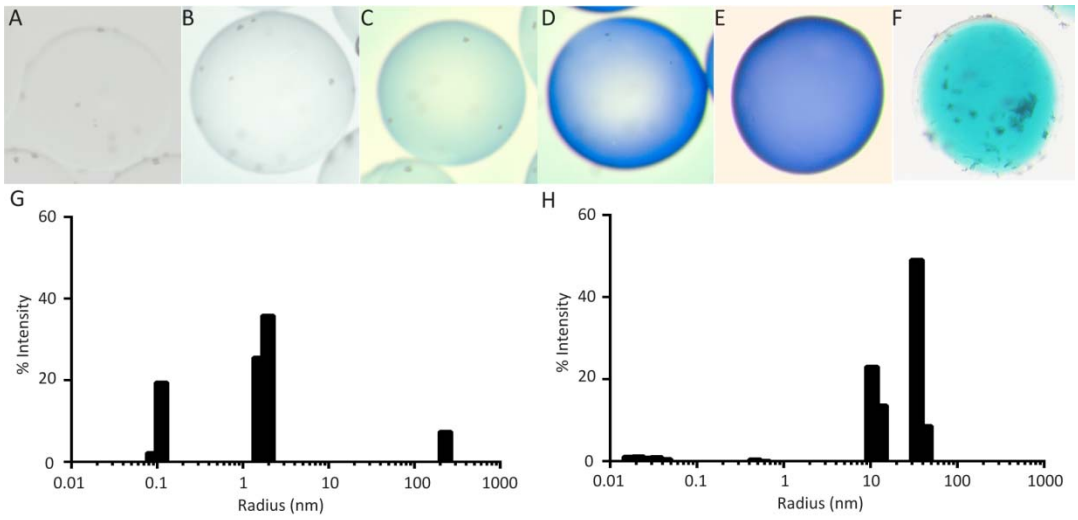

Figure 5-7 CONP retention within alginate and agarose hydrogels. Control alginate beads incubated with TMB and hydrogen peroxidase for 0 (A), 5 (B), 10 (C), and 15 minutes (D) demonstrate gradual color change as TMB is oxidized and penetrates the gels. Control alginate beads incubated with TMB and hydrogen peroxidase for 20 minutes and washed with excess PBS exhibit retention of oxidized TMB (E), likely due to interactions between oxidized TMB and alginate polymer. CONP-alginate retains nanoparticles long-term, as demonstrated by CONP-alginate oxidation of TMB after 1 year (F). DLS analysis of supernatants of CONP-alginate beads (G) and CONP-agarose beads (H) exhibits small debris and CONPs, respectively, further establishing that alginate gels effectively retain the incorporated nanoparticles.

5.3.4 CYTOTOXIC AND CYTOPROTECTIVE EFFECTS OF CONP-ALGINATE ENCAPSULATION GELS

Following identification of a stable CONP-hydrogel composite, we evaluated the potential of this system to protect cells from oxidative stress, as well as to investigate

potential cytotoxic effects. For these studies, MIN6 beta cells were encapsulated within alginate microbeads containing CONP at concentrations of 0, 1, 5, and 10 mM.

Cytotoxicity results for beta cells encapsulated within CONP-alginate composites found no impairment of cellular viability, per metabolic assay, even at 10 mM CONP concentration (**Figure 5-8A**, black bars). In comparison, exposure of cells to only 1 mM CONP free in solution induced statistically significant decreases in cell viability. Cellular internalization of CONPs for cells encapsulated in 10 mM CONP alginate was not observed in TEM images, contrary to the marked presence of CONPs within cellular lysosomes when only 1 mM free CONPs was added to the culture media (**Figure 5-9**). This suggests that entrapment of nanoparticles within the hydrogel decreases the potential for cellular internalization of the nanoparticles, a trend observed for other nanoparticle-hydrogel composites.(Meenach et al., 2009; Travan et al., 2009)

To evaluate the capacity of CONP-alginate composites to provide protection to embedded cells from external oxidative stress, encapsulated cells were exposed to superoxide radicals using the XA/XO system. A two-fold increase in concentration of XA/XO was required for these studies to induce significant cell death, as the time delay imparted by the diffusional barrier and the instability of the radical reduces potency.(Kavdia et al., 2002) Significant protective effects from free radical damage were observed for CONP-alginate composites. For 5 and 10 mM CONP-alginate groups, complete abrogation of free radical damage was observed, where cell viability was statistically identical from untreated controls (**Figure 5-9A**). This trend was further confirmed by Live/Dead imaging of encapsulated cells, where substantial cell death was observed in superoxide treated controls, while CONP-alginate composites demonstrated a

concentration dependent effect (**Figure 5-9B**). These studies illustrate the capacity of CONP-alginate composite hydrogels to provide significant protection of beta cells from oxidative stress.

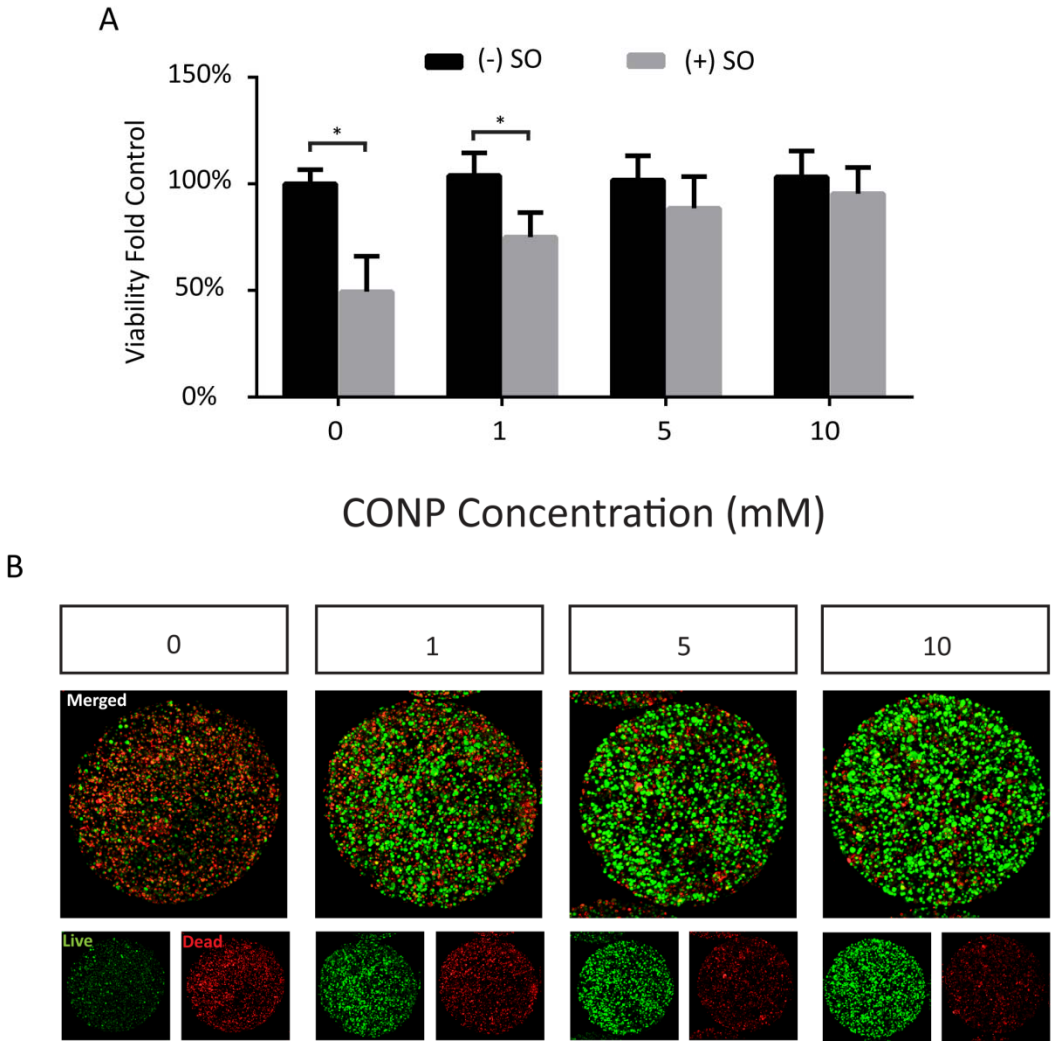

Figure 5-8.CONP-alginate composite hydrogels provide enhanced beta cell cytocompatibility and cytoprotection from oxidative stress. MIN6 beta cells were encapsulated within CONP-alginate hydrogels with varying CONP (0, 1, 5, 10 mM) and cultured for 48 hr. (A) Beta cell viability was evaluated after exposure to superoxide ($^{(+)}$SO; grey bars) via Alamar Blue. Controls were not exposed to superoxide ($^{(-)}$SO; black bars). Results were normalized to day 0 controls (no CONP, no superoxide). (B) Single plane Live/Dead (live, green; dead, red; merged) confocal imaging of beta cells within

alginate microbeads doped with 0, 1, 5, and 10 mM CONP. Error = standard deviation *$P < 0.05$

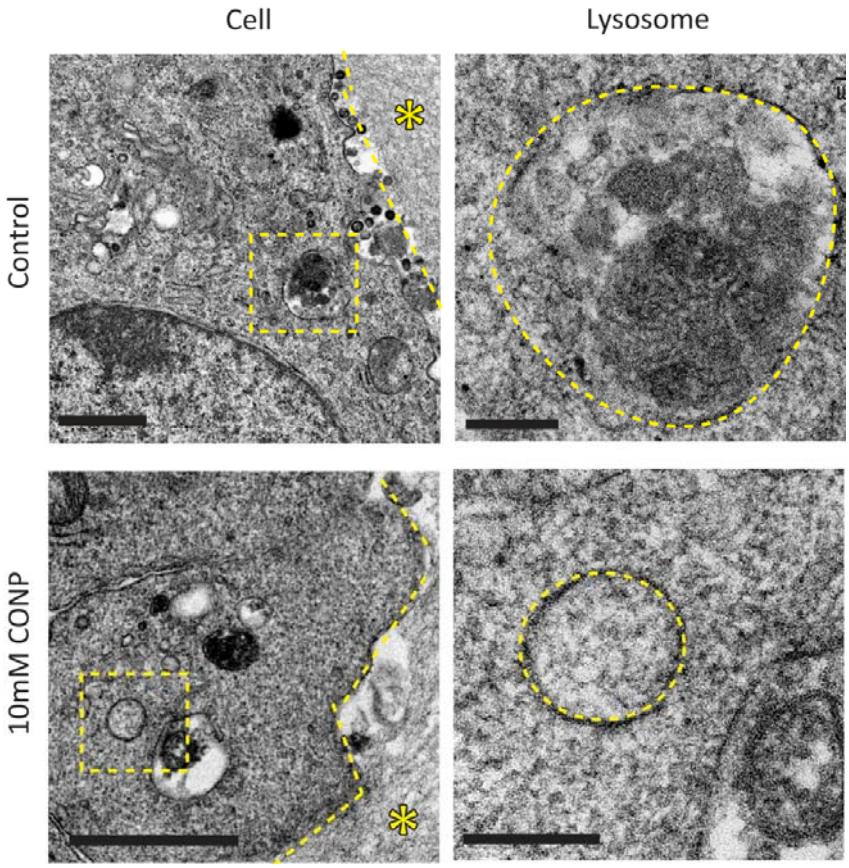

Figure 5-9. TEM imaging of MIN6 encapsulated in control (top row) or 10 mM CONP-alginate gels (bottom). Normal cell morphology was observed for both encapsulation groups (left column, scale bars = 1 μm), illustrating a close interface with encapsulating alginate hydrogel (* alginate hydrogel). High magnification images of a cellular lysosome (right column, scale bars = 200nm) exhibits an internal composition that lacking detectable CONPs for cells entrapped within 10 mM CONP-alginate.

5.3.5 LONG-TERM PROTECTIVE EFFECTS OF SELF-RENEWING CONP-ALGINATE ENCAPSULATION GELS

A notable advantage of CONP is their capacity to self-renew. To investigate the long-term, continuous protective effects of novel CONP-alginate encapsulation hydrogels, MIN6 beta cells, entrapped within control or 10 mM CONP-alginate composite hydrogels were exposed to repeated hits of oxidative stress, specifically day 2 and 6 post-encapsulation. **Figure 5-10** summarizes the effects of superoxide treatment on encapsulated beta cell viability. Following the first exposure to superoxide on day 2, significant impairment of cell viability was observed for control alginate hydrogels. Minimal recovery was observed on day 4. Cells were exposed again to superoxide on day 6, which resulted in significant impairment of cell viability for alginate-only hydrogel controls. A decreased capacity for protection was observed for CONP-alginate composites (e.g. comparison of protection on day 2 versus day 6), although still potent. Overall, for all time points except day 8, the CONP-alginate group exhibited a statistically significant ($p < 0.05$) improvement in viability over alginate-only controls, demonstrating the capacity of these gels to neutralize repeated exposure to superoxide radicals. This is further supported by confocal microscopy imaging of live/dead cells, whereby a significant decrease in the presence of viable beta cells was observed. Of note, the highly proliferative nature of the MIN6 beta cell line provides a means for cellular recovery following free radical damage. Primary islets, however, would exhibit limited ability to recuperate, given their low capacity for proliferation.

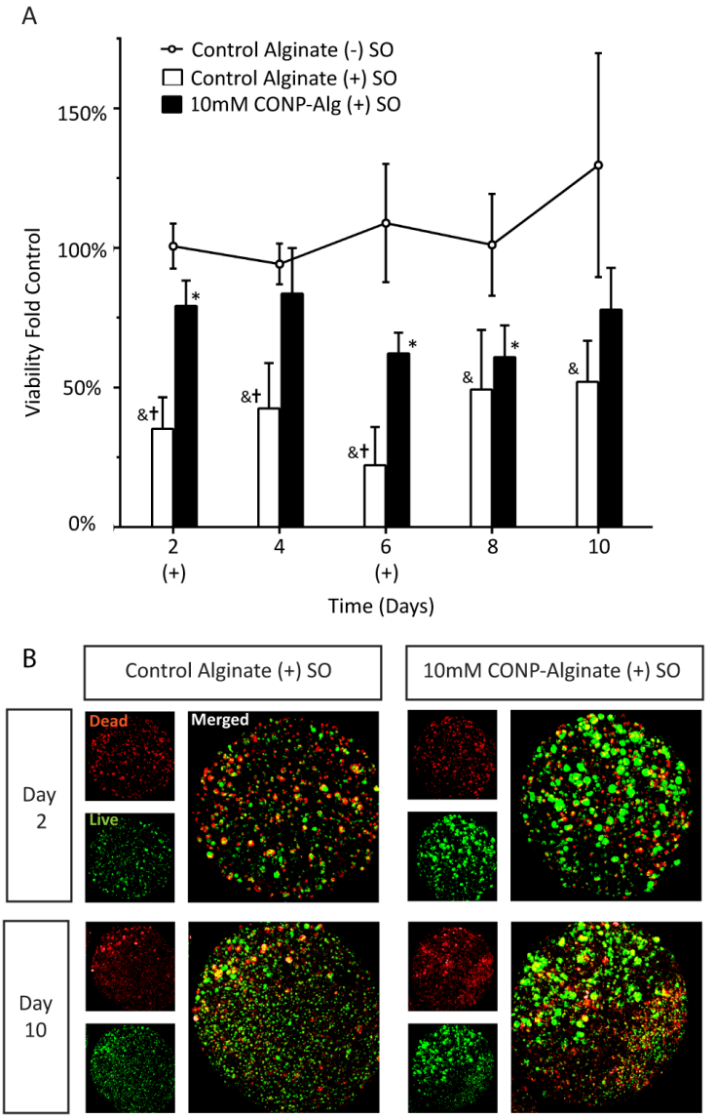

Figure 5-10. CONP-alginate composite hydrogels provide extended beta cell cytoprotection from multiple exposures to oxidative stress. MIN6 beta cells were encapsulated within CONP-alginate hydrogels (10 mM CONP) or control alginate and exposed to superoxide on 2 and 6 post-encapsulation day (indicated by (+)). (A) Beta cell viability was evaluated for groups exposed to superoxide without (open bars) or with CONP (filled bars) via Alamar Blue. Encapsulated controls (no superoxide) are also shown (open circles). Results were normalized to day 0 control (no CONP, no superoxide). (B) Single plane Live/Dead (live, green; dead, red; merged) confocal imaging of beta cells within alginate microbeads without and with CONP are shown at day 2 and 10 post-encapsulation. Error = standard deviation $^{*}P < 0.001$(10mM CONP-Alginate (+) SO vs. control alginate (-) SO), $^{\&}P < 0.005$ (control alginate (+) SO vs. control alginate (-) SO) $^{\dagger}P < 0.0001$ (control alginate (+) SO vs. 10mM CONP-Alginate (+) SO)

5.3.6 PRELIMINARY INVESTIGATIONS INTO CONP SOLUTION AND CONP-ALGINATE IMPACT ON ISLET VIABILITY AND FUNCTION

To assess CONP impact on primary cell viability and function, Lewis Rat islets were exposed to 0, 0.1, 1, or 10 mM CONP solution concentrations in media. As observed with the MIN6 cell line, CONP concentrations up to 0.1 mM demonstrated no toxicity, 1 mM concentrations exhibit a slight drop in viability (26%, p=0.119), and 10 mM results in a significant drop in islet viability (**Figure 5-11A**, black bars). Viability studies were further supported by evaluation of islet function (**Figure 5-11B**), wherein islets demonstrate responsive insulin secretion to environmental glucose at basal (Low 1 and Low 2) and elevated (High) levels at up to 1 mM CONP concentrations. At 10 mM CONP, islets demonstrate significant impairment in function, which correlates with the dramatic loss in metabolic function observed at this concentration.

Islets were encapsulated in CONP-alginate at concentrations of 0, 0.1, 1.0, and 10 mM CONP, and metabolic activity assessment (**Figure 5-11A**, gray bars) indicates no significant toxicity up to 10 mM CONP, which demonstrates a significant improvement in the biocompatibility of this delivery strategy over bolus methods. These findings agree with the MIN6 studies above, and Live/Dead imaging of encapsulated and free cells (**Figure 5-11C**) emphasizes the drastic reduction in non-viable cells (red) present when CONPs are incorporated into alginate rather than the culture medium. This illustrates the advantages of CONP-alginate over other delivery methods, where CONPs may be localized to the site with minimal toxic effects to donor or host cells.

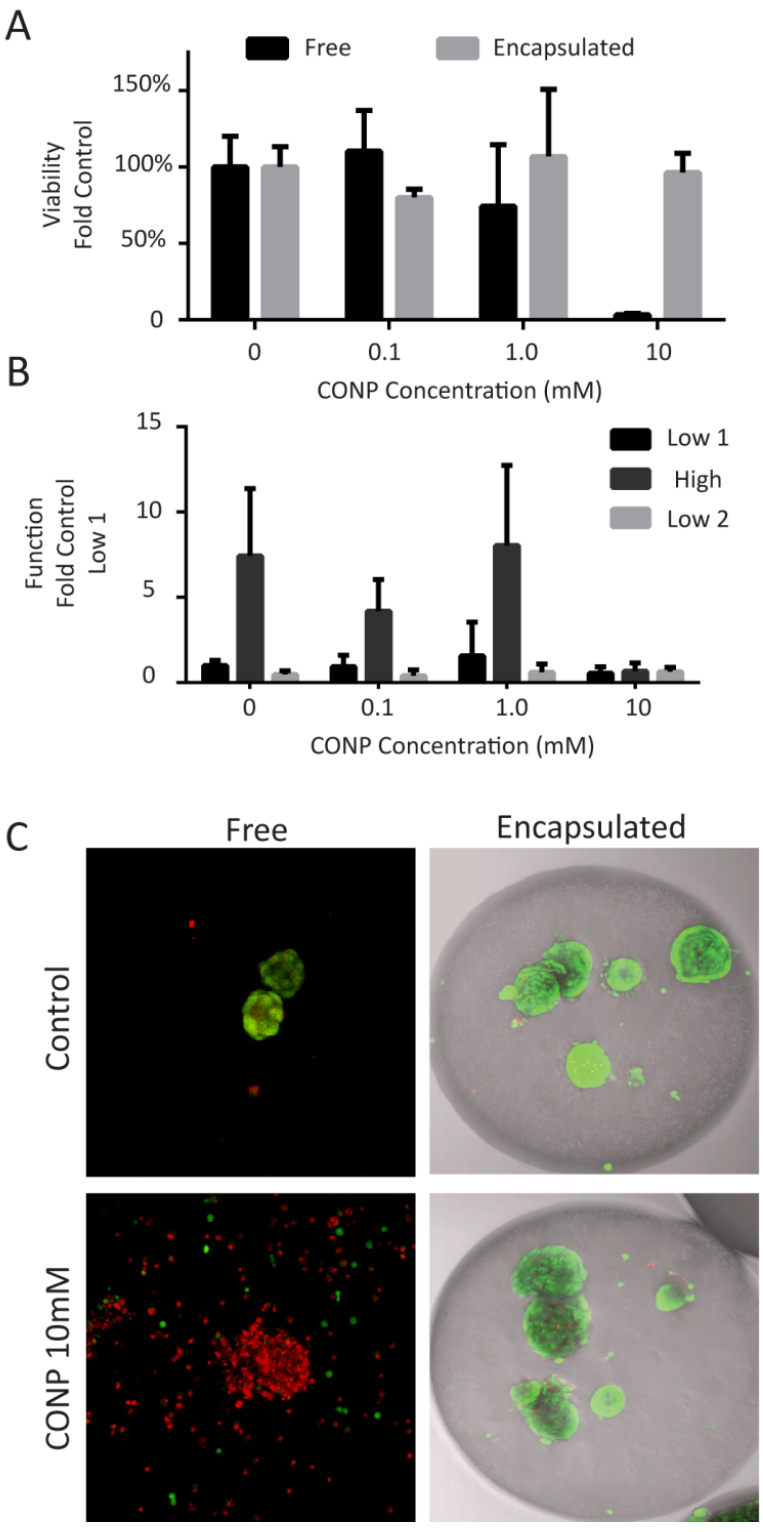

Figure 5-11. Rat islets exposed to CONP solutions and encapsulated within CONP-alginate. CONP solutions (black bars) demonstrate minimal impact on islet viability up to 0.1mM (A), with a slight drop in viability at 1mM, and a significant reduction at

10mM, whereas no significant toxicity is seen with CONP-alginate (gray bars) up to 10mM. GSIR function tests on islets incubated in CONP solutions indicate no significant impact up to 1mM CONP (B), and total loss of function at 10mM CONP. Live/Dead imaging (C) demonstrates the significant reduction in dead cells within the islets when CONPs are embedded within the alginate.

5.4 CONCLUSIONS

Herein, we designed a catalytically antioxidant hydrogel capable of efficiently scavenging free radicals, a major contributor to cell graft death post-transplantation. This hydrogel can also serve as a cellular encapsulation system to provide a bioactive barrier between transplanted cells and ambient radicals. This novel, nanocomposite CONP-alginate hydrogel provides significant protection to encapsulated cells, with the additional advantage of negligible cytotoxicity at nanoparticle concentrations of ten–fold higher than free CONP. For translational studies, this approach will provide enhanced cytocompatibility and safety over bolus injection methods. Consequently, incorporation of CONPs to the encapsulation material retains the particles to the site of transplantation, enabling the localized delivery of potent doses of nanoparticles with reduced concern for down-stream effects.

Chapter 6. Conclusions and Recommendations for Future Work

6.1 SUMMARY AND CONCLUDING REMARKS

Clinical islet transplantation has demonstrated superior blood glucose control and the promise of cell-based transplantation for the treatment of diabetes; however, one of the most pivotal challenges within the islet transplant model is inflammation. Inflammation remains a key issue in the engineering of a transplant site with stable islet engraftment and minimal fibrotic remodeling. Thus, the development of novel strategies to suppress this response in the islet microenvironment could be highly beneficial.

The central hypothesis of this dissertation was that application of anti-inflammatory biomaterials, optimized for the islet microenvironment, would improve beta cell and islet viability and function. We pursued this aim through two strategies: the novel application of localized drug delivery constructs in an islet transplant site utilizing a well-established PDMS platform; and the development of novel self-renewing catalytic antioxidant encapsulation hydrogels. The first strategy provided a means for tailored drug delivery, with optimized geometry and drug loading for application at the transplant site, wherein both the acute and chronic phases of inflammation may be addressed by application of an appropriate drug and dosage. The second strategy provided beta cell protection from harmful radical byproducts of inflammation through an antioxidant hydrogel, capable of shielding encapsulated cells for the lifetime of the graft.

6.1.1 DEXAMETHASONE-ELUTING PDMS CONSTRUCTS FOR LOCALIZED SUPPRESSION OF INFLAMMATION IN AN ISLET TRANSPLANT SITE

Dex-PDMS constructs of varying geometries (rod, cage and scaffold) were developed and assessed for drug release profile, and finite element modeling was utilized to optimize the key characteristics of localized delivery dose and spatial delivery (external or internal) within the islet graft. Dex-PDMS scaffolds exhibited the fastest rate of delivery due to high surface area-to-volume (SA/V) ratio; Dex-PDMS rod and cage geometries, which possess comparable SA/V ratios, exhibited controlled plateau release ranges amenable to facile optimization through variation of total surface area and drug loading. The three geometries were explored in rodent transplant models and engraftment assessed via histopathology. Our observations found that the rate of local drug delivery correlated highly with a reduction in remodeling; spatial characteristics of constructs also impacted remodeling, as evidenced by limited tissue in-growth proximal to Dex-PDMS constructs.

The most promising Dex-PDMS prototype was further evaluated for impact on inflammatory cells and primary islet. *In vitro* studies with monocytes and macrophages confirmed the anti-inflammatory effects of Dex-PDMS constructs, while islet studies exhibited minimal impact of locally delivered drug dose on primary cell function and viability. *In vivo* studies demonstrated minimal, but measurable, systemic Dex levels in mice, and an insignificant impact of local Dex-PDMS rods on graft function and efficacy of function. Histological assessments and FACS analysis of infiltrating cell phenotypes suggest local delivery of Dex was sufficient to reduce the presence of inflammatory cells at the transplant site. Reduced inflammatory cell infiltration at the transplant site, in

conjunction with low circulating Dex levels and the insignificant impact of local drug on graft function, demonstrate the feasibility of this strategy for application in a variety of transplant models.

6.1.2 CATALYTIC, ANTIOXIDANT CONP-ALGINATE ENCAPSULATION HYDROGELS FOR BETA CELL PROTECTION

CONPs were synthesized and fully characterized for composition and activity prior to exposure to a continuous beta cell line to evaluate cytotoxicity. The cytoprotective capacity of CONP solutions was demonstrated through the scavenging of potent superoxide radicals, providing measurable protective effects to the exposed beta cells. The development of CONP-functionalized encapsulation hydrogels was explored through the investigation of three common materials: alginate, agarose and matrigel. High CONP retention within alginate favored its use in subsequent studies.

CONP-alginate encapsulation hydrogels not only retained catalytic activity, but demonstrated minimal cytotoxicity in beta cells and islets, even at a dose 10-fold higher than that found to impart cytotoxicity for CONP solution. This illustrates the improved cytocompatibility of CONP-alginate gels over bolus delivery methods, where high concentrations of catalytic antioxidant may be localized to the transplant site while eliminating down-stream and systemic effects. CONP-alginate hydrogels convey significant cytoprotective effects to encapsulated beta cells, even after multiple exposures to toxic levels of superoxide radicals. The potent, renewable antioxidant activity and negligible toxicity of CONP-alginate gels makes this versatile biomaterial favorable for use in a wide variety of tissue engineering and transplant applications.

6.2 RECOMMENDATIONS FOR FUTURE WORK

The overarching goal of this work was to develop biomaterials capable of reducing inflammation and its impact on the islet microenvironment for the treatment of type I diabetes mellitus. The two strategies demonstrated within this dissertation met the primary objective of anti-inflammatory biomaterial development through alternative methods. Drug-eluting PDMS constructs designed for local delivery in an islet transplant site demonstrated the capacity for facile tailoring of therapeutic agent delivery through optimization of geometry and drug loading, as well as a marked impact on graft remodeling. CONP-alginate hydrogels conveyed potent, long-term antioxidant protection to beta cells, providing a cytocompatible method for localization of the therapeutic agent. Despite these achievements, future work is necessary in the optimization of these technology platforms for application in the islet transplant model.

In the development of a drug-eluting construct for localized suppression of inflammation, future work is recommended to further optimize geometry and drug loading. The construct designs presented herein achieved the goal of reduction in localized inflammation; however, trends in graft infiltration suggest that the optimal therapeutic dose lies in the range of 0.5-1.0 μg per day, with remodeling dependent on graft proximity to the construct. To achieve optimal three dimensional delivery at the periphery of the graft, a balance must be struck between construct geometry spatial structure and surface area-to-volume ratio. Future work focusing on COMSOL modeling of three-dimensional constructs to achieve this balance would improve and facilitate the application of this technology. Further, given the toxicity of dexamethasone to islets and host cell migration, it is likely not the ideal candidate for delivery in an islet transplant

model. Thus, future studies focusing on alternative drugs that demonstrate minimal impact on islet function and positive graft remodeling are warranted.

The CONP-alginate hydrogels developed herein were optimized for physical entrapment of nanoparticles within the biomaterial. The CONP formulation synthesized in our study utilizes a Dextran polymer coating as a surfactant to prevent particle aggregation in solution. While this coating enables the handling of CONP solutions at high concentrations, the stability of this formulation is limited due to weak interactions between Dextran and the nanoparticle surface, which results in particle aggregation after prolonged incubations at dilutions below 40 mM. The instability of this coating limits the capacity for covalent linkage of nanoparticles to biomaterials.

Future studies in the development of CONP-functionalized biomaterials would benefit from investigations into alternative coatings that are more amenable to covalent conjugation to biomaterials, such as PEG(Karakoti et al., 2009; Qi, L. et al., 2008) and PAA(Sehgal et al., 2005). Previous studies have demonstrated the potential for toxicity due to systemic nanoparticle exposure (Nel et al., 2006; Tsuji et al., 2006), and for CONPs in particular (Lin et al., 2006; Ma et al., 2010). Therefore, implementation of CONP-biomaterial technologies would optimally entail the physical tethering of CONPs to materials in order to minimize the potential for systemic exposure.

Additionally, the studies herein preliminarily investigated the effect of CONP solutions on primary islet viability and function, as well as the cytotoxic effects of CONP-alginate. Future studies are recommended to investigate the impact of CONP-alginate encapsulation hydrogels on islet function *in vitro*, as well as the potential for these gels to convey long-term *in vivo* cytoprotection in an islet transplant model.

References

Allen, T. M., et al. (2004). Drug delivery systems: entering the mainstream. *Science, 303*(5665), 1818-1822.

Anderson, J. M. (1988). Inflammatory response to implants. *ASAIO Trans, 34*(2), 101-107.

Anderson, J. M. (2001). Biological responses to materials. *Annual Review of Materials Research, 31*, 81-110.

Asati, A., et al. (2009). Oxidase-like activity of polymer-coated cerium oxide nanoparticles. *Angew Chem Int Ed Engl, 48*(13), 2308-2312.

Baecher-Allan, C., et al. (2006). Human regulatory T cells and their role in autoimmune disease. *Immunol Rev, 212*, 203-216.

Barshes, N. R., et al. (2005). Inflammation-mediated dysfunction and apoptosis in pancreatic islet transplantation: implications for intrahepatic grafts. *J Leukoc Biol, 77*(5), 587-597.

Bennet, W., et al. (2000). Isolated human islets trigger an instant blood mediated inflammatory reaction: implications for intraportal islet transplantation as a treatment for patients with type 1 diabetes. *Ups J Med Sci, 105*(2), 125-133.

Berman, D. M., et al. (2007). Interference with tissue factor prolongs intrahepatic islet allograft survival in a nonhuman primate marginal mass model. *Transplantation, 84*(3), 308-315.

Berman, D. M., et al. (2009). Long-term survival of nonhuman primate islets implanted in an omental pouch on a biodegradable scaffold. *Am J Transplant, 9*(1), 91-104.

Berney, T., et al. (2004). Immunosuppression for pancreatic islet transplantation. *Transplant Proc, 36*(2 Suppl), 362S-366S.

Bocca, N., et al. (2010). Long-term islet allograft survival in a biohybrid device by locally delivered immunosuppression. *Am. J. Transplant., 10*(S4), 149-149.

Bocca, N., et al. (2008). Soft corticosteroids for local immunosuppression: exploring the possibility for the use of loteprednol etabonate for islet transplantation. *Pharmazie, 63*(3), 226-232.

Borg, D., et al. (2011). The use of biomaterials in islet transplantation. *Current Diabetes Reports, 11*(5), 434-444.

Brady, A., et al. (2013). Pro-angiogenic hydrogels within macroporous scaffolds enhances islet engraftment in an extrahepatic site. *Tissue Engineering, in press*.

Brandt, W. W. (1959). Model calculation of the temperature dependence of small molecule diffusion in high polymers. *Journal of Physical Chemistry, 63*(7), 1080-1084.

Broe, G. A., et al. (2000). Anti-inflammatory drugs protect against Alzheimer disease at low doses. *Arch Neurol, 57*(11), 1586-1591.

Buchwald, P. (2008). Glucocorticoid receptor binding: a biphasic dependence on molecular size as revealed by the bilinear LinBiExp model. *Steroids, 73*(2), 193-208.

Buchwald, P., et al. (2010). Feasibility of localized immunosuppression: 1. Exploratory studies with glucocorticoids in a biohybrid device designed for cell transplantation. *Pharmazie, 65*(6), 421-428.

Buchwald, P., et al. (2009). Quantitative assessment of islet cell products: estimating the accuracy of the existing protocol and accounting for islet size distribution. *Cell Transplant, 18*(10), 1223-1235.

Bumajdad, A., et al. (2009). Cerium oxide nanoparticles prepared in self-assembled systems. *Adv Colloid Interface Sci, 147-148*, 56-66.

Celardo, I., et al. (2011). Pharmacological potential of cerium oxide nanoparticles. *Nanoscale, 3*(4), 1411-1420.

Chatenoud, L. (2008). Chemical immunosuppression in islet transplantation--friend or foe? *N Engl J Med, 358*(11), 1192-1193.

Chen, B., et al. (1998). Diffusion and reaction of nitric oxide in suspension cell cultures. *Biophys J, 75*(2), 745-754.

Cheung, C. Y., et al. (2006). Synthesis of immunoisolation barriers that provide localized immunosuppression for encapsulated pancreatic islets. *Bioconjug Chem, 17*(4), 1036-1042.

Cheung, C. Y., et al. (2008). Synthesis of polymerizable superoxide dismutase mimetics to reduce reactive oxygen species damage in transplanted biomedical devices. *Adv Funct Mater, 18*(20), 3119-3126.

Chiba, K., et al. (2005). Immunosuppressive activity of FTY720, sphingosine 1-phosphate receptor agonist: I. Prevention of allograft rejection in rats and dogs by FTY720 and FTY720-phosphate. *Transplant Proc, 37*(1), 102-106.

Cohen, H. J., et al. (1978). Superoxide production by digitonin-stimulated guinea pig granulocytes. The effects of N-ethyl maleimide, divalent cations; and glycolytic and mitochondrial inhibitors on the activation of the superoxide generating system. *J Clin Invest, 61*(4), 1088-1096.

Colon, J., et al. (2009). Protection from radiation-induced pneumonitis using cerium oxide nanoparticles. *Nanomedicine, 5*(2), 225-231.

Cronstein, B. N., et al. (1992). A mechanism for the antiinflammatory effects of corticosteroids: the glucocorticoid receptor regulates leukocyte adhesion to endothelial cells and expression of endothelial-leukocyte adhesion molecule 1 and intercellular adhesion molecule 1. *Proc Natl Acad Sci U S A, 89*(21), 9991-9995.

Croxatto, H. B. (2002). Progestin implants for female contraception. *Contraception, 65*(1), 15-19.

Cui, H., et al. (2009). Long-term metabolic control of autoimmune diabetes in spontaneously diabetic nonobese diabetic mice by nonvascularized microencapsulated adult porcine islets. *Transplantation, 88*(2), 160-169.

Das, M., et al. (2007). Auto-catalytic ceria nanoparticles offer neuroprotection to adult rat spinal cord neurons. *Biomaterials, 28*(10), 1918-1925.

Di Colo, G. (1992). Controlled drug release from implantable matrices based on hydrophobic polymers. *Biomaterials, 13*(12), 850-856.

Drews, G., et al. (2010). Oxidative stress and beta-cell dysfunction. *Pflügers Archiv - European Journal of Physiology, 460*(4), 703-718.

Freise, C. E., et al. (1991). Demonstration of local immunosuppression with methylprednisolone in the sponge matrix allograft model. *Transplantation, 52*(2), 318-325.

Frenning, G., et al. (2005). Finite element analysis of the release of slowly dissolving drugs from cylindrical matrix systems. *Journal of Controlled Release, 107*(2), 320-329.

Fridovich, I. (1970). Quantitative aspects of the production of superoxide anion radical by milk xanthine oxidase. *J Biol Chem, 245*(16), 4053-4057.

Frisch, H. L., et al. (1983). Diffusion of small molecules in polymers. *Crc Critical Reviews in Solid State and Materials Sciences, 11*(2), 123-187.

Fu, J. C., et al. (1973). Drug-incorporated silicone discs as sustained release capsules. I. Chloroquine diphosphate. *Journal of Biomedical Materials Research, 7*(1), 71-78.

Fu, Y., et al. (2010). Drug release kinetics and transport mechanisms of non-degradable and degradable polymeric delivery systems. *Expert Opinion on Drug Delivery, 7*(4), 429-444.

Fukudome, D., et al. (2008). The radical scavenger edaravone counteracts diabetes in multiple low-dose streptozotocin-treated mice. *Eur J Pharmacol, 583*(1), 164-169.

Galdi, I., et al. (2012). Drug release from matrix systems: analysis by finite element methods. *Heat and Mass Transfer, 48*(3), 519-528.

Gombotz, W. R., et al. (1998). Protein release from alginate matrices. *Advanced Drug Delivery Reviews, 31*(3), 267-285.

Goulding, N. J. (2004). The molecular complexity of glucocorticoid actions in inflammation - a four-ring circus. *Curr Opin Pharmacol, 4*(6), 629-636.

Greenwald, R. J., et al. (2005). The B7 family revisited. *Annu Rev Immunol, 23*, 515-548.

Griendling, K. K., et al. (2003). Oxidative stress and cardiovascular injury: part I: basic mechanisms and in vivo monitoring of ROS. *Circulation, 108*(16), 1912-1916.

Guo, Z., et al. (2001). Immunotherapy with nondepleting anti-CD4 monoclonal antibodies but not CD28 antagonists protects islet graft in spontaneously diabetic nod mice from autoimmune destruction and allogeneic and xenogeneic graft rejection. *Transplantation, 71*(11), 1656-1665.

Habicht, A., et al. (2006). Novel insights into the mechanism of action of FTY720 in a transgenic model of allograft rejection: implications for therapy of chronic rejection. *The Journal of Immunology, 176*(1), 36-42.

Hafiz, M. M., et al. (2005). Immunosuppression and procedure-related complications in 26 patients with type 1 diabetes mellitus receiving allogeneic islet cell transplantation. *Transplantation, 80*(12), 1718-1728.

Harlan, D. M., et al. (2009). Current advances and travails in islet transplantation. *Diabetes, 58*(10), 2175-2184.

Heckert, E. G., et al. (2008). The role of cerium redox state in the SOD mimetic activity of nanoceria. *Biomaterials, 29*(18), 2705-2709.

Ho, E., et al. (1999). Antioxidants, NFkappaB activation, and diabetogenesis. *Proc Soc Exp Biol Med, 222*(3), 205-213.

Hori, Y., et al. (1996). Differential effects of angiostatic steroids and dexamethasone on angiogenesis and cytokine levels in rat sponge implants. *Br J Pharmacol, 118*(7), 1584-1591.

Hosseini, A., et al. (2013). Antiapoptotic effects of cerium oxide and yttrium oxide nanoparticles in isolated rat pancreatic islets. *Hum Exp Toxicol, 32*(5), 544-553.

Huang, X., et al. (2001). On the importance and mechanisms of burst release in matrix-controlled drug delivery systems. *J Control Release, 73*(2-3), 121-136.

Hume, P. S., et al. (2011a). Polymerizable superoxide dismutase mimetic protects cells encapsulated in poly(ethylene glycol) hydrogels from reactive oxygen species-mediated damage. *J Biomed Mater Res A, 99*(1), 29-37.

Hume, P. S., et al. (2011b). Functionalized PEG hydrogels through reactive dip-coating for the formation of immunoactive barriers. *Biomaterials, 32*(26), 6204-6212.

Hussain, S., et al. (2012). Cerium dioxide nanoparticles induce apoptosis and autophagy in human peripheral blood monocytes. *ACS Nano, 6*(7), 5820-5829.

Johansson, E. D., et al. (2004). New delivery systems in contraception: vaginal rings. *Am J Obstet Gynecol, 190*(4 Suppl), S54-59.

Johansson, H., et al. (2005). Tissue factor produced by the endocrine cells of the islets of langerhans is associated with a negative outcome of clinical islet transplantation. *Diabetes, 54*, 1755-1762.

Johansson, U., et al. (2003). Inflammatory mediators expressed in human islets of Langerhans: implications for islet transplantation. *Biochem Biophys Res Commun, 308*, 474-479.

Kajihara, M., et al. (2001). Development of a new drug delivery system for protein drugs using silicone (II). *J Control Release, 73*(2-3), 279-291.

Kalliokoski, O., et al. (2010). Distribution and time course of corticosterone excretion in faeces and urine of female mice with varying systemic concentrations. *Gen Comp Endocrinol, 168*(3), 450-454.

Karakoti, A. S., et al. (2009). PEGylated nanoceria as radical scavenger with tunable redox chemistry. *J Am Chem Soc, 131*(40), 14144-14145.

Kavdia, M., et al. (2002). Free radical profiles in an encapsulated pancreatic cell matrix model. *Ann Biomed Eng, 30*(5), 721-730.

Kenyon, N., et al. (2010). Engineering alternative islet implant sites in a nonhuman primate model. *Transplantation, 90*(2S), 232.

Kenyon, N., et al. (2011). Scaffolds within an omental pouch site support long term survival of allogeneic, nonhuman primate islets. *Amer J Transplant, 11*(S2), 117.

Kenyon, N. S., et al. (1998). Islet transplantation: present and future perspectives. *Diabetes Metab Rev, 14*(4), 303-313.

Kim, H. I., et al. (2010a). Comparison of four pancreatic islet implantation sites. *J Korean Med Sci, 25*(2), 203-210.

Kim, J., et al. (2008). Extended delivery of ophthalmic drugs by silicone hydrogel contact lenses. *Biomaterials, 29*(14), 2259-2269.

Kim, J., et al. (2010b). Extended release of dexamethasone from silicone-hydrogel contact lenses containing vitamin E. *J. Control. Release, 148*(1), 110-116.

Kimoto, K., et al. (2003). Gliclazide protects pancreatic beta-cells from damage by hydrogen peroxide. *Biochem Biophys Res Commun, 303*(1), 112-119.

Kizilel, S., et al. (2010). Encapsulation of pancreatic islets within nano-thin functional polyethylene glycol coatings for enhanced insulin secretion. *Tissue Eng Part A, 16*(7), 2217-2228.

Kojima, Y., et al. (1996). Polymer conjugation to Cu,Zn-SOD and suppression of hydroxyl radical generation on exposure to H_2O_2: improved stability of SOD in vitro and in vivo. *Journal of Bioactive and Compatible Polymers, 11*(3), 169-190.

Korsgren, O., et al. (2009). Improving islet transplantation: a road map for a widespread application for the cure of persons with type I diabetes. *Curr Opin Organ Transplant, 14*(6), 683-687.

Korsvik, C., et al. (2007). Superoxide dismutase mimetic properties exhibited by vacancy engineered ceria nanoparticles. *Chem Commun (Camb)*(10), 1056-1058.

Koulmanda, M., et al. (2012). Alpha 1-antitrypsin reduces inflammation and enhances mouse pancreatic islet transplant survival. *Proc Natl Acad Sci U S A, 109*(38), 15443-15448.

Krautz, C., et al. (2013). Effects of immunosuppression on alpha and beta cell renewal in transplanted mouse islets. *Diabetologia, 56*(7), 1596-1604.

Lambillotte, C., et al. (1997). Direct glucocorticoid inhibition of insulin secretion. An in vitro study of dexamethasone effects in mouse islets. *J. Clin. Invest., 99*(3), 414-423.

Langer, R. (1983). Implantable controlled release systems. *Pharmacol Ther, 21*(1), 35-51.

Langer, R. S., et al. (1981). Present and future applications of biomaterials in controlled drug delivery systems. *Biomaterials, 2*(4), 201-214.

Lenzen, S., et al. (1996). Low antioxidant enzyme gene expression in pancreatic islets compared with various other mouse tissues. *Free Radic Biol Med, 20*(3), 463-466.

Li, X., et al. (2004). Metallothionein protects islets from hypoxia and extends islet graft survival by scavenging most kinds of reactive oxygen species. *J Biol Chem, 279*(1), 765-771.

Li, Z., et al. (2009). Injectable, highly flexible, and thermosensitive hydrogels capable of delivering superoxide dismutase. *Biomacromolecules, 10*(12), 3306-3316.

Lin, W. S., et al. (2006). Toxicity of cerium oxide nanoparticles in human lung cancer cells. *International Journal of Toxicology, 25*(6), 451-457.

Logie, J. J., et al. (2010). Glucocorticoid-mediated inhibition of angiogenic changes in human endothelial cells is not caused by reductions in cell proliferation or migration. *PLoS One, 5*(12), e14476.

Ma, J. Y., et al. (2010). Cerium oxide nanoparticle-induced pulmonary inflammation and alveolar macrophage functional change in rats. *Nanotoxicology*.

Maeda, H., et al. (2004). Study on accelerated evaluation system for release profiles of covered-rod type silicone formulation using indomethacin as a model drug. *J Control Release, 94*(2-3), 337-349.

Malcolm, K., et al. (2003). Influence of silicone elastomer solubility and diffusivity on the in vitro release of drugs from intravaginal rings. *J Control Release, 90*, 217-225.

Malcolm, R. K., et al. (2004). Controlled release of a model antibacterial drug from a novel self-lubricating silicone biomaterial. *J Control Release, 97*(2), 313-320.

Mancarella, R., et al. (2008). Beneficial effect of the nonpeptidyl low molecular weight radical scavenger IAC on cultured human islet function. *Cell Transplant, 17*(10-11), 1271-1276.

Marzorati, S., et al. (2009). Effects of systemic immunosuppression on islet engraftment and function into a subcutaneous biocompatible device. *Transplant Proc, 41*(1), 352-353.

Mattson, D., et al. (2004). Heat shock and the activation of AP-1 and inhibition of NF-kappa B DNA-binding activity: possible role of intracellular redox status. *Int J Hyperthermia, 20*(2), 224-233.

McDaniel, M. L., et al. (1996). Cytokines and nitric oxide in islet inflammation and diabetes. *Proc Soc Exp Biol Med, 211*(1), 24-32.

Meenach, S. A., et al. (2009). Biocompatibility analysis of magnetic hydrogel nanocomposites based on poly(N-isopropylacrylamide) and iron oxide. *Journal of Biomedical Materials Research Part A, 91A*(3), 903-909.

Merani, S., et al. (2008). Optimal implantation site for pancreatic islet transplantation. *Br J Surg, 95*(12), 1449-1461.

Moberg, L., et al. (2002). Productions of tissue factor by pancreatic islet cells as a trigger of detrimental thrombotic reactions in clinical islet transplantation. *Lancet, 360*, 2039-2045.

Muhammad, S., et al. (2009). Reactive oxygen species in diabetes-induced vascular damage, stroke, and Alzheimer's disease. *Journal of Alzheimer's Disease, 16*(4), 775-785.

Muller, D. W., et al. (1994). Site-specific dexamethasone delivery for the prevention of neointimal thickening after vascular stent implantation. *Coron. Artery Dis., 5*(5), 435-442.

Nakaoka, R., et al. (1997). Prolongation of the serum half-life period of superoxide dismutase by poly(ethylene glycol) modification. *Journal of Controlled Release, 46*(3), 253-261.

Nel, A., et al. (2006). Toxic potential of materials at the nanolevel. *Science, 311*(5761), 622-627.

Nilsson, B., et al. (2007). The role of complement in biomaterial-induced inflammation. *Mol Immunol, 44*(1-3), 82-94.

Niu, J., et al. (2007). Cardioprotective effects of cerium oxide nanoparticles in a transgenic murine model of cardiomyopathy. *Cardiovasc Res, 73*(3), 549-559.

Oberley, L. W. (1988). Free radicals and diabetes. *Free Radic Biol Med, 5*(2), 113-124.

Onuki, Y., et al. (2008). A review of the biocompatibility of implantable devices: current challenges to overcome foreign body response. *J Diabetes Sci Technol, 2*(6), 1003-1015.

Ozcay, N., et al. (1997). Budesonide, a locally acting steroid, prevents graft rejection in a rat model of intestinal transplantation. *Transplantation, 63*(9), 1220-1225.

Padmasekar, M., et al. (2013). Exendin-4 protects hypoxic islets from oxidative stress and improves islet transplantation outcome. *Endocrinology, 154*(4), 1424-1433.

Patil, S., et al. (2007a). Protein adsorption and cellular uptake of cerium oxide nanoparticles as a function of zeta potential. *Biomaterials, 28*(31), 4600-4607.

Patil, S. D., et al. (2007b). Concurrent delivery of dexamethasone and VEGF for localized inflammation control and angiogenesis. *J Control Release, 117*(1), 68-79.

Paul, D. R. (2011). Elaborations on the Higuchi model for drug delivery. *Int J Pharm, 418*(1), 13-17.

Pedraza, E., et al. (2013a). Macroporous three-dimensional PDMS scaffolds for extrahepatic islet transplantation. *Cell Transplant, 22*(7), 1123-1135.

Pedraza, E., et al. (2013b). Synthesis of macroporous poly(dimethylsiloxane) scaffolds for tissue engineering applications. *J Biomater Sci Polym Ed, 24*(9), 1041-1056.

Pedraza, E., et al. (2012). Preventing hypoxia-induced cell death in beta cells and islets via hydrolytically activated, oxygen-generating biomaterials. *Proc Natl Acad Sci U S A, 109*(11), 4245-4250.

Perez, J. M., et al. (2008). Synthesis of biocompatible dextran-coated nanoceria with pH-dependent antioxidant properties. *Small, 4*(5), 552-556.

Pernodet, N., et al. (1997). Pore size of agarose gels by atomic force microscopy. *Electrophoresis, 18*(1), 55-58.

Pileggi, A., et al. (2006). Reversal of diabetes by pancreatic islet transplantation into a subcutaneous, neovascularized device. *Transplantation, 81*(9), 1318-1324.

Pileggi, A., et al. (2004). Twenty years of clinical islet transplantation at the Diabetes Research Institute--University of Miami. *Clin Transpl*, 177-204.

Pires, N. M., et al. (2005). Histopathologic alterations following local delivery of dexamethasone to inhibit restenosis in murine arteries. *Cardiovasc Res, 68*(3), 415-424.

Pirmohamed, T., et al. (2010). Nanoceria exhibit redox state-dependent catalase mimetic activity. *Chem Commun (Camb), 46*(16), 2736-2738.

Pourkhalili, N., et al. (2012). Improvement of isolated rat pancreatic islets function by combination of cerium oxide nanoparticles/sodium selenite through reduction of oxidative stress. *Toxicol Mech Methods*.

Qi, D., et al. (2007). Glucocorticoids produce whole body insulin resistance with changes in cardiac metabolism. *Am. J. Physiol. Endocrinol. Metab., 292*(3), E654-E667.

Qi, L., et al. (2008). Redispersible hybrid nanopowders: cerium oxide nanoparticle complexes with phosphonated-PEG oligomers. *ACS Nano, 2*(5), 879-888.

Ranade, S. V., et al. (2005). Styrenic block copolymers for biomaterial and drug delivery applications. *Acta Biomater, 1*(1), 137-144.

Ratner, B. D., et al. (2004). Biomaterials: where we have been and where we are going. *Annu Rev Biomed Eng, 6*, 41-75.

Reffet, S., et al. (2006). Immunology of pancreatic islet transplantation. *Diabetes Metab, 32*(5 Pt 2), 523-526.

Reuter, S., et al. (2010). Oxidative stress, inflammation, and cancer: how are they linked? *Free Radical Biology and Medicine, 49*(11), 1603-1616.

Reynolds, T. D., et al. (2002). Investigation of the effect of tablet surface area/volume on drug release from hydroxypropylmethylcellulose controlled-release matrix tablets. *Drug Dev Ind Pharm, 28*(4), 457-466.

Roseman, T. J. (1972). Release of steroids from a silicone polymer. *J Pharm Sci, 61*(1), 46-50.

Roseman, T. J., et al. (1970). Release of medroxyprogesterone acetate from a silicone polymer. *J Pharm Sci, 59*(3), 353-357.

Ruers, T. J. M., et al. (1986). Local treatment of renal allografts, a promising way to reduce the dosage of immunosuppressive drugs. Comparison of various ways of administering prednisolone. *Transplantation, 41*(2), 156-161.

Ruers, T. J. M., et al. (1988). Sensitivity of graft rejection in rats to local immunosuppressive therapy. *Transplantation, 46*(6), 820-825.

Ryan, E. A., et al. (2001). Clinical outcomes and insulin secretion after islet transplantation with the Edmonton protocol. *Diabetes, 50*(4), 710-719.

Salvay, D., et al. (2008). Extracellular matrix protein-coated scaffolds promote the reversal of diabetes after extrahepatic islet transplantation. *Transplantation, 85*(10), 1456-1464.

Schmidt, J. J., et al. (2008). Hydrogels used for cell-based drug delivery. *J Biomed Mater Res A, 87*(4), 1113-1122.

Schubert, D., et al. (2006). Cerium and yttrium oxide nanoparticles are neuroprotective. *Biochem Biophys Res Commun, 342*, 86-91.

Schultz, C. L., et al. (2010). Contact lenses as a drug delivery device for epidermal growth factor in the treatment of ocular wounds. *Clin Exp Optom, 93*(2), 61-65.

Scott, M. D., et al. (1998). Cellular camouflage: fooling the immune system with polymers. *Curr Pharm Des, 4*(6), 423-438.

Sefton, M. V., et al. (2000). Making microencapsulation work: conformal coating, immobilization gels and in vivo performance. *J Control Release, 65*(1-2), 173-186.

Sehgal, A., et al. (2005). Precipitation-redispersion of cerium oxide nanoparticles with poly(acrylic acid): toward stable dispersions. *Langmuir, 21*(20), 9359-9364.

Siepmann, J., et al. (2000). Calculation of the required size and shape of hydroxypropyl methylcellulose matrices to achieve desired drug release profiles. *Int J Pharm, 201*(2), 151-164.

Siepmann, J., et al. (2011). Higuchi equation: derivation, applications, use and misuse. *Int J Pharm*, ePub.

Sipos, L., et al. (2005). Controlled delivery of paclitaxel from stent coatings using poly(hydroxystyrene-b-isobutylene-b-hydroxystyrene) and its acetylated derivative. *Biomacromolecules, 6*(5), 2570-2582.

Sivin, I., et al. (2002). Jadelle® levonorgestrel rod implants: a summary of scientific data and lessons learned from programmatic experience. (pp. 48). New York: Population Council.

Snorradottir, B. S., et al. (2009). Release of anti-inflammatory drugs from a silicone elastomer matrix system. *Pharmazie, 64*(1), 19-25.

Snorradottir, B. S., et al. (2011). Experimental design for optimizing drug release from silicone elastomer matrix and investigation of transdermal drug delivery. *Eur J Pharm Sci, 42*(5), 559-567.

Song, Y., et al. (2011). Feasibility of localized immunosuppression: 3. Preliminary evaluation of organosilicone constructs designed for sustained drug release in a cell transplant environment using dexamethasone. *Pharmazie, in press*.

Stern, S. T., et al. (2008). Induction of autophagy in porcine kidney cells by quantum dots: a common cellular response to nanomaterials? *Toxicological Sciences, 106*(1), 140-152.

Sun, A. M. (1988). Microencapsulation of pancreatic islet cells: a bioartificial endocrine pancreas. *Methods Enzymol, 137*, 575-580.

Tarnuzzer, R., et al. (2005). Vacancy engineered ceria nanostructures for protection from radiation-induced cellular damage. *Nano Letters, 5*(12), 2573-2577.

Tiedge, M., et al. (1997). Relation between antioxidant enzyme gene expression and antioxidative defense status of insulin-producing cells. *Diabetes, 46*(11), 1733-1742.

Tiedge, M., et al. (1998). Complementary action of antioxidant enzymes in the protection of bioengineered insulin-producing RINm5F cells against the toxicity of reactive oxygen species. *Diabetes, 47*, 1578-1585.

Travan, A., et al. (2009). Non-cytotoxic silver nanoparticle-polysaccharide nanocomposites with antimicrobial activity. *Biomacromolecules, 10*(6), 1429-1435.

Tsai, Y. Y., et al. (2007). Novel synthesis of cerium oxide nanoparticles for free radical scavenging. *Nanomed, 2*(3), 325-332.

Tsuji, J. S., et al. (2006). Research strategies for safety evaluation of nanomaterials, part IV: risk assessment of nanoparticles. *Toxicol Sci, 89*(1), 42-50.

Tuckermann, J. P., et al. (2005). Molecular mechanisms of glucocorticoids in the control of inflammation and lymphocyte apoptosis. *Crit Rev Clin Lab Sci, 42*(1), 71-104.

Udipi, K., et al. (2007). Development of a novel biocompatible polymer system for extended drug release in a next-generation drug-eluting stent. *J Biomed Mater Res A*.

Ueda, H., et al. (2005). Preoperative administration of FTY720 prolonged renal allograft survival. *Transplant Immunology, 14*(1), 1-8.

van der Windt, D. J., et al. (2007). Rapid loss of intraportally transplanted islets: an overview of pathophysiology and preventive strategies. *Xenotransplantation, 14*(4), 288-297.

Van Vlierberghe, S., et al. (2011). Biopolymer-based hydrogels as scaffolds for tissue engineering applications: a review. *Biomacromolecules, 12*(5), 1387-1408.

Vital, A. L., et al. (2003). Dexamethasone prevents granulocyte-macrophage colony-stimulating factor-induced nuclear factor-kappaB activation, inducible nitric oxide synthase expression and nitric oxide production in a skin dendritic cell line. *Mediators Inflamm, 12*(2), 71-78.

Walker, N. I., et al. (1988). Patterns of cell death. *Methods Achiev Exp Pathol, 13*, 18-54.

Ward, W. K., et al. (2002). The effect of microgeometry, implant thickness and polyurethane chemistry on the foreign body response to subcutaneous implants. *Biomaterials, 23*(21), 4185-4192.

Weber, L. M., et al. (2008). Cell-matrix interactions improve beta-cell survival and insulin secretion in three-dimensional culture. *Tissue Eng Part A, 14*(12), 1959-1968.

Weber, L. M., et al. (2007). The effects of cell-matrix interactions on encapsulated beta-cell function within hydrogels functionalized with matrix-derived adhesive peptides. *Biomaterials, 28*(19), 3004-3011.

Weber, T., et al. (1997). Local immunosuppression with budesonide after liver transplantation in the rat: a preliminary histomorphological analysis. *Transplantation, 64*(5), 705-708.

Wiegand, F., et al. (1993). Macrophage-generated nitric oxide as cytotoxic factor in destruction of alginate-encapsulated islets. Protection by arginine analogs and/or coencapsulated erythrocytes. *Transplantation, 56*(5), 1206-1212.

Wilson, J. T., et al. (2008a). Thrombosis and inflammation in intraportal islet transplantation: a review of pathophysiology and emerging therapeutics. *J Diabetes Sci Technol, 2*(5), 746-759.

Wilson, J. T., et al. (2008b). Layer-by-layer assembly of a conformal nanothin PEG coating for intraportal islet transplantation. *Nano Lett, 8*(7), 1940-1948.

Wu, P., et al. (2006). Drug/device combinations for local drug therapies and infection prophylaxis. *Biomaterials, 27*(11), 2450-2467.

Xu, J., et al. (2011). In vitro and in vivo evaluation of ketotifen fumarate-loaded silicone hydrogel contact lenses for ocular drug delivery. *Drug Deliv, 18*(2), 150-158.

Yang, Z., et al. (2004). Inflammation blockade improves pancreatic islet function. *Transplant Proc, 36*, 2864-2865.

Zaman, M. H., et al. (2006). Migration of tumor cells in 3D matrices is governed by matrix stiffness along with cell-matrix adhesion and proteolysis. *Proceedings of the National Academy of Sciences, 103*(29), 10889-10894.

Zawalich, W. S., et al. (2006). Dexamethasone suppresses phospholipase C activation and insulin secretion from isolated rat islets. *Metabolism-Clinical and Experimental, 55*(1), 35-42.

Zhou, Y., et al. (1997). Finite element analysis of diffusional drug release from complex matrix systems. I. Complex geometries and composite structures. *Journal of Controlled Release, 49*(2-3), 277-288.

Zhu, H., et al. (2010). Bilirubin protects grafts against nonspecific inflammation-induced injury in syngeneic intraportal islet transplantation. *Exp Mol Med, 42*(11), 739-748.

Zimmermann, H., et al. (2007). Alginate-based encapsulation of cells: past, present, and future. *Curr Diab Rep, 7*(4), 314-320.

Zisch, A. H., et al. (2003a). Cell-demanded release of VEGF from synthetic, biointeractive cell ingrowth matrices for vascularized tissue growth. *FASEB J, 17*(15), 2260-2262.

Zisch, A. H., et al. (2003b). Biopolymeric delivery matrices for angiogenic growth factors. *Cardiovasc Pathol, 12*(6), 295-310.